

Electronic Thesis and Dissertation Repository

---

7-28-2015 12:00 AM

## Effect of Temperature and Successive Sprays on Liquid Distribution in Fluidized Beds

Liliana Andrea Pardo Reyes  
*The University of Western Ontario*

Supervisor

Dr. Cedric Briens

*The University of Western Ontario* Joint Supervisor

Dr. Franco Berruti

*The University of Western Ontario*

Graduate Program in Chemical and Biochemical Engineering

A thesis submitted in partial fulfillment of the requirements for the degree in Master of Engineering Science

© Liliana Andrea Pardo Reyes 2015

Follow this and additional works at: <https://ir.lib.uwo.ca/etd>

 Part of the [Other Chemical Engineering Commons](#)

---

### Recommended Citation

Pardo Reyes, Liliana Andrea, "Effect of Temperature and Successive Sprays on Liquid Distribution in Fluidized Beds" (2015). *Electronic Thesis and Dissertation Repository*. 2959.

<https://ir.lib.uwo.ca/etd/2959>

This Dissertation/Thesis is brought to you for free and open access by Scholarship@Western. It has been accepted for inclusion in Electronic Thesis and Dissertation Repository by an authorized administrator of Scholarship@Western. For more information, please contact [wlsadmin@uwo.ca](mailto:wlsadmin@uwo.ca).

EFFECT OF TEMPERATURE AND SUCCESSIVE SPRAYS ON LIQUID  
DISTRIBUTION IN FLUIDIZED BEDS

(Thesis format: Monograph)

by

Liliana Andrea Pardo Reyes

Graduate Program in Chemical and Biochemical Engineering

A thesis submitted in partial fulfillment  
of the requirements for the degree of  
Master of Engineering Science

The School of Graduate and Postdoctoral Studies  
The University of Western Ontario  
London, Ontario, Canada

© Liliana Andrea Pardo Reyes 2015

## Abstract

Liquid injection in gas-solid fluidized beds is used in several industrial processes including food additive production, manufacturing of fertilizers, intermediate processing of pharmaceutical capsules and oil refining (i.e., Fluid Coking<sup>TM</sup> and Fluid Catalytic Cracking (FCC)). Good quality in the liquid distribution on the fluidized particles is fundamental in these processes either to ensure uniformity in the formation of desirable agglomerates, or to minimize their formation when undesirable. In the Fluid Coking process, for example, improving the liquid distribution and minimizing agglomerate formation will result in increasing the overall yield of the process and avoid operability problems.

A new experimental model that simulates agglomerate formation in fluidized beds and investigates their stability was developed and tested at pilot plant scale. The model can be adapted to model different processes, but, in this work, Fluid Coking<sup>TM</sup> was selected as an example of a system to model. The liquid content of the agglomerates was estimated with a new, simple and accurate procedure that can be applied to the whole mass of the recovered agglomerates. This procedure was extended to estimate the recoating of individual agglomerates by different sprays resulting from multiple feed jets.

The results indicated that reducing the average bed temperature or the mass of injected liquid (liquid load) enhanced the liquid distribution. Also, the maximum extent of liquid spread from wet to dry particles was estimated. The results indicated that the spreading is not a significant factor in reactors such as Fluid Cokers.

Keywords: Liquid injection, fluidized bed, liquid distribution, agglomeration, Fluid Coking<sup>TM</sup>, liquid spreading

## **Acknowledgments**

I would like to thank my supervisors Dr. Cedric Briens and Dr. Franco Berruti not only for the opportunity to complete my degree under their guidance, but also for all the insights, advices and challenges that helped me to successfully accomplish all my objectives in this project.

I would also like to sincerely thank Syncrude Canada Limited and ExxonMobil for their financial support, guidance and technical contributions for the completion of this research.

I would like to express my gratitude to all ICFAR staff members. Thank you Tom Johnston, Quinn Rush and Rob Taylor for all the technical assistance with the experimental set-up and thank you Caitlin Marshall for the support with the analytical characterization. I would like to thank as well my colleagues at ICFAR for their help and collaboration in different ways, especially Helal, Caro, Ana, Vale, and Francisco.

Finally, my deepest gratitude goes to my family, especially to my lovely husband, my daughter, my parents, my brother, Clau and Juanis. Oscar, thanks for holding my hand in the hardest moments, for helping me keep working hard and never letting me give up. Mom thanks for all you have done for me and for my baby. Gabi, a lot of this is for you.

## Table of Contents

Abstract.....	ii
Acknowledgments.....	iii
Table of Contents.....	iv
List of Tables.....	vii
List of Figures.....	viii
List of Symbols.....	xi
Chapter 1.....	1
1. Introduction.....	1
1.1 Wet Agglomeration.....	1
1.2 Industrial applications of liquid injection (wet granulation) in fluidized beds.....	5
1.2.1 Food Industry.....	5
1.2.2 Pharmaceutical Industry.....	6
1.2.3 Fluid Coking <sup>TM</sup> .....	7
1.3 Previous studies on liquid distribution and agglomerate formation in fluidized beds.....	9
1.4 Research Objectives.....	13
Chapter 2.....	14
2. Methodology.....	14
2.1 Experimental Set-up.....	14
2.1.1 Equipment.....	14
2.1.2 Liquid Solution.....	16
2.2 Agglomerate Characterization.....	17
2.2.1 Determination of Agglomerate Size Distribution.....	17
2.2.2 Estimation of Liquid-to-Solid Ratio.....	20

2.2.2.1	<i>Dye Concentration in Agglomerates when Injecting a Single Colour</i> .....	20
2.2.2.2	<i>Dye Concentration in Agglomerates when Injecting more than One Dye</i> .....	23
2.3	Colour distribution in individual agglomerates.....	28
2.4	Estimation of time for a Jet Expansion .....	30
2.5	Estimation of Liquid Concentration in Solids after End of Jet Expansion (Small Number of Jet Expansions) .....	33
2.6	Estimation of fraction of agglomerates (from earlier injections) entering the jet cavity with bubbles .....	34
2.7	Liquid Spreading Estimation.....	36
2.7.1	Digital Image Analysis .....	36
2.7.2	Statistical Analysis of Liquid Spreading in Bed Particles .....	38
Chapter 3	.....	40
3.	Development of an experimental low temperature model for the study of agglomerate formation and stability in fluidized beds.....	40
3.1	Introduction .....	40
3.2	Materials and methods .....	41
3.3	Results and Discussion.....	42
3.3.1	General Characteristics of the model.....	42
3.3.2	Injection Experiments in a Large Scale Fluidized Bed.....	44
3.3.3	Average Bed Temperature Effect .....	47
3.3.4	Effect of binder concentration and pH (viscosity).....	54
Chapter 4	.....	58
4.	Impact of pulse duration on agglomerate formation, recoating and breakup .....	58
4.1	Introduction .....	58
4.2	Materials and methods .....	58
4.3	Results and Discussion.....	61

4.3.1	Effect of Pulse Duration on Agglomerates Formation .....	61
4.3.2	Effect of Pulse Duration on the Liquid Concentration .....	67
Chapter 5	.....	80
5.	Evaluation of liquid spreading from wet to dry particles .....	80
5.1	Introduction .....	80
5.2	Materials and methods .....	80
5.2.1	Operating conditions .....	81
5.2.2	Equations.....	82
5.3	Results and discussion.....	82
5.3.1	Characterization of initial liquid distribution.....	82
5.3.2	Spreading of liquid from wet to dry particles .....	87
Chapter 6	.....	92
6.	Conclusions and recommendations.....	92
6.1	Conclusions .....	92
6.2	Recommendations .....	93
References	.....	95
Appendix A	.....	101
CURRICULUM VITAE	.....	104

## List of Tables

Table 2-1: Wavelength of maximum absorbance ( $\lambda_{\max}$ ) for the different dyes .....	21
Table 2-2: Calibration factors for the system equation for Blue + Yellow mixtures .....	24
Table 2-3: Calibration factors for Blue + Yellow + Red mixtures .....	26
Table 3-1: Operating conditions for Plexiglas and Gum Validation Experiments .....	42
Table 3-2: Physical properties of Gum Solutions Tested, Plexiglas Model and Bitumen.....	43
Table 3-3: Heat of vaporization for AVR from Syncrude Canada Ltd (i.e. Bitumen), Plexiglas model and Gum Arabic solution (5 wt% GA + 2 wt% colour + 93 wt% water .....	44
Table 4-1: Operating conditions for Injection Experiments .....	59
Table 4-2: Physical properties of Gum Solutions Used.....	60
Table 4-3: Sequence of colour injected for each type of experiment .....	60
Table 5-1: Operating conditions for Injection Experiments .....	81
Table 5-2: Physical properties of Gum Solution Used .....	82
Table 5-3: Free moisture available in individual particles for experiments with different fluidization velocities.....	84
Table 5-4: Results for ANOVA test; $V_g = 0.3$ m/s, Defluidized just after injection .....	86
Table 5-5: Results for ANOVA test; $V_g = 0.3$ m/s, Drying time = 10 min .....	88
Table 5-6: Results for Welch Two Sample t-test; $V_g$ 0.3 m/s,.....	91
Table A 1: Gum Arabic Physical Properties, adapted from (ROEPER, 2015)	102



## List of Figures

Figure 1-1: Mechanism of agglomeration process (Adapted from Ivenson et al., 2001) .....	3
Figure 1-2: Wet agglomeration mechanism for Fluid Coking <sup>TM</sup> (Morales M, 2013).....	4
Figure 1-3: Block flow diagram for drug production (Adapted from Aulton, 2002) .....	6
Figure 1-4: Informal Classification of Organic Sediments (Adapted from Speight, 2011).....	7
Figure 1-5: Simplified Fluid Coking <sup>TM</sup> Scheme ExxonMobil (Adapted from Exxon Mobil, 2014).....	8
Figure 2-1: Schematic of the Experimental Setup .....	14
Figure 2-2: Particle size distribution of the silica sand used in the experiments .....	15
Figure 2-3: Schematic of the TEB nozzle .....	16
Figure 2-4: Example of particle size distribution of a washed and dried sample for step 3 in the micro-agglomerates determination procedure .....	19
Figure 2-5: Calibration Curve for Blue No. 1, $\lambda_{\max} = 630 \text{ nm}$ .....	22
Figure 2-6: Calibration Curve for Yellow No.5, $\lambda_{\max} = 427 \text{ nm}$ .....	22
Figure 2-7: Calibration Curve for Red No. 40, $\lambda_{\max} = 503 \text{ nm}$ .....	23
Figure 2-8: Calculated concentrations for blue in blue + yellow mixtures using either the full model (Equation 2-5) which accounts for interactions, or the calibration curve of.....	25
Figure 2-9: Calculated concentrations for yellow in blue + yellow mixtures using either the full model (Equation 2-6) which accounts for interactions, or the calibration curve of.....	25
Figure 2-10: Calculated concentrations for blue in blue + yellow + red mixtures using either the full model (Equation 2-7) which accounts for interactions, or the calibration curve of Figure 2-5, which neglects interactions .....	27
Figure 2-11: Calculated concentrations for yellow in blue + yellow + red mixtures using either the full model (Equation 2-8) which accounts for interactions, or the calibration curve of Figure 2-6, which neglects interactions .....	27
Figure 2-12: Calculated concentrations for red in blue + yellow + red mixtures using either the full model (Equation 2-9) which accounts for interactions, or the calibration curve of Figure 2-7, which neglects interactions .....	28
Figure 2-13: Ternary plot for colour mixing representation .....	30
Figure 2-14: Schematic representation of a jet expansion .....	30
Figure 2-15: Example of picture used for total particles counting after pre-processing.....	37
Figure 2-16: Example of picture used for blue dyed particles counting .....	38

Figure 3-1: Effect of binder concentration on agglomerate formation; .....	45
Figure 3-2: Effect of binder concentration on the initial liquid concentration in agglomerates, $T_0 = 130\text{ }^\circ\text{C}$ , 1 x 1200 g, Solution pH = 3.0.....	46
Figure 3-3: Bed temperatures for one pulse and four pulse injections; .....	48
Figure 3-4: Effect of average bed temperature (number of pulses) on agglomerate formation; $T_0 = 130\text{ }^\circ\text{C}$ , Solution: 5 wt% GA - 2 wt% Blue No. 1 – pH 3.....	49
Figure 3-5: Effect of average bed temperature (number of pulses) on the initial liquid concentration in agglomerates; $T_0 = 130\text{ }^\circ\text{C}$ , Solution: 5 wt% GA - 2 wt% Blue No. 1 – pH 3 .....	50
Figure 3-6: Schematic representation of the agglomerate drying for one and four pulse injections ...	51
Figure 3-7: Bed temperature for four pulse injection with different initial bed temperatures; Solution: 5 wt% GA - 2 wt% Blue No. 1 – pH 3.....	52
Figure 3-8: Effect of average bed temperature (initial bed temperature) on agglomerate formation; Type of Injection: 4 x 300 g, Solution: 5 wt% GA - 2 wt% Blue No. 1 – pH 3 .....	53
Figure 3-9: Effect of average bed temperature (initial bed temperature) on the initial liquid concentration in agglomerates; Type of Injection: 4 x 300 g, Solution: 5 wt% GA - 2 wt% Blue No. 1 – pH 3.....	54
Figure 3-10: Effect of pH and binder concentration on the viscosity of the model solutions .....	55
Figure 3-11: Effect of solution pH on agglomerate formation; .....	56
Figure 3-12: Effect of solution pH on the initial liquid concentration in agglomerates; .....	57
Figure 4-1: Bed temperatures for two, three and six pulses injections; .....	62
Figure 4-2: Effect of pulse duration on agglomerate formation .....	63
Figure 4-3: Average liquid concentration of wetted solids obtained with the model corresponding to different injection strategies.....	64
Figure 4-4: Total mass of agglomerates formed for an experiment with a single pulse and for an experiment with two pulse of 600 g each .....	65
Figure 4-5: Comparison of agglomerates smaller than $d_{\text{aggl}}$ formed for an experiment with a single pulse and an experiment with two pulse of 600 g each .....	66
Figure 4-6: Mass of agglomerates formed per gram of liquid injected for an experiment with a single pulse and an experiment with two pulse of 600 g each .....	66
Figure 4-7: Concentration of the liquid from the first pulse (blue) and the second pulse (yellow) in agglomerates; $T_{0, 2 \times 600 \text{ g}} = 116\text{ }^\circ\text{C}$ .....	67

Figure 4-8: Particle size distribution of the initial silica sand in the fluidized bed at the beginning of the experiment, and of the sand trapped in the macro-agglomerates recovered after the end of the experiment.....	68
Figure 4-9: Example of agglomerates recovered after the second pulse in an experiment of two pulse of 600 g each.....	70
Figure 4-10: Colour distribution in agglomerates $d_{\text{aggl}} \geq 9500 \mu\text{m}$ for two pulse injection.....	71
Figure 4-11: Colour distribution in agglomerates $9500 \mu\text{m} > d_{\text{aggl}} \geq 4000 \mu\text{m}$ for two pulse injection.....	71
Figure 4-12: Effect of colour sequence on the total liquid concentration in agglomerates for a three pulse injection; $T_{0, 3 \times 400 \text{ g}} = 112.5 \text{ }^\circ\text{C}$ .....	73
Figure 4-13: Samples of agglomerates recovered for three pulse injection: 3 x 400 g (colour sequence of: blue, yellow and red).....	74
Figure 4-14: Colour distribution in agglomerates recovered for three pulse injection (colour sequence of: blue, yellow and red).....	75
Figure 4-15: Effect of the colour sequence on the total liquid concentration in agglomerates in a six pulse injection; $T_{0, 6 \times 200 \text{ g}} = 111 \text{ }^\circ\text{C}$ .....	77
Figure 4-16: Colour distribution in agglomerates recovered for six pulse injection a) $d_{\text{aggl}} \geq 9500 \mu\text{m}$ b) $9500 \mu\text{m} > d_{\text{aggl}} \geq 4000 \mu\text{m}$ c) $4000 \mu\text{m} > d_{\text{aggl}} \geq 2000 \mu\text{m}$ .....	78
Figure 4-17: Effect of the pulse duration on the total mass of liquid trapped in agglomerates.....	79
Figure 5-1: Effect of fluidization time after injection on agglomerate formation,.....	83
Figure 5-2: Effect of fluidization time after injection on the initial liquid concentration in agglomerates; $V_g = 0.3 \text{ m/s}$ .....	84
Figure 5-3: Fraction of dyed particles for different individual size particles;.....	85
Figure 5-4: Concentration of wetted particles according to the model for the Estimation of Liquid Concentration in Solids after End of Jet Expansion.....	86
Figure 5-5: Fraction of dyed particles for different individual size particles;.....	88
Figure 5-6: Fraction of dyed particles for different individual size particles;.....	89
Figure 5-7: Effect of fluidization time after injection in liquid spreading;.....	90
Figure A 1: Proposed Structure of Gum Arabic.....	101
Figure A 2: Gum Arabic solution viscosity as function of GA concentration.....	103

## List of Symbols

$A_{blue}^0$	Absorbance of blue in solution without any colour added
$A_{red}^0$	Absorbance of red in solution without any colour added
$A_{yellow}^0$	Absorbance of yellow in solution without any colour added
B	Fraction mass of blue in individual agglomerate (g/g)
c	Concentration of liquid in wetted solids at steady state (kg/kg)
$C_{blue}$	Concentration of blue in individual agglomerate (mg/kg)
$C_{red}$	Concentration of red in individual agglomerate (mg/kg)
$C_{yellow}$	Concentration of yellow in individual agglomerate (mg/kg)
$C_{Blue}^*$	Normalized mass of blue in individual agglomerate
$C_{Red}^*$	Normalized mass of red in individual agglomerate
$C_{Total}^*$	Normalized total mass of colour in individual agglomerate
$C_{Yellow}^*$	Normalized mass of yellow in individual agglomerate
D	Diameter of the jet projection (m)
$d_{aggl}$	Agglomerate diameter ( $\mu\text{m}$ )
$d_b$	Diameter of the detached bubbles from the jet (m)
$d_p$	Individual particle diameter ( $\mu\text{m}$ )
$d_N$	Spray nozzle diameter (m)
$d_{pH}$	Higher size limit for a given sieve size
$d_{pL}$	Lower size limit for a given sieve size
$F_L$	Liquid flow rate (kg/s)
$F_{ga}$	Mass flow rate of gas coming into the jet from the atomization gas (kg/s)
$F_{gB}$	Mass flow rate of gas coming into the jet with the bubbles (kg/s)
$F_{SB}$	Mass flow rate of solids entering jet cavity in the wakes of bubbles captured by jet (kg/s)
$f_w$	Wake volume, as fraction of gas bubble volume
GA	Gum Arabic

$L$	Liquid wetting he solids in one jet expansion (kg)
$L_{jet}$	Jet length (m)
$L_{max}$	Maximum jet penetration length (m)
$L_{min}$	Minimum jet penetration length (m)
$m_B$	Initial bed mass (g)
$m_d$	Mass of dye (g)
$m_{GA}$	Gum Arabic mass (g)
$m_M$	Total mass of macro-agglomerates recovered (g)
$M_p$	Mass of particles trapped in agglomerates (g)
$m_R$	Representative sample taken from $m_{<600\mu m}$ (g)
$m_{sand}$	Mass of washed and dried sand particles (g)
$m_{\mu aggl,Ri}$	Mass of micro-agglomerates in the size cut sample (g)
$m_{\mu aggl,i}$	Total mass of micro-agglomerates in the bed for a given size cut (g)
$m_{<600\mu m}$	Bed mass after recovery of macro-agglomerates (g)
$Q_{cB}$	Volumetric gas flow rate into the jet cavity from captured bubbles ( $m^3/s$ )
$Q_g$	Total gas volumetric flow rate into the jet cavity ( $m^3/s$ )
$Q_{g_a}$	Volumetric atomization gas flow rate into the jet cavity ( $m^3/s$ )
$S_B$	Mass of solids entering jet cavity in 1 jet expansion (kg)
$S_R$	Mass of solids in wake of bubble released from jet (kg)
$U_{mf}$	Minimum fluidization velocity (m/s)
$V_g$	Superficial gas velocity for fluidization (m/s)
$v_{B_e}$	Estimated volume of the detached bubbles from the jet (m)
$v_B$	Volume of the detached bubbles from the jet (m)
$R$	Fraction mass of red in individual agglomerate (g/g)
$S$	Solids wetted in one jet expansion (kg)
$x_f$	Weight fraction of fines (g)

$Y$	Fraction mass of yellow in individual agglomerate (g/g)
$\alpha$	Mass fraction of solids in wakes bubbles captured by the jet cavity that are agglomerates
$\Gamma$	Calibration factor for colours
$\lambda_{\max}$	Characteristic wavelength of a dye colour
$\rho_{mf}$	Emulsion phase density ( $\text{kg/m}^3$ )
$\theta$	Angle of the jet projection ( $^\circ$ )

## Chapter 1

### 1. Introduction

Wet agglomeration in gas-solid fluidized beds is utilized in different industries, such as oil and gas, food, fertilizer and pharmaceutical. In the process of size enlargement of the agglomerates, the quality of the liquid distribution is fundamental to achieve the desired final product characteristics and enhance its yield and quality. The initial liquid distribution will determine the agglomerates growth rate, strength and thus their persistence or breakage rate (Salman, et al., 2007). Different researchers have studied the effect of operating conditions on the liquid distribution, such as, for example, binder concentration, liquid binder viscosity, fluidization velocity, among others. However, determining the impact of these parameters requires further research so that the agglomeration process and stability can be fully understood.

The present work aimed at a better understanding of the agglomeration processes resulting from the injection of liquid sprays in gas-solid fluidized beds. A new experimental method was developed to estimate the effect of bed temperature, liquid properties and liquid loading. Fluid Coking<sup>TM</sup> was used as the specific industrial application due its economic importance in a country like Canada.

This chapter presents a brief literature review on the fundamentals of the wet agglomeration process and its applications, and on previous studies on the liquid distribution in gas-solid fluidized beds. At the end of this chapter, the objectives of the present thesis are introduced.

#### 1.1 Wet Agglomeration

When individual particles join by binding and form a new larger particle in which the original particles can still be discerned, this individual particle is known as agglomerate (Parveen, 2011). Agglomeration processes can be classified in different ways, such as dry and wet agglomeration, depending on whether a liquid binder has been used (Dhanalakshmi, et al., 2011).

In wet agglomeration, a liquid binder is sprayed onto a group of moving particles to promote their adhesion by forming solid bridges when the liquid is evaporated (Iveson, et al., 2001). In wet agglomeration, binders are dissolved in the granulation solvent. Gas-solid fluidized beds are commonly used for this process, since the solid mixing in these reactors is rapid and the temperature is uniform (Woolard & Potter, 1968) leading to a uniform evaporation of the solvent used to distribute the binder. Agglomerate formation is the objective of some processes to achieve improved product appearance, increased bulk density for storage, control of solubility or other characteristics (Parikh, 2005). On the contrary, for processes like Fluid Coking<sup>TM</sup> the formation of agglomerates should be minimized since their presence degrades operability because of the fouling of internals and reduces the yield of valuable products. Excessive agglomeration may ultimately lead to the loss of fluidity of the bed (bed bogging).

Wet agglomeration occurs in three stages, clearly defined by Ivenson et al (2000) and illustrated in **Figure 1-1**:

- i. *Wetting and nucleation*: initial liquid distribution over the moving individual particles followed by the formation “seeds” of subsequent agglomerates (nuclei). The size of the sprayed droplets of liquid will determine the mechanism of the nuclei formation: droplets bigger than the individual particles will form nuclei by immersion and droplets smaller than the individual particles will form nuclei by dispersion. Nuclei kinetics depends on factors such as liquid properties and solids mixing.
- ii. *Consolidation and coalescence*: collisions between granules and other granules (coalescence) and / or individual particles (layering) occur, resulting in particle enlargement. Mechanical properties of the granules and the availability of liquid binder will affect the consolidation strength. The agglomerate strength will be determined by capillary forces, viscous forces, and inter-particle forces (Iveson & Page, 2001). It has been established that, in most cases, capillary forces have more impact on the agglomerate stability and growth than viscous forces (Pont, et al., 2001). Operating conditions such as nozzle design, bed temperature and droplet velocity affect the agglomerate consolidation.



- iii. *Attrition and breakage*: still wet (breakage) or dry granules (attrition) fracture due to shear forces within the fluidized bed, chemical or thermal changes (Shamlou, et al., 1990). Also, it has been established that the breakage rate is higher in vessels where mixing is intense (Iveson & Page, 2001). The bed geometry and the gas atomization conditions also have an effect in the break up process (Benali, et al., 2009)

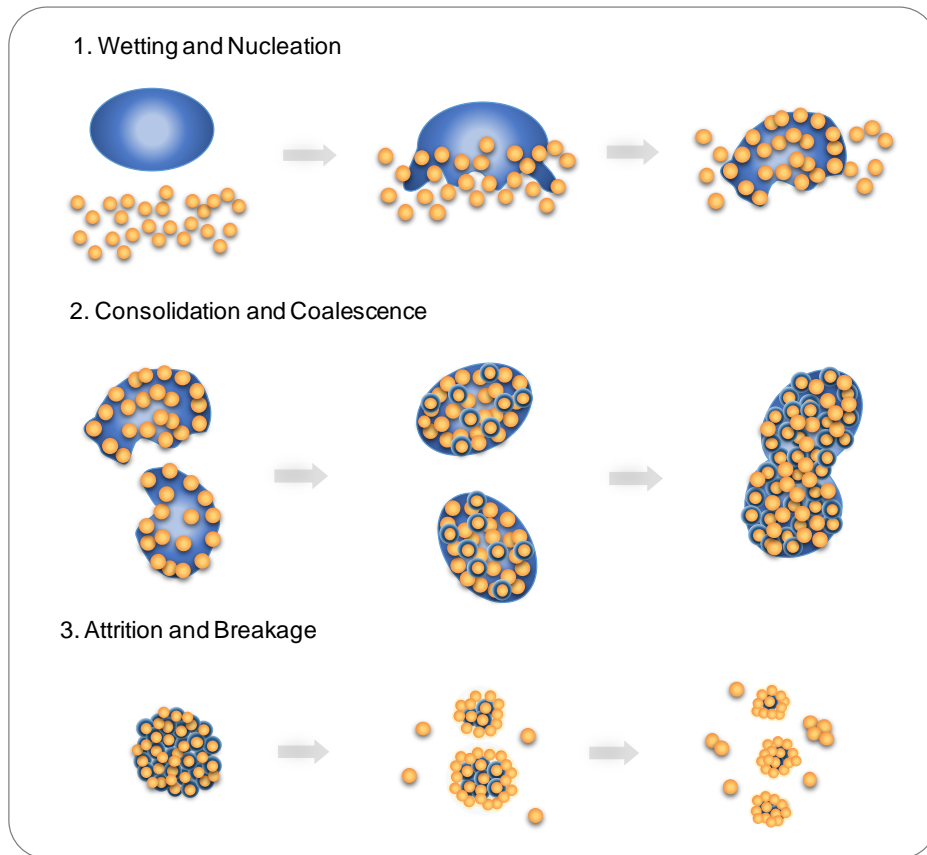


**Figure 1-1: Mechanism of agglomeration process (Adapted from Ivenson et al., 2001)**

Gray (2002), using the granulation process as a reference, proposed a mechanism for the agglomeration process in Fluid Coking<sup>TM</sup>. Morales (2013) considered this mechanism and suggested the different properties that could affect each of the stages proposed by Gray. According to this mechanism, the agglomeration process in Fluid Coking<sup>TM</sup> consists of three consecutive stages (**Figure 1-2**):

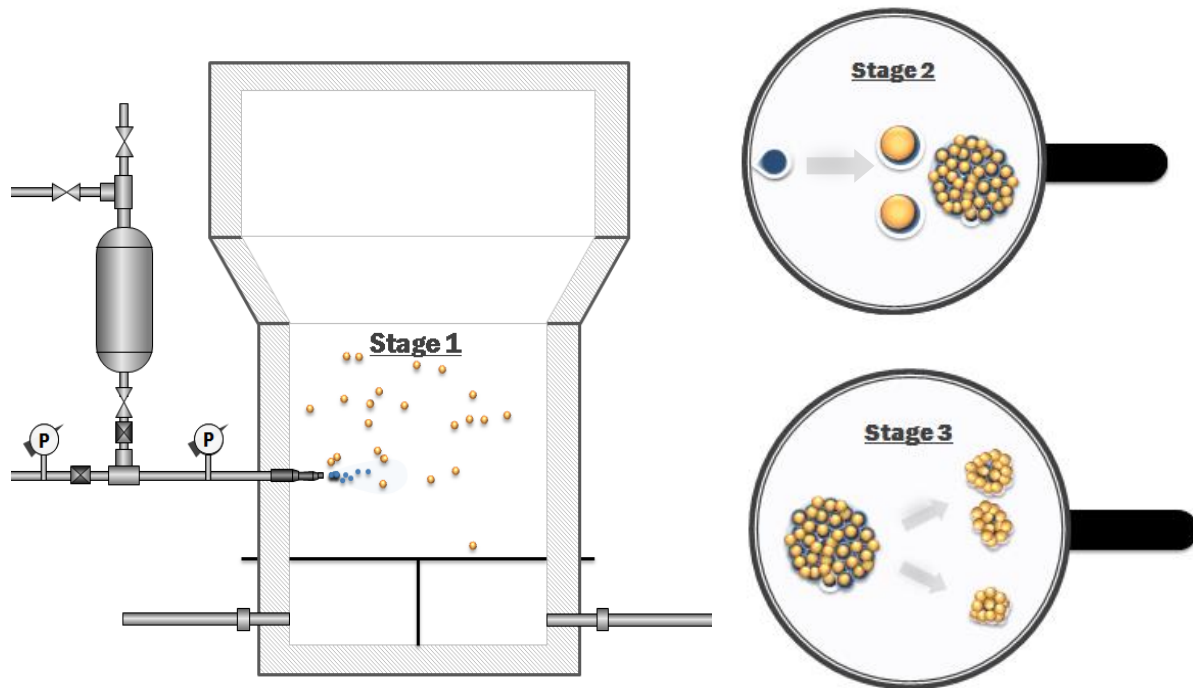


**Figure 1-2: Wet agglomeration mechanism for Fluid Coking™ (Morales M, 2013)**

- i. *Stage 1:* liquid sprayed together with atomizing gas form droplets that come in contact with the solid particles entering the jet cavity formed by the two-phase feed jet. Reducing the binder solution viscosity and/or increasing the atomization gas will improve the initial liquid distribution, since the droplets contacting the particles would be smaller and thus, the spreading more even.
- ii. *Stage 2:* the particles get wetted and the liquid is spread when collisions occur. When the liquid content within particles is high enough to resist the shear forces in the bed, agglomerates will form. The liquid will spread more easily if the solids are wettable by the binder solution; therefore, if the contact angle is reduced, more agglomerates will form but their liquid concentration will be lower.
- iii. *Stage 3:* fragmentation of the agglomerates due to bed dynamic induced stresses. Increasing the superficial gas velocity will promote breakage of agglomerates.

## 1.2 Industrial applications of liquid injection (wet granulation) in fluidized beds

### 1.2.1 Food Industry

The production of different food additives (i.e. flavors, thickeners, stabilizers, etc...) and products are often carried out with wet agglomeration. The aim of the agglomeration is often to improve the flowability, handling, dissolution characteristics, shelf life, resistance to degradation, and minimize dust formation and product losses among others (Dhanalakshmi, et al., 2011).

In the food industry, wet agglomeration in fluidized beds is selected when more porous products are desired. Usually, the binder is suspended in an organic solvent and this mix is injected in a fluidized bed where heated fluidization gas evaporates the solvent and dries the granules. The most common fluidization gases used in the food industry are nitrogen and air and the binders are artificial polymers, natural polymers or sugars (Gaonkar, et al., 2014). Some common binders are gelatine, gum Arabic, methylcellulose and sorbitol (Ortega-Rivas, et al., 2005).

For instance, wet agglomeration has been introduced in the production of baby food. A suspension of 2% lecithin solution and 50% sugar solution is used as a liquid binder. It has been proven that performing this agglomeration greatly improves the flowability and the handling of the product (Szulc & Lenart, 2010).

Also, in order to produce iron fortified salt, different forms of iron have been microencapsulated using the wet agglomeration technique. If the iron is not encapsulated, a reaction between the iodine and the iron will produce unwanted coloration and flavors in the fortified salt (Andersson, et al., 2008).

Agglomerated powder beverages, soups mixes and a wide variety of dairy products are some other examples of products that are currently manufactured by agglomeration resulting from the injection of a liquid in fluidized beds (Dhanalakshmi, et al., 2011).

### 1.2.2 Pharmaceutical Industry

Similarly to the food industry, in the pharmaceutical industry agglomeration is used to improve different physical properties of the product, such as bulk density, or to avoid segregation in formulation mixes. Nowadays, fluidized beds are considered a multiprocessor unit since not only agglomeration but drying and granulation can be performed in these reactors (Parikh, 2005).

The successful agglomeration of drugs during fluid bed granulation is a very complex process that can be affected by equipment characteristics (i.e. geometry, capacity, etc.) and process conditions. Segregation of multi-component mixtures and moisture control throughout the fluidized bed are the most common issues in this process (Faure, et al., 2001).

A block flow process for drug tablet production was proposed by Aulton (2002) (**Figure 1-3**) where wet agglomeration is mainly applied in the second stage of the process.

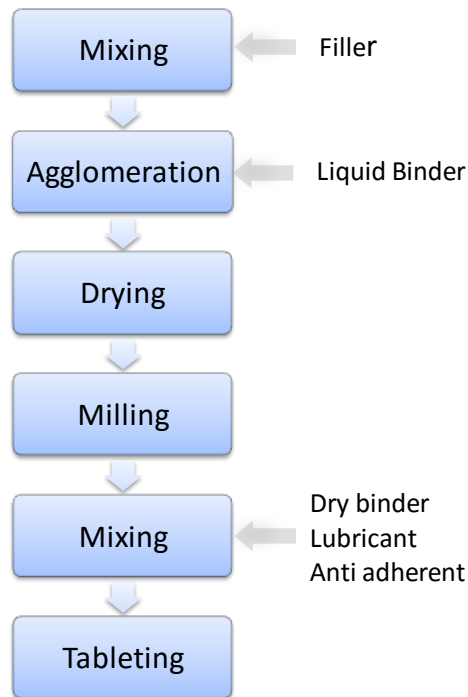


**Figure 1-3: Block flow diagram for drug production (Adapted from Aulton, 2002)**

### 1.2.3 Fluid Coking™

The bitumen extraction and upgrading industries are currently two of the most important players in the Canadian economy. The Canadian Association of Petroleum Producers indicates that these industries cumulatively represent the largest single private investor in Canada (\$61 billions), representing 20% of the Toronto Stock Exchange and providing over 550,000 direct/indirect jobs in the country (Canadian Association of Petroleum Producers, 2014). The bituminous oil represents approximately 98% of Canada’s oil reserves, which are now the third largest reserves in the world, according to the Oil & Gas journal (National Energy Board, 2014). As a consequence of the importance of the bituminous oil industry, there is an increasing interest with regard to the upgrading alternatives, and particularly, the study of the thermal cracking processes.

The National Energy Board describes bitumen or crude bitumen as “a highly viscous mixture, mainly of hydrocarbons heavier than pentanes”, which, due to its physical characteristics, is unsuitable for conventional processing (National Energy Board, 2014). **Figure 1-4** presents a classification of several organic sediments based on their ability to produce hydrocarbons. As observed, bitumen (Tar Sand Bitumen in the figure) requires additional upgrading operations in order to produce lighter hydrocarbons to be used in midstream/downstream petroleum plants:

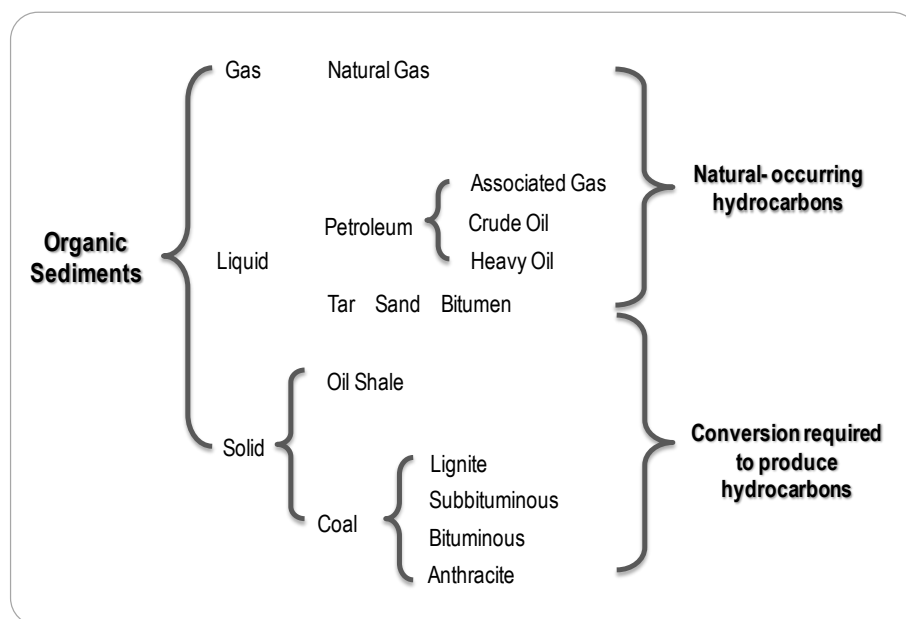


**Figure 1-4: Informal Classification of Organic Sediments (Adapted from Speight, 2011).**

Nowadays, the methods available for bitumen conversion into upgraded products can be divided in three large groups: thermal, catalytic and fluid catalytic processes (Sato, et al., 1992). Due to the normal presence of catalyst poisons in the bituminous materials (metals, resins, asphaltenes), thermal processes are preferred over catalytic processes as less severe pre-processing operations are required for treating the feedstock before entering the conversion units (Singh, et al., 2012). Thermal processes are those that use pressure (low to moderate) and heat (temperatures between 360 and 520°C (Phillips, et al., 1985)) to “break down, re-arrange and combine hydrocarbon molecules” (Gary, 2007). Among the most important technologies, FlexCoking, Fluid Coking<sup>TM</sup>, Delayed Coking and the Eureka Process are the most commonly used industrially. **Figure 1-5** shows a simplified process flow scheme of a Fluid Coker unit for thermal cracking.

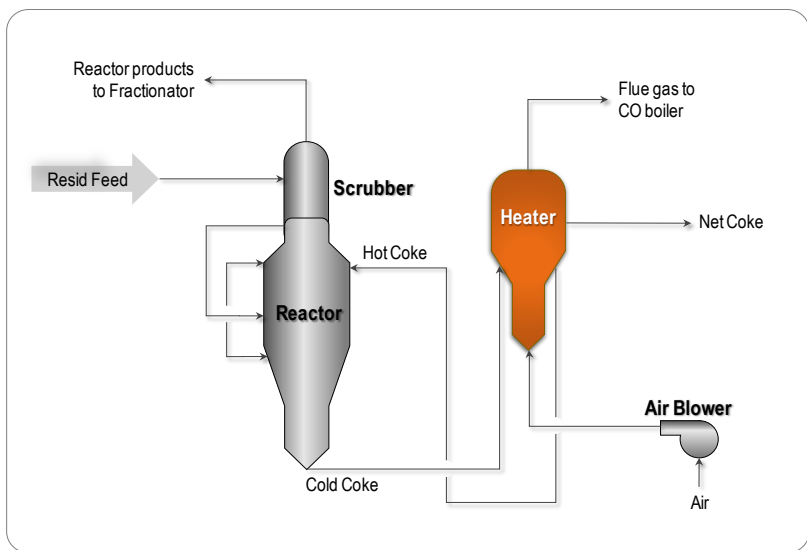


**Figure 1-5: Simplified Fluid Coking<sup>TM</sup> Scheme ExxonMobil (Adapted from Exxon Mobil, 2014)**

In Fluid Coking<sup>TM</sup>, pre-heated liquid bitumen (300 – 400 °C) is mixed with steam and injected in the form of droplets through specially designed nozzles into a fluidized bed of hot coke particles. The bitumen is heated to reduce the viscosity and, and thus, to improve the initial distribution of the liquid feed over the fluidized hot coke particles; however, as the cracking reaction occurs, the viscosity increases due to the evaporation of volatile material (Aminu, et al., 2004). The reactions take place over the hot coke surface, where heat transfer occurs, enabling the endothermic cracking

processes. It is fundamental that the liquid covers uniformly the coke particles to avoid the formation of coke agglomerates and, thus, create regions with considerable heat and mass transfer limitations that lead to a lower yield of valuable liquid and poor reactor operability (Gray, 2002).

The coking reaction temperatures typically range from 500 to 540 °C (Gray, 2002) and a mix of vapour and coke are produced. The produced vapours along with the steam rise to the top of the reactor where they are removed and sent to a scrubber, in which lighter and heavier products are separated. Lighter vapours are directed to the fractionation section and heavier liquid compounds are recycled by mixing them with the feed and reinjecting them into the Coker. In a stripper section, at the bottom of the reactor, hydrocarbons trapped in the coke particles are recovered before sending the coke particles to a burner to reheat them by partial combustion. Any agglomerate formed due to poor liquid distribution will also segregate in the bottom section, pass through the stripper and carry unreacted liquid to the burner, thus reducing the overall yield.

Although Fluid Coking<sup>TM</sup> is not intended as a wet agglomeration process per se, it can be considered as a wet-agglomeration process; since the bitumen injected acts as a liquid binder of the coke particles aggregates (Gray, 2002). As explained in a previous section, the mechanism of agglomerate formation proposed by Gray (2002) was based on wet-agglomeration, as thus, a lot of studies to understand and improve the liquid distributions are taken from this process.

### 1.3 Previous studies on liquid distribution and agglomerate formation in fluidized beds

Regardless of whether or not agglomerates are desired in any process, a better understanding of agglomerate formation and stability is needed to achieve the specific process objectives. In the case of Fluid Coking, agglomerate formation needs to be minimized. Therefore, different models have been proposed to study the agglomeration process during fluid coking at the pilot plant scale. This review focuses on the studies that were concerned with agglomerate minimization.

Portoghese (2007) characterised the quality of the liquid distribution by using triboelectric probes that monitored the moisture of the bed solids during the spreading, mixing, and drying phases. The

probes measured a current that was a monotonic function of the bed moisture. The effect of fluidization velocity was studied, finding that, at lower velocities, more agglomerates would form; in addition, increasing the gas atomization flow rate would help to achieve a more uniform liquid distribution.

House (2007) developed a water-based cold model with sugar as a binder for coke particles. To harden the initial agglomerates formed without breaking them as a result of shear in the fluid bed, the bed was dried under fixed bed conditions. The main advantage of this experimental model was that the initially formed agglomerates could be recovered and their liquid content could be determined using the sugar as a tracer. The drawback of this system was that the slow drying did not properly simulate the fast evaporation/reaction occurring in industrial processes such as Fluid Coking™ and that only the initially formed agglomerates, resulting from the interaction of the spray jet and the fluidized particles, could be investigated.

Following the previous studies, Weber (2009) investigated the stability of agglomerates of known characteristics (since they were fabricated in the laboratory) in fluidized beds. These agglomerates were manufactured using different solids (silica sand, glass beads and coke) and different liquids (water, oil, or sugar solutions) and were tested directly in a pilot plant. Knowing the initial characteristics of the agglomerates allowed the author to have a better idea of how their stability was influenced by their characteristics (i.e. liquid content, shape and size). The author established that there is a critical content of liquid in the agglomerates that, if exceeded, would give the agglomerates more chances to survive the bed stresses and grow. In general, larger agglomerates with high liquid content are the hardest to fragment in a fluid bed. Increasing the liquid viscosity increased the total mass of agglomerates and, on the other hand, increasing the superficial gas velocity, reduced this mass.

Parveen (2011) developed a model using Radio Frequency Identification (RFID) to detect the agglomerate breakup. The author investigated how fluidization velocity, agglomerate size, shape, density and liquid content would impact the breakage rate. Like Portoghese (2007), in this study



it was found that high fluidization velocities favour agglomerate breakup. Also, it was concluded that agglomerates that are bigger, denser or with a higher liquid content are more stable and thus, are less likely to break.

Saha (2012) used the sugar solution first introduced by House (2007), and coke particles, but increased the bed temperature to achieve caramelization conditions and thus model more closely the evaporation and agglomeration process in Fluid Cokers. High temperatures (250 °C) were needed to caramelize the sugar and thus, harden the agglomerates for subsequent recovery and analysis. Due to the caramelization reaction, further analysis of the liquid content of agglomerates was not possible. The author also investigated the impact of mass flow rate of atomization gas and the use of some attachments to the spray nozzle and peripheral jets; both conditions were found beneficial in the reduction of large agglomerates in the fluidized bed.

Morales M. (2013) developed a novel cold model to simulate the agglomeration process in Fluid Coking<sup>TM</sup>. The model consisted of Plexiglas (binder) dissolved in an acetone-pentane mixture. The model allowed the author to recover the total mass of agglomerates formed after injection, to measure their liquid content and in addition, to simulate more realistically the fast evaporation typical of Fluid Coking<sup>TM</sup>. In agreement with other authors (Aminu, et al., 2004) and (Gray, 2002), Morales concluded that agglomeration hinders liquid vaporization and so, in Fluid Coking, it would result in lower yields of desirable products. Also, the impact of the liquid properties and some operational conditions were evaluated by the author. Reduction of the total mass of agglomerates formed was found when the viscosity and the contact angle of the binder solution were lowered. Agglomeration reduction was also achieved by increasing the superficial gas velocity or the atomization gas flow rate, since the mixing of the solids within the bed is enhanced in the first scenario and the initial liquid distribution (smaller droplets at the tips of the nozzle) is enhanced in the second one. This model was tested in a pilot plant fluidized bed and the agglomerate size distribution obtained with the Plexiglas system matched the agglomerate size distribution obtained in a hydrodynamically similar pilot plant Fluid Coker. One drawback of this model is the complex procedure that is required to estimate the initial concentration of liquid in agglomerates (Soxhlet extraction); consequently, it could be estimated only in a small proportion

of the agglomerates. Also, nitrogen had to be used as fluidization gas making difficult to perform experiments at high fluidization velocities.

Mohagheghi Dar Ranji (2014) used a capacitance method to measure the liquid distribution in a fluidized bed. Varsol and coke particles were used to simulate the conditions in the Fluid Coking<sup>TM</sup> process under cold flow conditions. The capacitance of the bed increases with the amount of free liquid in the bed (the author defined free liquid as all the liquid that is not trapped in agglomerates). In this study, the injection pulse duration was investigated and it was found that an increment of the pulse duration in a stationary nozzle resulted in a reduction of the quality of the liquid distribution.

To fully understand the effect of different operating conditions on agglomerate formation and stability, it is necessary to be able to measure the agglomerate size distribution and the initial liquid concentration in agglomerates. Due to some limitations of the models described before, this was not always possible. Also, these limitations did not allow to study the effect of some operating conditions in the agglomerate size distribution and liquid content. For instance, high superficial gas velocity could be not used in experiments using the capacitance or the conductance method since the redistribution and evaporation of the liquid would occur really fast and the detection of the changes in the free moisture would be difficult. Also, the effect of high temperatures could not be evaluated since, in the case of the sugar solution the liquid content could not be estimated due to the caramelization of the sugar or due to safety reasons in the case of the Plexiglas solution. Moreover, the models were not flexible enough to study other cases like the liquid transfer due to particle collisions, effect of position of the spray nozzle, liquid loading, etc... None of the methods could be used to identify agglomerates formed with different nozzles or at different times.

Therefore, there is a need for an experimental model that can overcome all these limitations. This model could be used to study the dispersion of wet agglomerates in the bed, the dispersion of agglomerates formed at different times. It could also be used to study the transfer of liquid from wetted, individual particles to originally dry particles.

## 1.4 Research Objectives

The main objective of the present thesis work was to develop a new experimental model and associated measurement methods to reach a better understanding of agglomerate formation and stability in fluidized beds, and the effect of different variables on the process of formation and breakage. In order to address this main objective, the following steps were required:

- Develop a low temperature, water based, safe and realistic experimental model that could simulate the agglomerate formation and breakage in different industrial processes, but mainly focused on the Fluid Coking<sup>TM</sup> process. Show how the model could be adapted to various industrial systems by changing binder concentration, pH or initial bed temperature.
- Use the developed model to study the effect of bed temperature by changing the type of injection or the initial bed temperature.
- Use the developed model to study the impact of injection duration, at a constant liquid flow rate, on agglomerate formation and recoating.
- Determine the maximum extent of liquid spreading from wet to dry particles.

The present thesis work is part of a set of projects associated with NSERC/Syncrude/ExxonMobil Senior Industrial Research Chair in Fluid Coking Technologies. One of the main contributions of this thesis is the development of a convenient, versatile and accurate method to study liquid distribution in fluidized beds. This method is essential to the successful completion of the following projects:

- The effect of local bed hydrodynamics on liquid distribution. This will be achieved by changing the nozzle position, the fluidization velocity and the radial gas distribution.
- Independent measurements of the effects of bed temperature and liquid viscosity on agglomerate properties.
- The effects of interacting spray nozzles on liquid distribution.
- The effects of the relative motion between spray nozzle and fluidized solids on liquid distribution.

## Chapter 2

### 2. Methodology

#### 2.1 Experimental Set-up

##### 2.1.1 Equipment

A schematic diagram of the fluidized bed used in this study is presented in **Figure 2-1**.

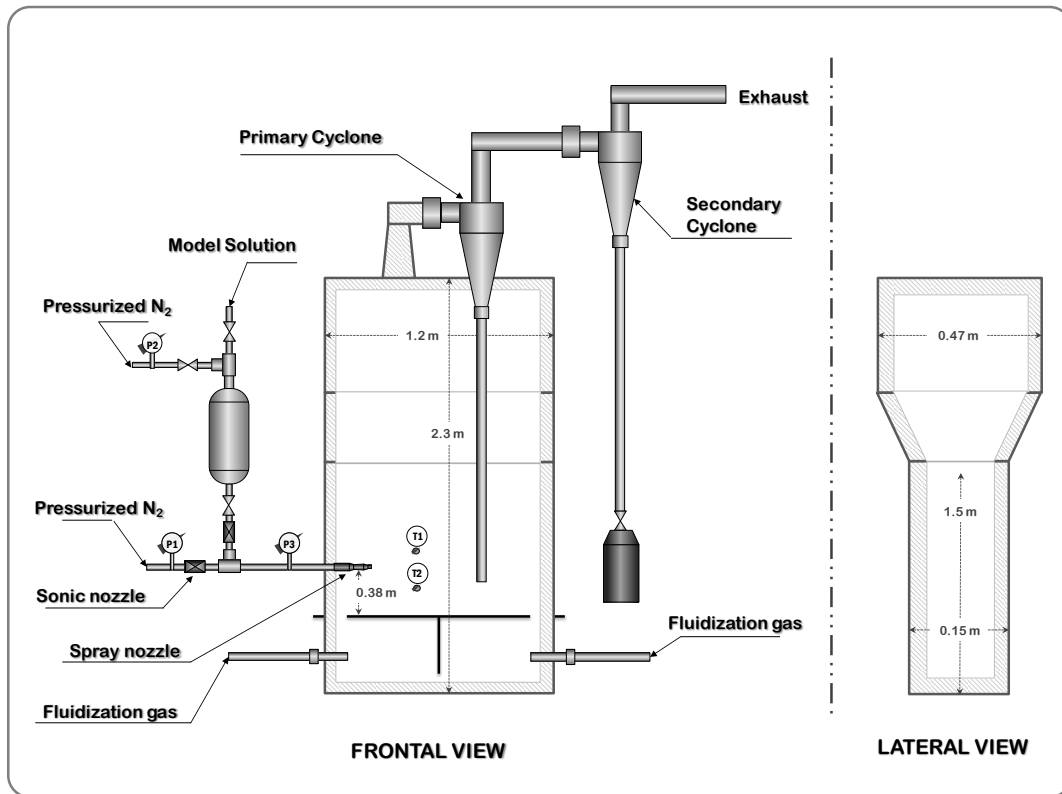


**Figure 2-1: Schematic of the Experimental Setup**

The total height of the bed was 2.3 m and at 1.5 m it had an expansion zone of 1.2 m by 0.47 m. The dimensions of its cross sectional area in the lower section were 1.2 m by 0.15 m. Air was used as a fluidization gas and a calibrated sonic bank of nozzles was used to control the mass flow rate.

For all the experiments, 150 kg of silica sand with a Sauter mean diameter of 190  $\mu\text{m}$  (**Figure 2-2**) and a particle density of 2650  $\text{kg}/\text{m}^3$  were used, resulting in a fixed bed height of 0.63 m. From a tank pressurized with nitrogen, a water based solution (described in the following section) was injected at room temperature at constant flow rate. Water and sand were chosen, since water wets the silica sand well, as bitumen wets coke in commercial Fluid Coker reactors (Prociw, 2014)

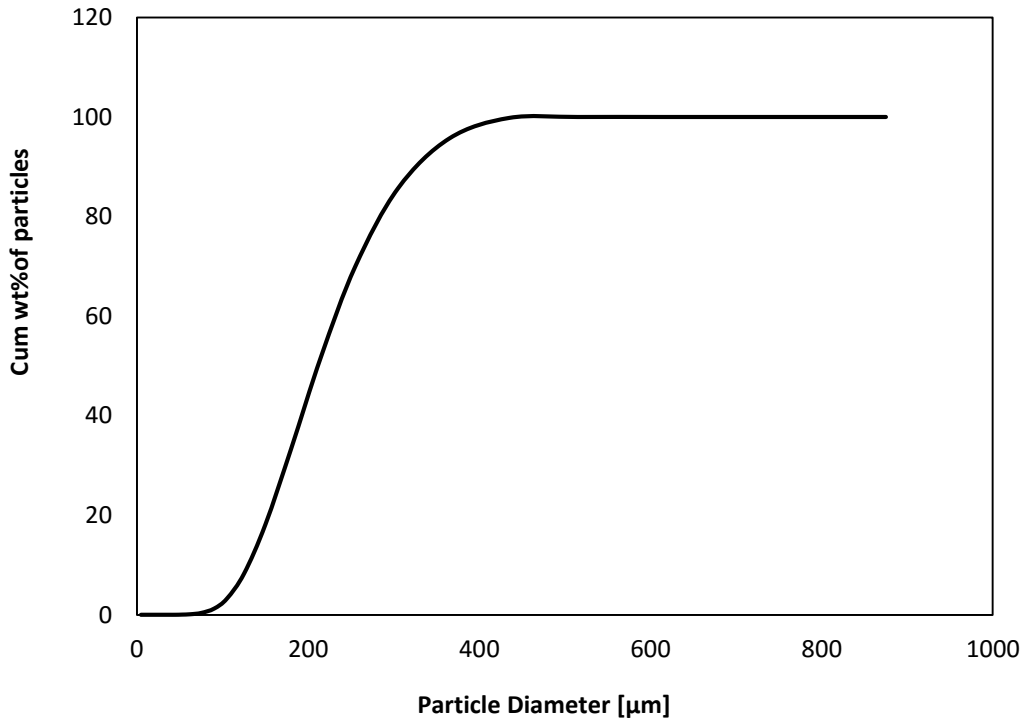


**Figure 2-2: Particle size distribution of the silica sand used in the experiments**

In most of the experiments (Chapter 3 and 4), the liquid was injected through a scaled down version of an industrial spray nozzle (TEB nozzle) with an internal tip diameter of 2.7 mm illustrated in **Figure 2-3** (Base, et al., 1999). Given the objectives for Chapter 5 (presented at the beginning of the chapter), a special spray nozzle that requires a high atomization gas to liquid mass ratio (GLR) was also used. This nozzle consisted of a straight cylindrical tube with an internal diameter of 3.6 mm.

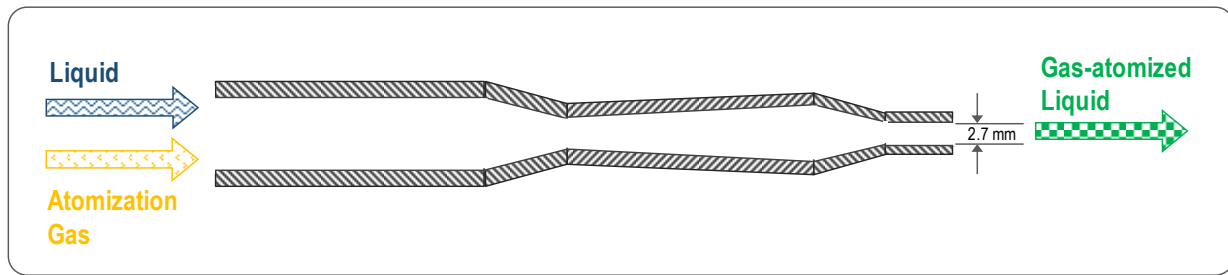


**Figure 2-3: Schematic of the TEB nozzle**

A Bilateral Flow Conditioner (BFC) pre-mixer located upstream the spray nozzle was used to mix the liquid and the atomization gas (nitrogen) (Farkhondehkavaki, 2012). In order to achieve the required Gas-to Liquid Ratio (GLR, wt/wt), pressure regulators and transducers were used to control the atomization and liquid tank pressures and a calibrated sonic orifice was installed to control the mass flow rate of the atomization gas.

Further details of the operating conditions for each experiment are given at the beginning of each chapter.

### 2.1.2 Liquid Solution

The liquid solution (binder solution) proposed in this new model is a mixture of Gum Arabic (GA), food dye (Blue No. 1, Yellow No. 5 or Red No. 40) and water. Since gum Arabic is a polysaccharide that carries a net negative charge (Yadong, et al., 2012), almost neutral or anionic dyes were selected to avoid interactions with the gum that could interfere with the estimation of the dye concentration (Flury & Flühler, 1994). Hydrochloric acid was added to adjust the viscosity of the binder solution. Water was selected as solvent since there is no risk of explosion with air; therefore, air can be used as a fluidization gas. The binder (GA) was chosen since it is completely soluble in water, non-toxic and stable up to approximately 200 °C (Imeson, 1997).

As mentioned before, the liquid solution was injected horizontally in the bed at a constant flow rate for a pre-determined injection time. The specific binder solution used in each experiment and its physical properties will be described at the beginning of each chapter.

## 2.2 Agglomerate Characterization

### 2.2.1 Determination of Agglomerate Size Distribution

Agglomerate size distribution analysis is important since heat transfer limitations are strongly related with the agglomerate size: the bigger the agglomerate the more the limitations. The procedure followed in this thesis is based on the one established by Morales M. (2013). After each liquid injection, all bed mass solids were recovered and classified in three groups:

- a. Macro-agglomerates: agglomerates recovered with a diameter  $d_{\text{aggl}} > 600 \mu\text{m}$
- b. Micro-agglomerates: agglomerates recovered with a diameter  $355 \mu\text{m} \leq d_{\text{aggl}} < 600 \mu\text{m}$
- c. Individual bed particles

The method to collect the agglomerates was different for macro and micro-agglomerates. For macro-agglomerates, since there were no initial bed particles with a diameter greater than  $600 \mu\text{m}$ , all the bed mass (150 kg) was sieved with the desired sieve sizes to recover agglomerates of various sizes. The sieve sizes used were:

$$\begin{aligned}d_{\text{aggl}} &\geq 9500 \mu\text{m} \\9500 \mu\text{m} &> d_{\text{aggl}} \geq 4000 \mu\text{m} \\4000 \mu\text{m} &> d_{\text{aggl}} \geq 2000 \mu\text{m} \\2000 \mu\text{m} &> d_{\text{aggl}} \geq 1400 \mu\text{m} \\1400 \mu\text{m} &> d_{\text{aggl}} \geq 850 \mu\text{m} \\850 \mu\text{m} &> d_{\text{aggl}} \geq 600 \mu\text{m}\end{aligned}$$

In the case of the micro-agglomerates, one should consider that there were individual bed particles with a diameter within the range size of the micro-agglomerates ( $355 \mu\text{m} \leq d_{\text{aggl}} < 600 \mu\text{m}$ ). Initial silica sand fines inside the micro-agglomerates could be used as a tracer to estimate the total mass of micro-agglomerates. The steps for this estimation were:

a. Recovery of Micro-agglomerates:

The bed mass that was left after the recovery of the macro-agglomerates was calculated as:

$$m_{<600\mu m} = m_{Bed} - m_M \quad 2-1$$

where  $m_{Bed}$  is the initial bed mass and  $m_M$  is the total mass of recovered macro-agglomerates. From  $m_{<600\mu m}$ , a representative sample ( $m_R$ ) was taken and sieved using the following sieve sizes:

$$\begin{aligned} 600 \mu\text{m} > d_p \geq 500 \mu\text{m} \\ 500 \mu\text{m} > d_p \geq 425 \mu\text{m} \\ 425 \mu\text{m} > d_p \geq 355 \mu\text{m} \end{aligned}$$

b. Determination of Dye in the Micro - Agglomerates

The mass of dye ( $m_d$ ) in the agglomerates was estimated using UV – spectroscopy. Agglomerates recovered in each sieve size cut were dissolved in enough water to ensure all the dye and the gum were dissolved (the dyes and the Gum Arabic used in the experiments are completely soluble in water) and that the values of absorbance would fall within between 0.1 - 1. The absorbance of the wash liquid was measured at the characteristic wavelength ( $\lambda_{max}$ ) of the dye colour used.

If one dye was used in the injection, the calibration curve of the corresponding colour was used to determine the concentration of dye in the solution. If several dyes were used, the system of equations described in Section 2.2.2.2 was used.

Once the mass of dye in the sample was estimated, the initial amount of liquid in the sample was calculated by mass balance since the initial mass of dye in the solution was known. Also, knowing the initial liquid in the sample and the gum concentration in the solution, the mass of dry gum ( $m_{GA}$ ) was calculated. Finally, the washed sand particles ( $m_{sand}$ ) were dried and weighed using a laboratory scale with an accuracy of 0.1 mg.



c. Determination of the Mass of Fine Particles in the agglomerates

A particle size distribution analysis of the sand particles dried in the previous step ( $m_{sand}$ ) and of a representative sample of the initial silica sand in the fluidized bed at the beginning of the experiment, was performed using a laser diffraction method (HELOS of Sympatec). With this analysis, the weight fractions of fines in the  $m_{sand}$  ( $x_f$ ) and in the initial silica sand ( $x_{fbed}$ ) could be determined.

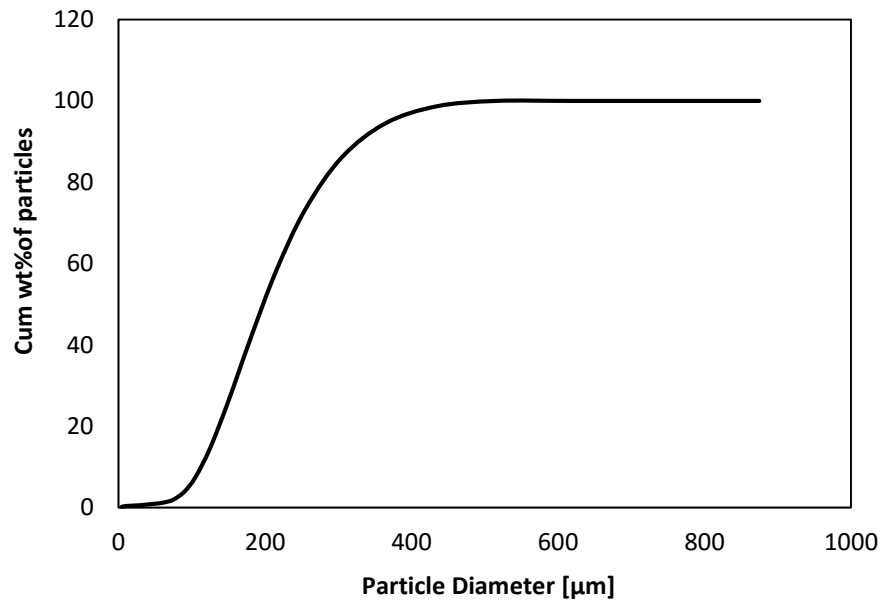


**Figure 2-4: Example of particle size distribution of a washed and dried sample for step 3 in the micro-agglomerates determination procedure**

For each sieve size, fines were all the individual particles that would have passed the lower limit of the size range ( $d_{pL}$ ), if they had not been agglomerated. Assuming that there was no segregation in the fines when trapped in the agglomerates, the size distribution of the particles trapped in the agglomerates was the same as the size distribution of the bed particles, so the mass of particles trapped in the agglomerates ( $m_p$ ) was calculated as:

$$m_p = m_{sand} \times \frac{x_f}{x_{fbed}} \quad 2-2$$

Hence, the mass of micro-agglomerates in the sample ( $m_{\mu aggl,Ri}$ ) could be calculated for each sieve size, considering that the agglomerates were formed of sand, dye and gum. Therefore, the mass of agglomerates in the sample could be defined as:

$$m_{\mu aggl,Ri} = m_p + m_{GA} + m_d \quad 2-3$$

Finally, knowing the mass of micro-agglomerates in the sample for each sieve size, the total mass of micro-agglomerates ( $m_{\mu aggl,i}$ ) in the bed mass per sieve size ( $d_{pH} > d_p \geq d_{pL}$ ) was calculated as:

$$m_{\mu aggl,i} = m_{\mu aggl,Ri} \times \frac{m_{<600\mu m}}{m_R} \quad 2-4$$

## 2.2.2 Estimation of Liquid-to-Solid Ratio

To calculate the liquid trapped in the recovered agglomerates, the dyes added to the gum solution were used as a tracer of the liquid. In the experiments for the evaluation of pulse duration (Chapter 4), different dyes were used in order to be able to identify from which pulse the liquid was coming. With the different procedures described below, the concentration of dye in the agglomerates was estimated and thus the amount of liquid trapped in agglomerates was also estimated by mass balance, since the initial concentration of dye in the solution was known. Also, knowing the mass of liquid, the mass of sand in the agglomerates could be estimated and thus, the liquid-to-solid ratio.

### 2.2.2.1 Dye Concentration in Agglomerates when Injecting a Single Colour

The procedure to estimate the dye concentration was the same for macro-agglomerates and micro-agglomerates and involved the following steps:

1. The mass recovered for each sieve size was weighed using a scale with an accuracy of 0.1 mg.

2. The agglomerates were dissolved in water using an approximate weight ratio of water / agglomerates = 3:1. This quantity of water was required to ensure that all the dye was in solution and that its absorbance would fall within 0.1 – 1.
3. The solution was centrifuged for 10 minutes at 4500 rpm (Thermo Scientific Sorvall Legend X1 Centrifuge).
4. The solution absorbance was measured at the characteristic wavelength corresponding to the maximum absorbance of the dye used ( $\lambda_{\max}$ ).
5. The calibration curve for the dye was used to determine the concentration of dye in the solution.

**Table 2-1: Wavelength of maximum absorbance ( $\lambda_{\max}$ ) for the different dyes**

<b>Colour</b>	<b><math>\lambda_{\max}</math> [nm]</b>
Blue No. 1	630
Yellow No. 5	427
Red No. 40	503

The samples used to build the calibration were prepared to simulate the agglomerates that were formed in the bed after injecting the liquid solution:

1. Approximately 10 g of sand were weighed.
2. A known quantity of liquid solution was added to the sand.
3. The sample (sand + binder solution) was dried in a moisture analyzer (Mettler Toledo HB43 Halogen) at 130°C (maximum bed temperature used in injection experiments), until all liquid had disappeared.
4. The dry sample was mixed with 30 g of water to dissolve all its dye.
5. The solution was centrifuged for 10 minutes at 4500 rpm (Thermo Scientific Sorvall Legend X1 Centrifuge) to remove all the sand particles from the liquid solution.
6. A sand-free sample of the liquid solution was taken.
7. The sample absorbance was measured at the characteristic wavelength of the dye used ( $\lambda_{\max}$ ) with a spectrophotometer (Thermo Scientific Evolution 220 UV-Visible Spectrophotometer).

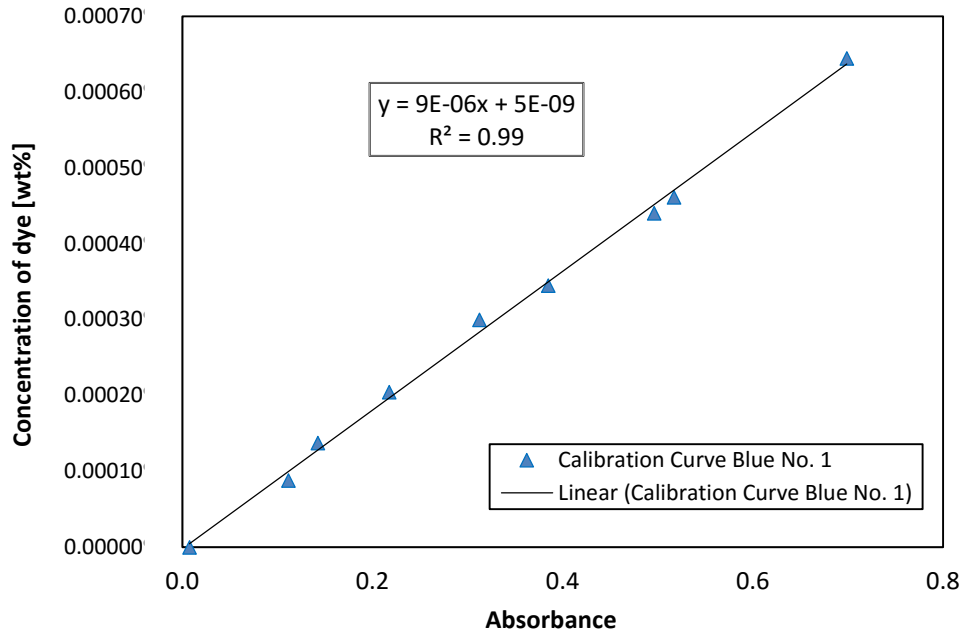


**Figure 2-5: Calibration Curve for Blue No. 1,  $\lambda_{\text{max}} = 630 \text{ nm}$**

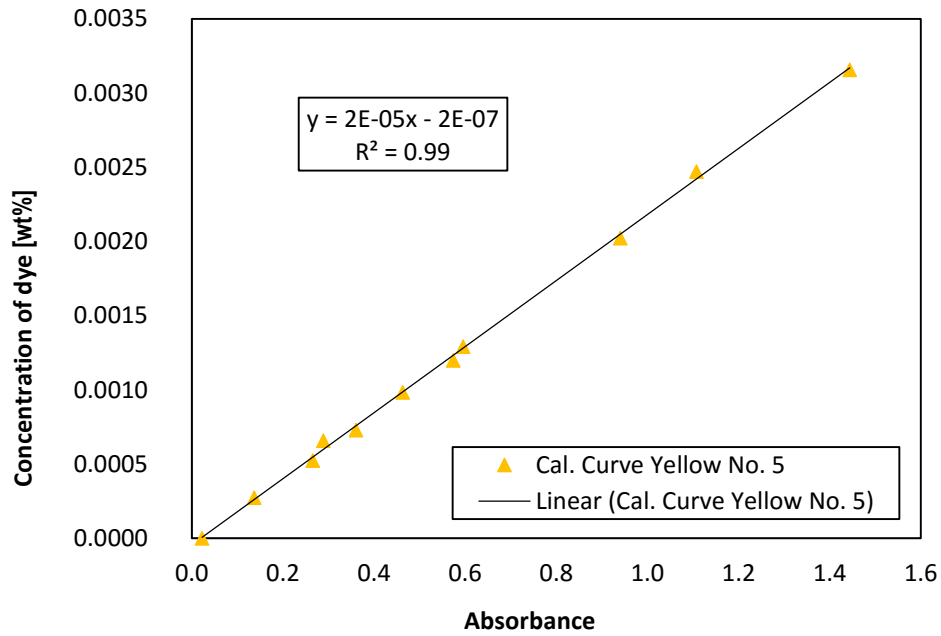


**Figure 2-6: Calibration Curve for Yellow No. 5,  $\lambda_{\text{max}} = 427 \text{ nm}$**

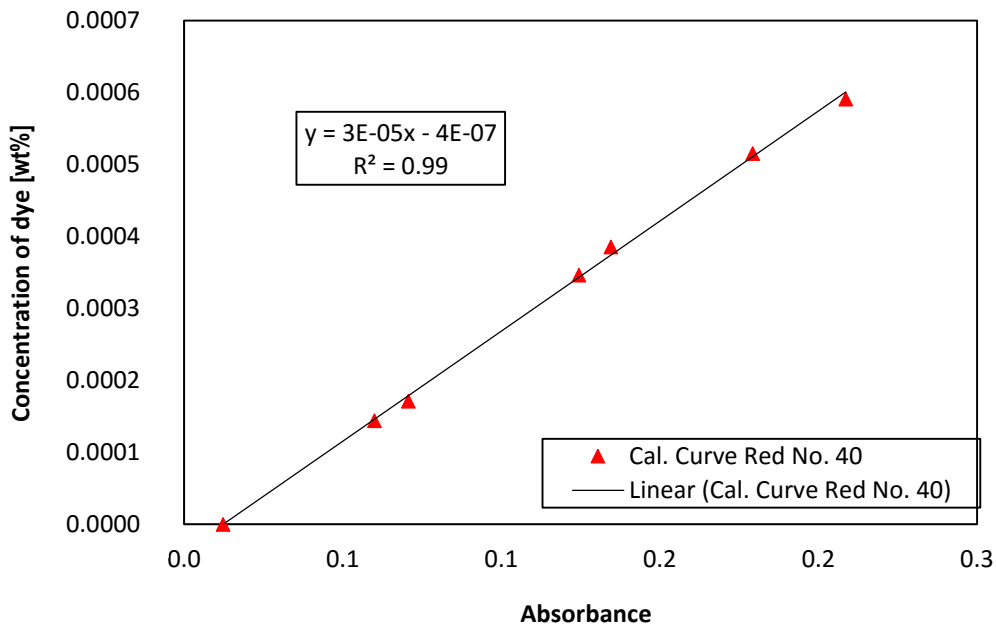


**Figure 2-7: Calibration Curve for Red No. 40,  $\lambda_{\text{max}} = 503 \text{ nm}$**

#### 2.2.2.2 Dye Concentration in Agglomerates when Injecting more than One Dye

Two mixtures of dyes were used in the injection experiments: blue + yellow and blue + yellow + red. To estimate the dye concentrations when two or three dyes were injected, the agglomerates for each sieve size were mixed with water and the wash liquid was centrifuged as described in the above section. However, since there was a mixture of dyes, interactions between different dyes were taken into account to determine the accurate dye concentrations.

##### a. System of Equations for Blue + Yellow Mixture

The absorbance of the binary mixture consisted of two linear equations that consider the interactions between the two colours. Absorbance measurements were performed at two wavelengths: the “blue wavelength”, i.e. the wavelength of maximum absorbance for the blue dye, and the “yellow wavelength”, i.e. the wavelength of maximum absorbance for the yellow dye (see **Table 2-1**).

**Equation (2-5)** includes the three contributions to the measured absorbance at the blue wavelength:

1.  $A_{blue}^0$  is the background absorbance at the blue wavelength when no dye is present in the binder solution.
2. The absorbance from the blue dye, which is proportional to the concentration of blue dye (**Figure 2-5**).
3. The absorbance from any yellow dye present in the sample, which is proportional to the concentration of yellow dye.

$$A_{(b+y)}^{blue} = A_{blue}^0 + A_{blue}^{blue} + A_{yellow}^{blue} = A_{blue}^0 + (\gamma_{blue}^{blue} \times C_{blue}) + (\gamma_{yellow}^{blue} \times C_{yellow}) \quad 2-5$$

Similarly, **Equation (2-6)** refers to the absorbance of the mixture at the yellow wavelength:

$$A_{(b+y)}^{yellow} = A_{yellow}^0 + A_{blue}^{yellow} + A_{yellow}^{yellow} = A_{yellow}^0 + (\gamma_{blue}^{yellow} \times C_{blue}) + (\gamma_{yellow}^{yellow} \times C_{yellow}) \quad 2-6$$

Different mixtures with known concentrations of blue and yellow were prepared and analyzed to find the values of the calibration factors ( $\gamma$ ) using the SOLVER function of Excel™ that minimized the sum of the square errors between the expected colour concentration and the calculated colour concentration. **Table 2-2** lists the calibration factors found for this mixture where x refers to the colour listed in the left column.

**Table 2-2: Calibration factors for the system equation for Blue + Yellow mixtures**

<i>Colour</i>	$A_x^0$	$\gamma_{x,blue}$	$\gamma_{x,yellow}$
<i>Blue</i>	0.0074	0.1081	0.0003
<i>Yellow</i>	0.0222	0.0069	0.0449

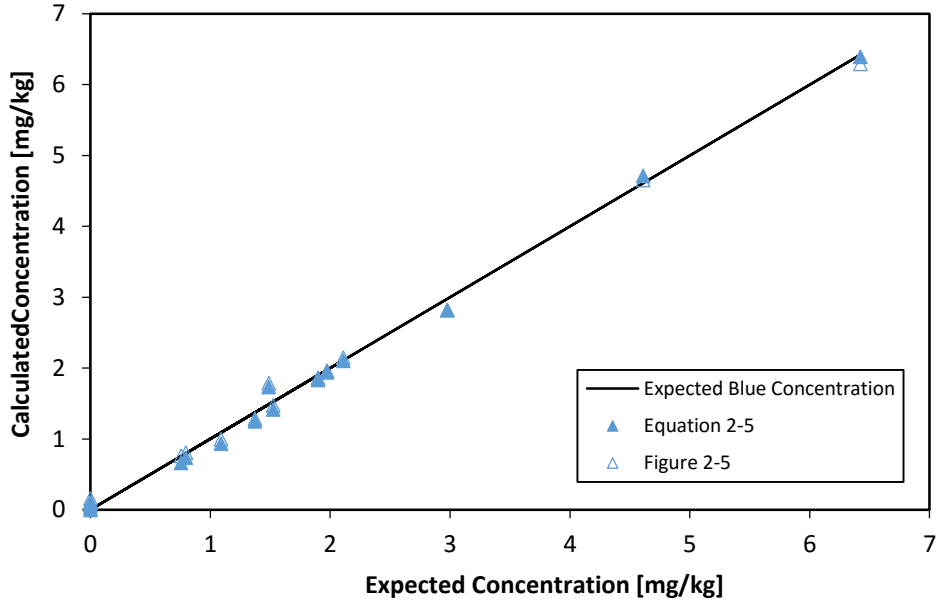


**Figure 2-8: Calculated concentrations for blue in blue + yellow mixtures using either the full model (Equation 2-5) which accounts for interactions, or the calibration curve of Figure 2-5, which neglects interactions.**

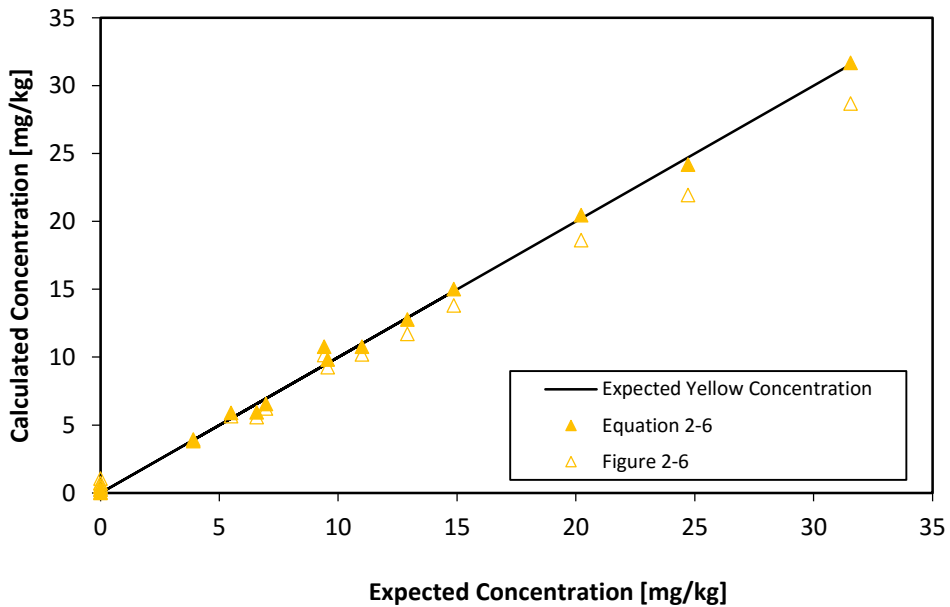


**Figure 2-9: Calculated concentrations for yellow in blue + yellow mixtures using either the full model (Equation 2-6) which accounts for interactions, or the calibration curve of Figure 2-6, which neglects interactions**

b. System of Equations for Blue + Yellow + Red mixture

**Equation 2-7** includes the four contributions to the measured absorbance at the blue wavelength:

1.  $A_{blue}^0$  is the background absorbance at the blue wavelength when no dye is present in the binder solution.
2. The absorbance from the blue dye, which is proportional to the concentration of blue dye (**Figure 2-5**).
3. The absorbance from any yellow dye present in the sample, which is proportional to the concentration of yellow dye.
4. The absorbance from any red dye present in the sample, which is proportional to the concentration of red dye.

$$A_{(b+y+r)}^{blue} = A_{blue}^{blue} + A_{yellow}^{blue} + A_{red}^{blue} = (\gamma_{blue}^{blue} \times C_{blue}) + (\gamma_{yellow}^{blue} \times C_{yellow}) + (\gamma_{red}^{blue} \times C_{red}) \quad 2-7$$

Similarly, **Equations 2-8** and **2-9** refer to the absorbance of the mixture at the yellow and red wavelengths, respectively:

$$A_{(b+y+r)}^{yellow} = A_{blue}^{yellow} + A_{yellow}^{yellow} + A_{red}^{yellow} = (\gamma_{blue}^{yellow} \times C_{blue}) + (\gamma_{yellow}^{yellow} \times C_{yellow}) + (\gamma_{red}^{yellow} \times C_{red}) \quad 2-8$$

$$A_{(b+y+r)}^{red} = A_{blue}^{red} + A_{yellow}^{red} + A_{red}^{red} = (\gamma_{blue}^{red} \times C_{blue}) + (\gamma_{yellow}^{red} \times C_{yellow}) + (\gamma_{red}^{red} \times C_{red}) \quad 2-9$$

In the same way as the previous mixture, different mixtures with known concentrations of blue, yellow and red were prepared and analyzed to find the values of the calibration factors ( $\gamma$ ).

**Table 2-3: Calibration factors for Blue + Yellow + Red mixtures**

<i>Colour</i>	$A_x^0$	$\gamma_{x,b}$	$\gamma_{x,y}$	$\gamma_{x,r}$
<i>Blue</i>	0.0074	0.1095	0.0005	0.0010
<i>Yellow</i>	0.0222	0.0081	0.0450	0.0090
<i>Red</i>	0.0123	-0.0020	0.0014	0.0420



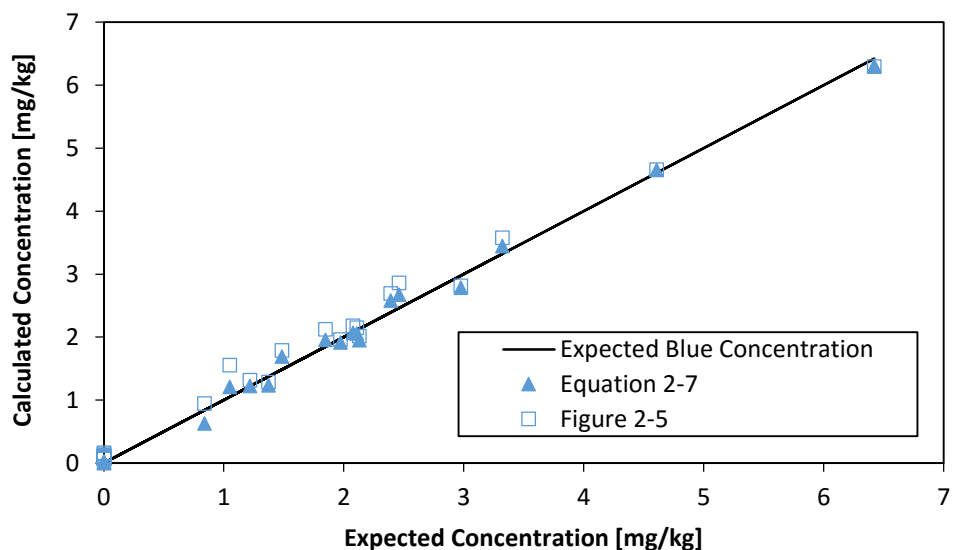


**Figure 2-10: Calculated concentrations for blue in blue + yellow + red mixtures using either the full model (Equation 2-7) which accounts for interactions, or the calibration curve of Figure 2-5, which neglects interactions**

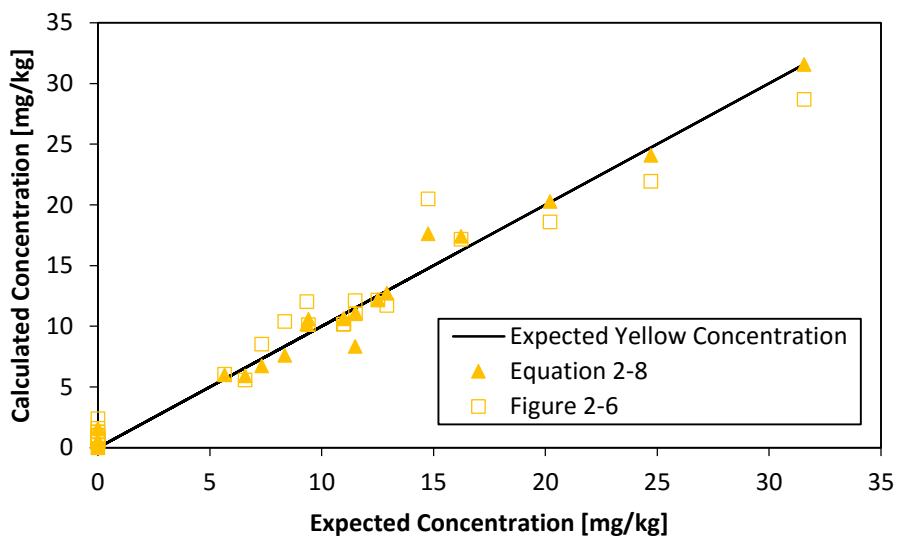


**Figure 2-11: Calculated concentrations for yellow in blue + yellow + red mixtures using either the full model (Equation 2-8) which accounts for interactions, or the calibration curve of Figure 2-6, which neglects interactions**

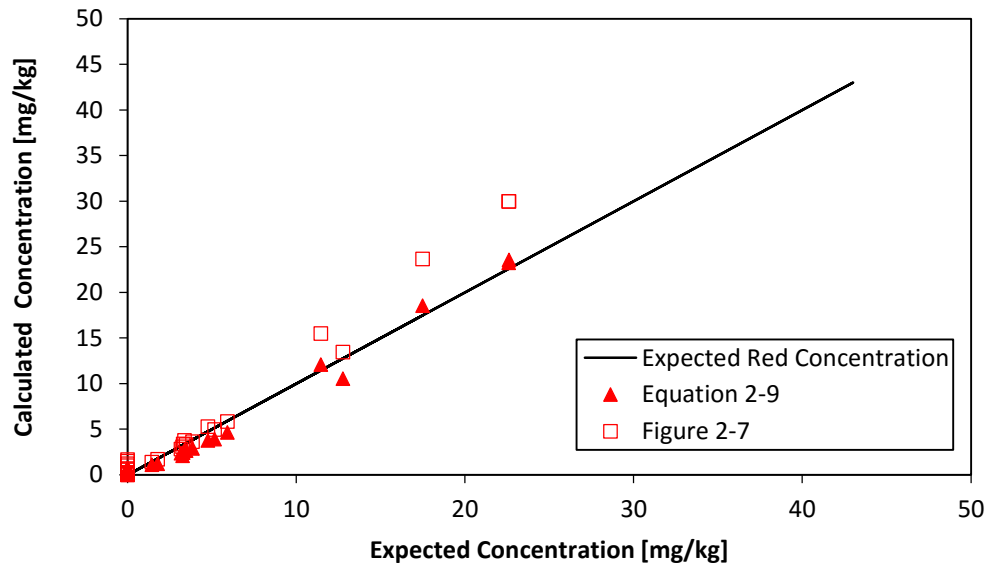


**Figure 2-12: Calculated concentrations for red in blue + yellow + red mixtures using either the full model (Equation 2-9) which accounts for interactions, or the calibration curve of Figure 2-7, which neglects interactions**

### 2.3 Colour distribution in individual agglomerates

As mentioned before, in the experiments of the pulse duration effect different colours were used to identify from which pulse the liquid trapped in agglomerate was coming from. In addition to this, the use of different dyes allowed to study the colour distribution in individual agglomerates and thus identify possible recoating. A ternary diagram (**Figure 2-13**) was used to visualize the colour distribution within individual agglomerates. After the sieving process of the total bed mass (150 kg) and recovery of all macro-agglomerates, forty individual agglomerates from the three biggest sieve sizes (i.e.  $d_{\text{aggl}} \geq 9500 \mu\text{m}$ ,  $9500 \mu\text{m} > d_{\text{aggl}} \geq 4000 \mu\text{m}$ , and  $4000 \mu\text{m} > d_{\text{aggl}} \geq 2000 \mu\text{m}$ ) were taken randomly to be analyzed. To perform the random sampling, all agglomerates recovered for a given size were passed through a splitter until around 40 agglomerates were left. The colour composition of each sample was measured using the methods described in the above section.

Since the initial mass of the dye was not the same for each one of the colours used, the following dimensionless normalized concentrations were used:

$$C_{Blue}^* = \frac{\text{mass of Blue measured in the agglomerate}}{\text{initial mass of Blue injected}} \quad 2-10$$

$$C_{Yellow}^* = \frac{\text{mass of Yellow measured in the agglomerate}}{\text{initial mass of Yellow injected}} \quad 2-11$$

$$C_{Red}^* = \frac{\text{mass of Red measured in the agglomerate}}{\text{initial mass of Red injected}} \quad 2-12$$

Then, the total normalized mass of dye was calculated as:

$$C_{Total}^* = C_{Blue}^* + C_{Yellow}^* + C_{Red}^* \quad 2-13$$

Finally, the mass proportion of each was calculated and plotted in the ternary diagram.

$$B = \frac{C_{Blue}^*}{C_{Total}^*} \quad Y = \frac{C_{Yellow}^*}{C_{Total}^*} \quad R = \frac{C_{Red}^*}{C_{Total}^*} \quad 2-14$$

In the ternary plot, the horizontal lines correspond to the red concentration, increasing from the bottom of the triangle to the top (100% Red) and the percentage scale at the right of the triangle represents the concentration of the red in the agglomerate. In the same way, if the left corner of the triangle is considered (100% Blue), the right side of the triangle becomes the baseline of it and all the parallel lines to this side represent blue concentrations which increase from the “new” bottom of the triangle to the “new” top. Finally, all parallel lines of the opposite side of the right corner (100% Yellow) correspond to yellow concentration and the scale located at the bottom of the triangle represents concentration values increasing from left to right. For example, the composition of the point shown in the diagram is: 10% Red, 70% Blue and 20% Yellow. Therefore, any point located on any side of the triangle will represent a binary mixture.

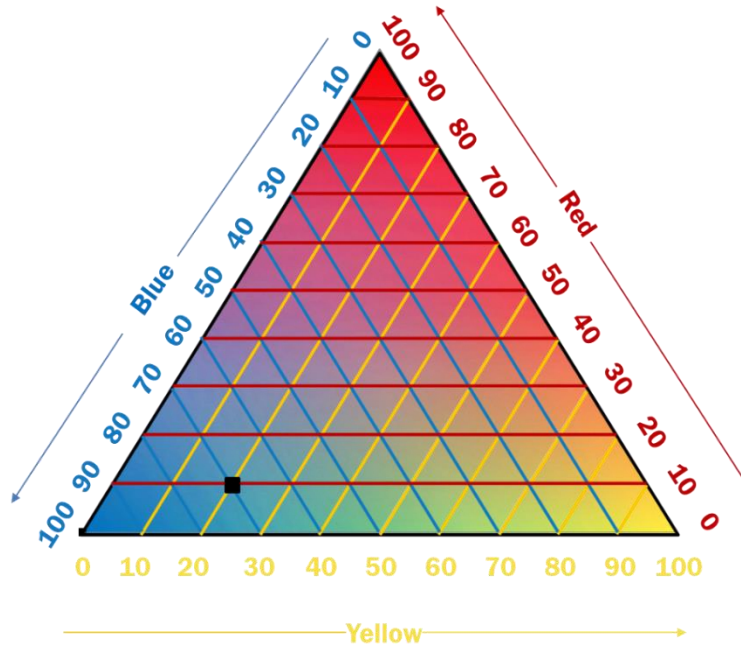


**Figure 2-13: Ternary plot for colour mixing representation**

## 2.4 Estimation of time for a Jet Expansion

When liquid is being injected in a gas-solid fluidized beds, the liquid forms a jet and the projection of this jet is considered as it is shown in **Figure 2-14**. The time for a jet expansion from  $L_{min}$  to  $L_{max}$  is known as cycle time ( $\Delta t$ ). An adaptation to the model developed by Mohagheghi Dar Ranji, 2014 was made to calculate the time in which a jet expansion occurs.

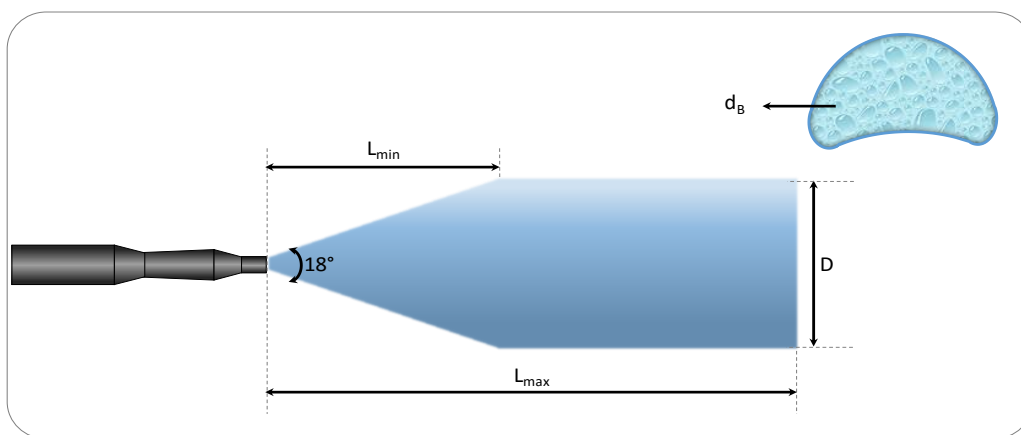


**Figure 2-14: Schematic representation of a jet expansion**

The calculation of the parameters associated with each cycle involved the following main steps:

1. Estimation of the minimum jet penetration length ( $L_{min}$ ) and the volume of the bubble released from the jet tip ( $v_{Be}$ ):

The average jet penetration  $L_{jet}$  was calculated using the correlation for gas jets from Benjelloun (1995) as adapted to gas-liquid jets by Ariyapadi et al. (2003). Then, the maximum jet penetration length ( $L_{max}$ ) was calculated using the equation reported by Xuereb, et al., 1991:

$$L_{max} = L_{jet} \times 1.23 \quad 2-15$$

If the section of the jet cavity between  $L_{min}$  and  $L_{max}$  is assumed to be cylindrical, as illustrated in **Figure 2-14**, then the average jet length  $L_{jet}$  is the arithmetic average of  $L_{min}$  and  $L_{max}$  and:

$$L_{min} = \frac{L_{jet}}{1.3} \quad 2-16$$

The volume of the detached bubbles can be defined as:

$$v_{Be} = \frac{\pi}{6} d_{Be}^3 \quad 2-17$$

Assuming that the angle of the projection of the jet is  $18^\circ$  (Mohagheghi Dar Ranji, 2014), one could calculate the diameter of the jet cylindrical part (**Figure 2-14**) ( $D$ ) as:

$$\theta = \tan 9^\circ = \frac{D - d_N}{2 \times L_{min}} \quad 2-18$$

$$D = d_N + 2\theta L_{min}$$

The volume of the detached bubbles was obtained from a volume balance, using **Equation 2-19**:

$$v_{Be} = \frac{\pi}{4} D^2 \times (L_{max} - L_{min}) \quad 2-19$$

Combining equations 2-15 to 2-19 yields:

$$d_{be} = \frac{L_{jet}}{2.8975} \quad 2-20$$

This equation is nearly identical to the empirical correlation proposed by (Xuereb, et al., 1991):

$$d_{be} = \frac{L_{jet}}{2.88} \quad 2-21$$

## 2. Estimation of the cycle time from $L_{min}$ to $L_{max}$

Once the maximum and the minimum jet penetration were calculated using the procedure described above, the time for a jet expansion could be defined as:

$$\frac{\pi}{4} D^2 (L_{max} - L_{min}) = Q_g \times \Delta t \quad 2-22$$

where  $\Delta t$  is the time for a jet expansion from  $L_{min}$  to  $L_{max}$ . The total gas flow into the jet cavity ( $Q_g$ ) includes the atomization gas ( $Q_{g_a}$ ) and the gas that is in the bubbles that are captured by the expanding jet cavity ( $Q_{c_B}$ ) (**Equation 2-23**):

$$Q_g = Q_{g_a} + Q_{c_B} \quad 2-23$$

However, the total gas flow into the jet cavity changes with time as the jet cavity expands, since the gas that is being captured by the bubbles changes. Then, that  $Q_{c_B}$  can be defined as:

$$Q_{c_B} = D(L - L_{min}) \times (V_g - U_{mf}) \quad 2-24$$

**Equation 2-24** assumes that:

- a. There is a uniform superficial gas velocity ( $V_g$ ) profile along the jet cavity.
- b. Only the cylindrical part of the jet cavity, which is past  $L_{min}$  (**Figure 2-14**) captures bubbles.

Then, **Equation 2-22** can be written as:

$$\frac{\pi}{4}D^2 dL = [D(L - L_{min}) \times (V_g - u_{mf}) + Q_a]dt \quad 2-25$$

Defining:

$$\varphi = L - L_{min} + \frac{Q_a}{(V_g - u_{mf})D} \quad 2-26$$

with:

$$d\varphi = dL$$

After the corresponding integration, the expansion time was calculated as:

$$t_{exp} = \frac{\pi D}{4(V_g - u_{mf})} \times \ln \frac{\varphi_{max}}{\varphi_{min}} \quad 2-27$$

## 2.5 Estimation of Liquid Concentration in Solids after End of Jet Expansion (Small Number of Jet Expansions)

At steady state, the concentration of liquid in wetted solids can be defined as:

$$c = \frac{L}{S} \quad 2-28$$

where S is the mass of solids wetted in one jet expansion and L is the mass of liquid wetting the solids in one jet expansion. The mass of solids that is located in the wake of the bubbles that are released from the jet is:

$$f_w \frac{\pi}{6} d_{Be}^3 \rho_{mf} = S_R \quad 2-29$$

The mass of solids wetted in one jet expansion can be assumed to be equal to the sum of the mass of bed solids displaced by one jet expansion and the total mass of solids in the wakes of the captured bubbles:

$$S = \rho_{mf} \times \frac{\pi}{4} \times D^2 (L_{max} - L_{min}) + \rho_{mf} \times f_w (v_{Be} - Q_a \times t_{exp}) \quad 2-30$$

Given a liquid flow rate  $F_L$ , the amount of liquid in every new expansion is:

$$L = t_{exp} \times F_L \quad 2-31$$

After the first expansion, the liquid balance can be defined as:

$$c_1 = \frac{L}{S} \quad 2-32$$

Therefore, the concentration of liquid in the solids immediately after the release of the bubble from the jet tip, after the first expansion, can be calculated as:

$$c_2 = c_1 \left(1 - \frac{S_R}{S}\right) + \frac{L}{S} \quad 2-33$$

Then, if the above equation is considered for expansion number  $n$ , the amount of liquid after the expansion can be expressed as:

$$c_n = c_{n-1} \left(1 - \frac{S_R}{S}\right) + \frac{L}{S} \quad 2-34$$

## 2.6 Estimation of fraction of agglomerates (from earlier injections) entering the jet cavity with bubbles

Knowing that the gas entering into the jet cavity should be equal to the gas exiting the jet, one can express the gas balance as:

$$(F_{ga} + F_{gB})t_{exp} = \rho_g \times v_{Be} \quad 2-35$$



where  $F_{gB}$  is the gas mass flow rate coming into the jet with the bubbles and  $F_{ga}$  is the gas mass flow coming into the jet from the atomization gas. If  $f_w$  is defined as the fraction of gas bubble volume, the mass flow rate of solids entering the jet cavity in the wakes of the bubbles can be obtained as:

$$F_{sB} = \left[ f_w \times \frac{\rho_{mf}}{\rho_g} \right] \times F_{gB} \quad 2-36$$

Then, for a complete jet expansion, the mass of solids entering the jet cavity with the bubbles is:

$$s_B = F_{sB} \times t_{exp} \quad 2-37$$

After the first injection, the agglomerates formed with concentration of first dyed liquid ( $c_1$ ) segregate near the bottom of the bed. After the second injection, the solids that are being released in the bubbles will have as concentration:

$$c_2 = \frac{L}{s_R} \quad 2-38$$

The released solids  $s_R$  contain individual bed particles and agglomerates that formed after the first injection. If  $\alpha$  is the fraction of agglomerates in the solids that are in the wakes of the bubbles captured by the jet cavity, one can define the mass of agglomerates and individual particles carried by bubbles as:

$$\text{Mass of agglomerates in bubbles} = s_B \times \alpha \quad 2-39$$

$$\text{Mass of individual particles in bubbles} = s_B(1 - \alpha) \quad 2-40$$

The total mass of individual particles that are in the wakes of the bubbles that are released from the jet tip is the sum of the individual particles coming from the wakes of the bubbles captured by the jet cavity and the individual particles that are being displaced by the expansion of the jet cavity. Then,

$$\text{Total mass of individual particles in released wakes} = s_R - \alpha s_B \quad 2-41$$

The relationships between the two concentrations can be defined as:

$$\frac{c_1}{c_2} = \frac{\alpha \times s_B}{s_R - \alpha s_B} \quad 2-42$$

Then, from **Equation 2-42**, the concentration of agglomerates being carried in the wake bubbles can be calculated as:

$$\alpha = \frac{s_R}{s_B \left( \frac{c_2}{c_1} + 1 \right)} \quad 2-43$$

## 2.7 Liquid Spreading Estimation

### 2.7.1 Digital Image Analysis

The study of the liquid spreading required the following new method. Subsequent to the sieving process to collect micro-agglomerates (i.e. particles  $600 \mu\text{m} > d_p \geq 355 \mu\text{m}$ ), the remaining sand (i.e.  $d_p < 355 \mu\text{m}$ ) was sieved using the following size cuts:

$$355 \mu\text{m} > d_p \geq 250 \mu\text{m}$$

$$200 > d_p \geq 125 \mu\text{m}$$

$$125 > d_p \geq 75 \mu\text{m}$$

Twenty samples of each sieve size cut were taken randomly for image analysis with a microscope (ZEISS Stemi 305 Stereomicroscope) using a 1.5x lens. To perform the random sampling, all sand obtained for a given size was passed through a splitter until 20 samples of approximately 1 g were obtained.

A script written in Python based on the scikit-image library (a collection of algorithms that facilitates image processing) was used to count the total number of particles in each microscope image. The program detected the contours of the particles using the differences between the

colours of the pixels in a given region. The pixels of the images with red or green intensity  $> 30$  and Blue  $< 100$  were converted to white to reduce background image noise and, thus, facilitate the identification of the particles (**Figure 2-15**). This, however, did not affect particle counting (setting image) as the script implemented a pre-processing step of thresholding<sup>1</sup> using Otsu's method (Hoover, et al., 1996) (Jia, et al., 2014) and then labels regions connected with the same value. As a consequence, any reduction in noise background would result in better identification. It is important to notice that other pixels were not modified, allowing a better segmentation in particles that overlap in the image.

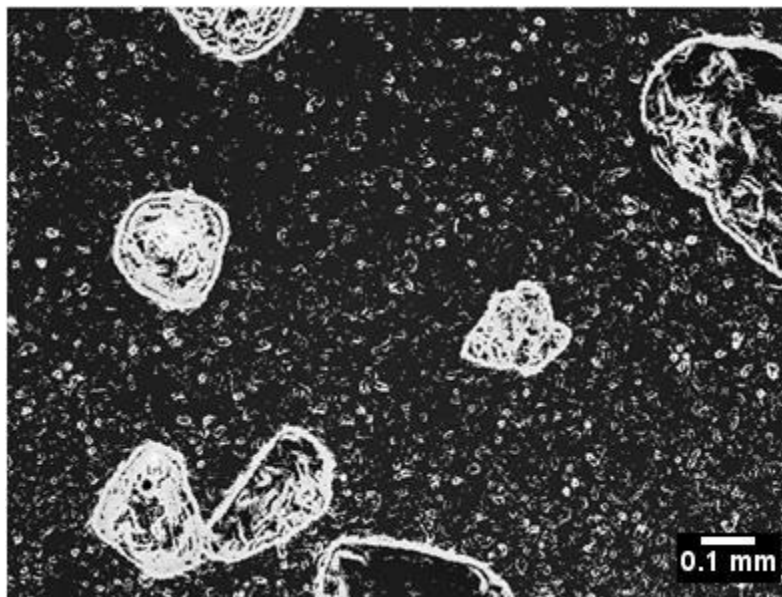


**Figure 2-15: Example of picture used for total particles counting after pre-processing**

After counting the total number of particles, dyed blue particles were identified using the intensity of blue in the original image (RGB). The pixel method was chosen since the interpretation of intensities and/or colours by humans can be very subjective. However, as the program could be very sensitive and identify more than one blue dot on the same particle, a subsequent check was performed to address this issue. To facilitate final verification by the human operator, the program inserted a blue circle over all blue tinted points identified on top of the original image (**Figure 2-16**).

---

<sup>1</sup> Creating a simplified binary image, containing only pure black or white

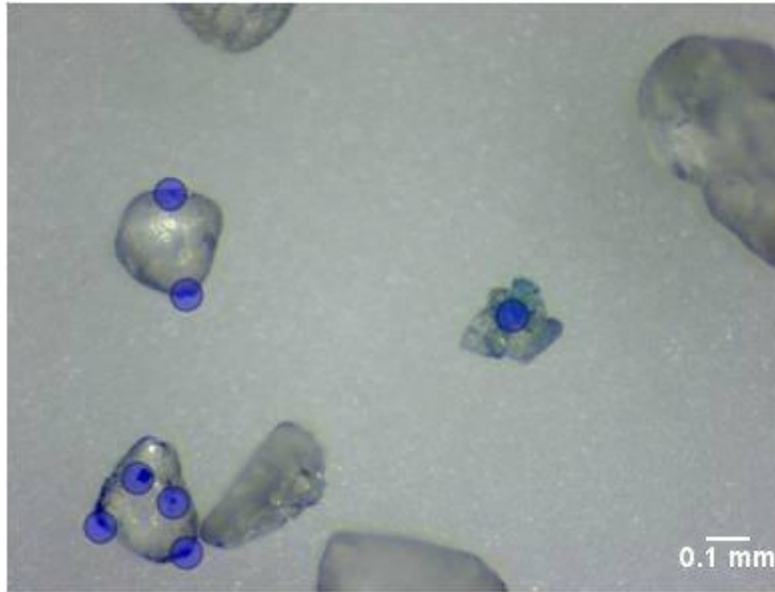


**Figure 2-16: Example of picture used for blue dyed particles counting**

### 2.7.2 Statistical Analysis of Liquid Spreading in Bed Particles

The fraction of blue particles was calculated in each sample and thus the mean of dyed particles for each sieve size for each injection experiment. Two statistical analyses were used to determine whether there was liquid transferring from wet to dry particles and whether it was promoted by changes in operating conditions (fluidization velocity).

To analyze the differences of liquid spreading (fraction of blue dyed particles) within the same experiment a *One-Way Analysis of Variance (ANOVA)* was used. The *ANOVA* allows testing the difference between multiple populations (more than two) and it analyzes the total variation in the groups (i.e. the variation of the fraction within the same sieve size and the other sieves sieve sizes). The following assumptions must be satisfied to apply this technique (Chambers & Hastie, 1991):

- All observations are independent of each other.
- All observations are randomly selected.
- The distribution of each set of observations is approx. normal.
- The variances of the set of observations are close to each other.

When analysing the spreading in two different experiments, a *Two – Sample T Test* was performed. Since the experiments were independent, the null hypothesis assumes that for a random sampling, there will not be statistical differences between the two experiments. Therefore, with the t-test one assessed whether the two means from the injection experiments were not equal, so that the null hypothesis was rejected. Thus, the fractions of particles means from each experiment significantly differed and the difference was due to the operating condition that was changed (Chambers & Hastie, 1991).

## Chapter 3

### **3. Development of an experimental low temperature model for the study of agglomerate formation and stability in fluidized beds**

#### 3.1 Introduction

As previously discussed, injection of liquid in gas-solid fluidized beds is widely used in different industrial processes such as FCC, granulation, polymerization and Fluid Coking<sup>TM</sup>. In all of them, good distribution of the liquid phase is essential for the consistency of product quality and in general, for the efficiency of the overall process. It is important to notice that agglomeration may or may not be desired, depending on subsequent processing stages or final product characteristics. For instance, agglomeration is desired when particle enlargement is required in the final product, or to improve the in-process product handling (Parikh, 2005). However, in other process such as Fluid Coking<sup>TM</sup>, the presence of agglomerates cause detrimental consequences on reactor operability and yield of valuable products (Knapper, et al., 2003). The quality of the liquid distribution depends greatly, among others, on different operating conditions, such as fluidization velocity and bed temperature. Considering the important impact of the agglomerates on the efficiency of the overall process, a better understanding of the agglomeration process, including formation and stability, is needed.

This chapter describes a low temperature model that contributes to a further understanding of the processes of agglomerate formation and stability in gas-solid fluidized beds. The impact of bed temperature (evaporation kinetics) on the agglomerate properties is investigated as well. Fluid Coking<sup>TM</sup> was taken as the example of industrial system to model. Previous studies have shown that a Plexiglas experimental model gives an agglomerate distribution that matches the agglomerate distribution obtained in a pilot plant Fluid Coker (Morales M, 2013).

## 3.2 Materials and methods

The experimental set up was described in Section 2.1 and the operating conditions that were used in this section are listed in **Table 3-1**. Since the Plexiglas model (Morales M, 2013) was the reference model, the operating conditions used in this study were, as much as possible<sup>2</sup>, the same used in the development of the Plexiglas model. For example, the initial bed temperatures differ and they were selected to guarantee that the average bed temperature in the bed was always above the boiling point of the water, so that the liquid could evaporate as soon as it was freed from agglomerates.

The total amount of liquid injected in the bed was always the same (i.e. 1200 g), but it was injected either in just one single pulse of 1200 g or in 4 pulses of 300 g each. When all the liquid was injected in one pulse, at the end of injection the bed was kept fluidized at 0.08 m/s (just above the minimum fluidization velocity) for 10 min to make sure that the bed solids were completely dry and, in this way, minimize agglomerate breakage to preserve the formed agglomerates.

In the case of injection of the liquid in four pulse, the fluidization velocity was kept at 0.3 m/s at the end of pulse one, two and three, so that the bed temperature could return to its initial value before starting the subsequent pulse. At the end of the fourth pulse, the bed was kept at 0.08 m/s for 10 min to fully dry the bed solids and preserve the agglomerates formed.

The agglomerates were recovered and characterized following the procedures described in Chapter 2.

---

<sup>2</sup> Due to physical/chemical differences between Plexiglas and the solution used in the present study, some adjustments were required in the experiments and the new value used as well as the reasons that originated the change are described in the text.

**Table 3-1: Operating conditions for Plexiglas and Gum Validation Experiments**

Parameter	Plexiglas Model*	Gum Model
Spray Nozzle	TEB 2.7 mm	
Solids	190 $\mu$ m Sand	
Fluidization Gas	Nitrogen	Air
Atomization Gas	Nitrogen	
Mass of Solids [kg]	150	
Total Liquid Injected [kg]	1.2	
Liquid Flow Rate [g/s]	30	
$t_{inj}$	40 s	1 x 40 s / 4 x 10 s
Fluidization Velocity [m/s]	0.3	
GLR [%]	2	
Initial Bed Temperature $T_0$ [°C]	68	110 / 120 / 130

(\*) (Morales M, 2013)

### 3.3 Results and Discussion

#### 3.3.1 General Characteristics of the model

The model presented in this study was developed with the purpose of having a “cold model” (i.e. a low temperature model) that could be used to simulate the agglomeration process not only for Fluid Coking<sup>TM</sup> but also, possibly, for other industrial processes. As described in Chapter 2, it consisted of a mixture of water, Gum Arabic and a food dye. Because of the dye, this model provides an easy and accurate procedure to estimate the initial liquid concentration within the agglomerates (as explained in Section 2.2.2), that can be applied to the whole mass of the agglomerates recovered. This procedure can also be used to estimate the total mass of agglomerates, including agglomerates that may be smaller than the larger particles of original bed material.



Fluid Coking<sup>TM</sup> can be considered as a wet-agglomeration process, since the bitumen injected acts as a liquid binder of the coke particles aggregates (Gray, 2002); because of that, models with dissolved binders (like the Plexiglas model) have been used to study it. Initial concentrations of Gum Arabic (GA) were selected so that the viscosity of the solution used in the model was in the range of bitumen viscosity at injection conditions (**Table 3-2**). The viscosity of the injected bitumen changes with the operation since the amount of recycle and the composition of the bitumen may vary. The liquid viscosity of the GA solutions increases as the water evaporates, similarly to the bitumen viscosity with the evaporation of volatile compounds as the reaction progresses. The following table presents the measurements of physical properties for several GA solutions compared with the same properties of the Plexiglas model and bitumen (used as reference):

**Table 3-2: Physical properties of Gum Solutions Tested, Plexiglas Model and Bitumen**

<b>Parameter</b>	<i>Gum Arabic 5 wt% + 2 wt% Blue No. 1 (room temperature )</i>	<i>Gum Arabic 5 wt% + 2 wt% Blue No. 1 (room temperature )</i>	<i>Gum Arabic 6 wt% + 2 wt% Blue No. 1 (room temperature )</i>	<i>Plexiglas Model (room temperature )</i>	<i>Bitumen (300 – 400 °C)</i>
pH	1.5	3.0	3.0	N/A	N/A
Viscosity [cP]	2.2	2.6	2.9	0.8	1 – 4*
Wettability: Contact angle with sand [°]	≈ 0	≈ 0	≈ 0	45	≈ 0** (with coke)

(\* ) (Aminu, et al., 2004) (McDougal, 2004) (\*\*) (House, 2007)

While the previous table denotes the feasibility of using GA solutions based on the liquid viscosity, other characteristics of this model should also be considered. An advantage is that Gum Arabic has shown its stability in different processes that use high temperatures (Imeson, 1997). Another important characteristic is the latent heat of vaporization, since the fast evaporation in Fluid Cokers should be simulated.

**Table 3-3** presents the heat of vaporization values for GA, Plexiglas and a Syncrude's AVR (Atmospheric Vacuum Residue). It is observed that the GA model has a higher latent heat of vaporization when compared to the other two systems. Using both the Gum Arabic and Plexiglas models would make it possible to bracket the bitumen total effective heat required by the process.

**Table 3-3: Heat of vaporization for AVR from Syncrude Canada Ltd (i.e. Bitumen), Plexiglas model and Gum Arabic solution (5 wt% GA + 2 wt% colour + 93 wt% water**

<b>Parameter</b>	<i>Gum Arabic Solution</i>	<i>Plexiglas Model*</i>	<i>Syncrude AVR*</i>
Energy required to heat the liquid from injection temperature to bed temperature [kJ/kg]	362	74	544
Latent heat of vaporization [kJ/kg]	2256	451	430
Heat of reaction [kJ/kg]	-	-	178
Total [kJ/kg]	2618	525	1152

(\*) (Morales M, 2013)

### 3.3.2 Injection Experiments in a Large Scale Fluidized Bed

The results of the injection experiments for the model proposed in this thesis were compared to the results obtained with the Plexiglas model, since it was demonstrated by Morales (2013) that they were applicable to the Fluid Coking™ process. The reproducibility of the experiments and the technique used to characterize the agglomerate size distribution is shown in **Figure 3-1**.

Two solutions with different concentrations of gum, but with viscosities close to the Plexiglas model (and that are believed to simulate the bitumen viscosity at injection conditions, (Aminu, et al., 2004) were tested.

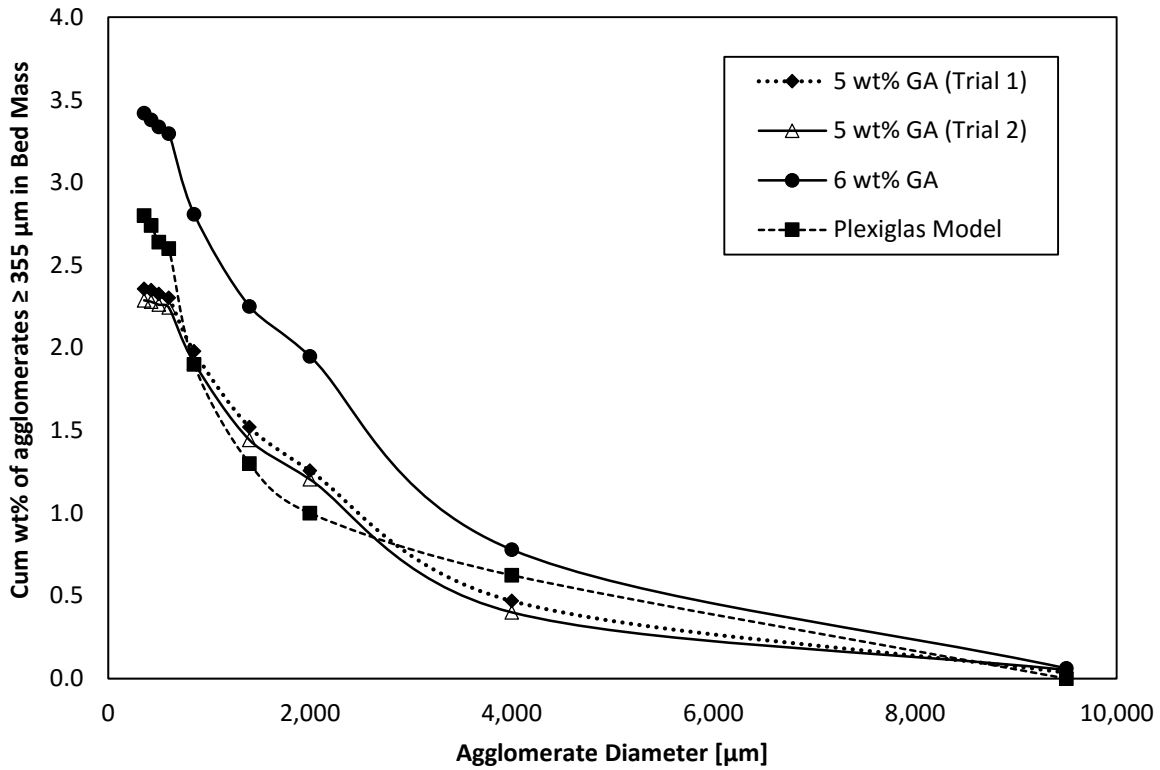


**Figure 3-1: Effect of binder concentration on agglomerate formation;  
 $T_0 = 130\text{ }^\circ\text{C}$ , 1 x 1200 g, 2 wt% Blue No. 1, pH = 3.0**

The total mass of agglomerates formed was higher when the concentration of gum Arabic was increased. It is believed that, with a higher concentration, the wear resistance of the aggregates was also increased, making it harder to break them (Salman, et al., 2007). As less liquid was required to form stable agglomerates, more liquid was available and a larger quantity of agglomerates was expected (Weber, 2009), which agrees with the results obtained and presented in the **Figure 3-1**.

Plexiglas solution is less viscous (i.e. 0.8 cP) than both of the GA solutions (i.e. 2.6 and 2.9 cP), and silica sand is less wettable by this solution. Hence, the formation of the liquid bridges (Stage 2 of the mechanism of agglomerate formation as explained in Chapter 1 (Morales M, 2013)) is not favored and so is not the agglomerate growth.

However, larger amounts of agglomerates were formed with Plexiglas (5 wt%) at same concentration of gum Arabic (5 wt%). These results can be explained by the difference in the type of binder, as some authors have shown that two different binders at same concentration can produce different amounts and sizes of agglomerates due to different binder properties (Davies & Gloor, 1972).

**Figure 3-2** shows that agglomerates formed with a solution with a higher concentration of Gum were dryer. The solvent removal depends on the heat available for evaporation and the characteristics of the solids (Nieuwmeyer, 2009), since the operating conditions in both experiments were the same, the evaporation rate was the same. Therefore, the mass of water evaporated at a given time was the same, but more binder was available at the surface of the particles in the case of the more concentrated solution. Therefore, the agglomerates could collect more dry sand particles and, as a result, the final agglomerates were drier.

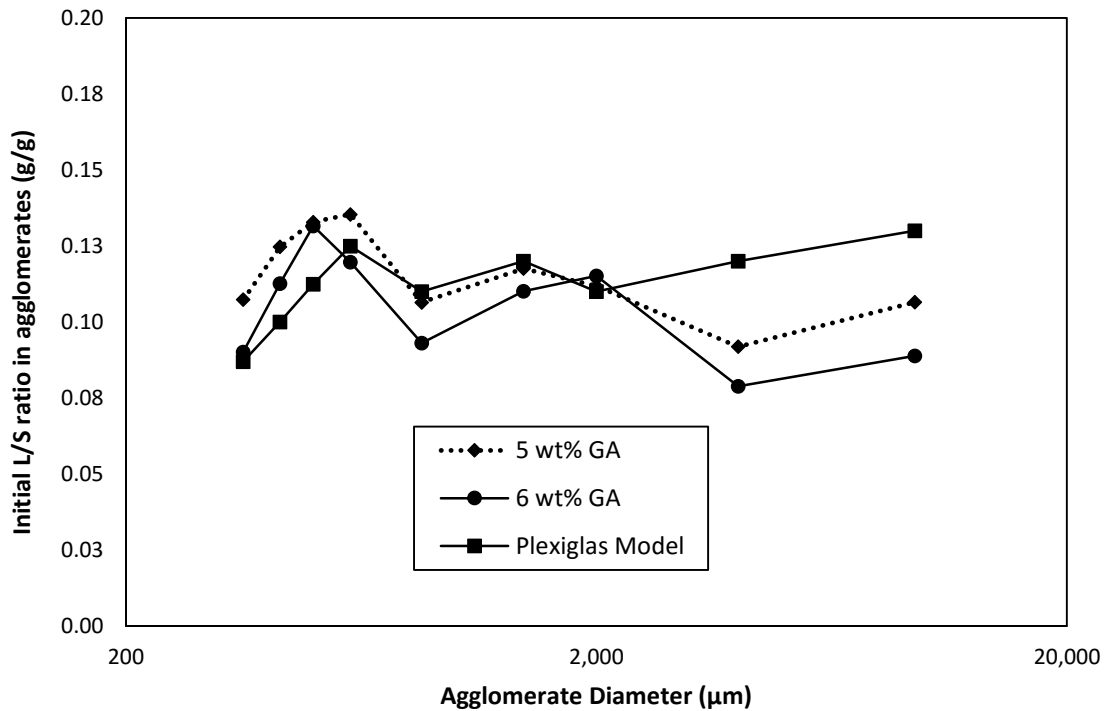


**Figure 3-2: Effect of binder concentration on the initial liquid concentration in agglomerates,  $T_0 = 130\text{ }^\circ\text{C}$ ,  $1 \times 1200\text{ g}$ , Solution pH = 3.0**

**Figure 3-2** also shows that there was more liquid trapped in the large agglomerates formed with the Plexiglas solution. The Gum model has a better wetting mechanism (the contact angle is close to zero); therefore, lower amounts of liquid are required for successful agglomeration (Morales M, 2013).

Even though the total mass of agglomerates obtained with the 5 wt% GA – pH 3 solution is in good agreement with the one obtained with the Plexiglas model (0.4 wt% of difference), there are still some differences that must be analyzed. Among the possible factors that could explain such differences, the variation in the temperature drop after one pulse injection seems to be the most significant (Morales M, 2013). It is important to recall at this point, the differences between GA and Plexiglas solutions in the total energy required to heat/vaporize the liquid (**Table 3-3**). As observed in that table, the GA solution requires over five times more energy to bring the liquid from ambient temperature (or operating temperature in the liquid feed tank) to the bed temperature and then vaporize it. Although the increment in bed temperature<sup>3</sup> is relevant, the major reason for this change is explained by the differences in latent heat of vaporization between GA and Plexiglas. To achieve comparable temperature drops, it was proposed to modify the injection scheme, and perform the liquid injection in pulses. The following section presents a more detailed analysis of the impact of the average bed temperature on the model results.

### 3.3.3 Average Bed Temperature Effect

**Figure 3-3** compares the bed temperatures for one pulse injection and the four pulse injection, with the same total mass of injected liquid. As expected, by doing the total injection of liquid in four pulse (with the same amount of liquid in each pulse), the temperature drop was reduced considerably. A temperature drop of about 6 °C with each of the 4 pulses and 25 °C with 1 large pulse was observed, which corresponds to the expected temperature drop that is approximately proportional to the mass of injected liquid.

---

<sup>3</sup> As previously indicated, the bed operating temperature was changed to ensure continuous vaporization of the injected solution. The saturation temperature of water at operating pressure was used as minimum value.

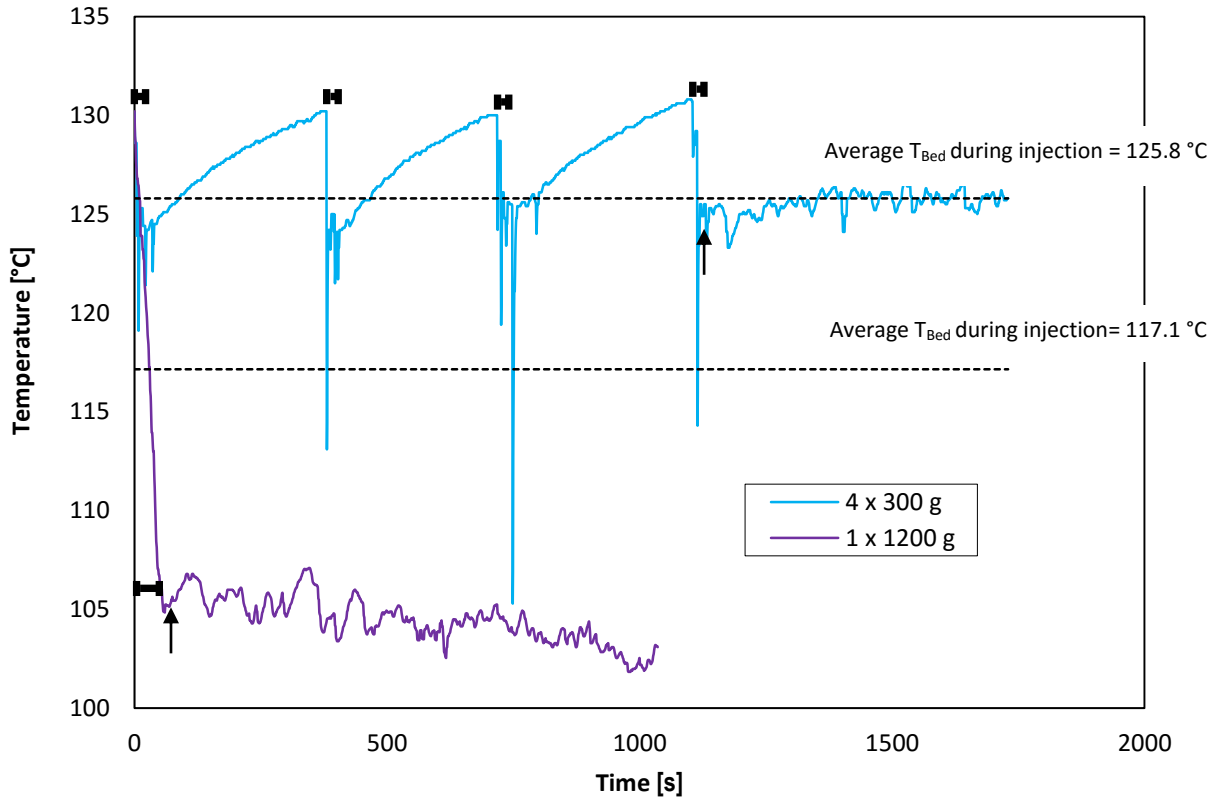


**Figure 3-3: Bed temperatures for one pulse and four pulse injections;  
 $T_0 = 130\text{ }^\circ\text{C}$ , Solution: 5 wt% GA - 2 wt% Blue No. 1 – pH 3  
 ↑ : reduction of  $V_g$  and heating turned off  
 ── : injection time**

The average temperature drop for one injection of 1200 g of the Plexiglas model was around 6 °C. Therefore, an injection of the total liquid divided in 4 equal parts (300 g) matched this characteristic of the Plexiglas model.

**Figure 3-4** shows a significant impact of the new type of injection and, thus, of the corresponding average bed temperature on the total mass of agglomerates formed. The total mass of agglomerates increased by nearly 50% with the new type of injection (i.e. four pulse of 300 g of binder liquid). The total mass of agglomerates that was formed when injecting the liquid in 4 pulses was much higher than when injecting the whole liquid in one single pulse. Since the average temperature during injection was higher, the heat available for the drying process was increased. As a consequence, the agglomerates dried faster and they had less time to break. The liquid bridges

solidified faster and, consequently, the breakage and the attrition processes are reduced and, correspondingly, the mass of agglomerates was greater (Poutiainen, 2013).

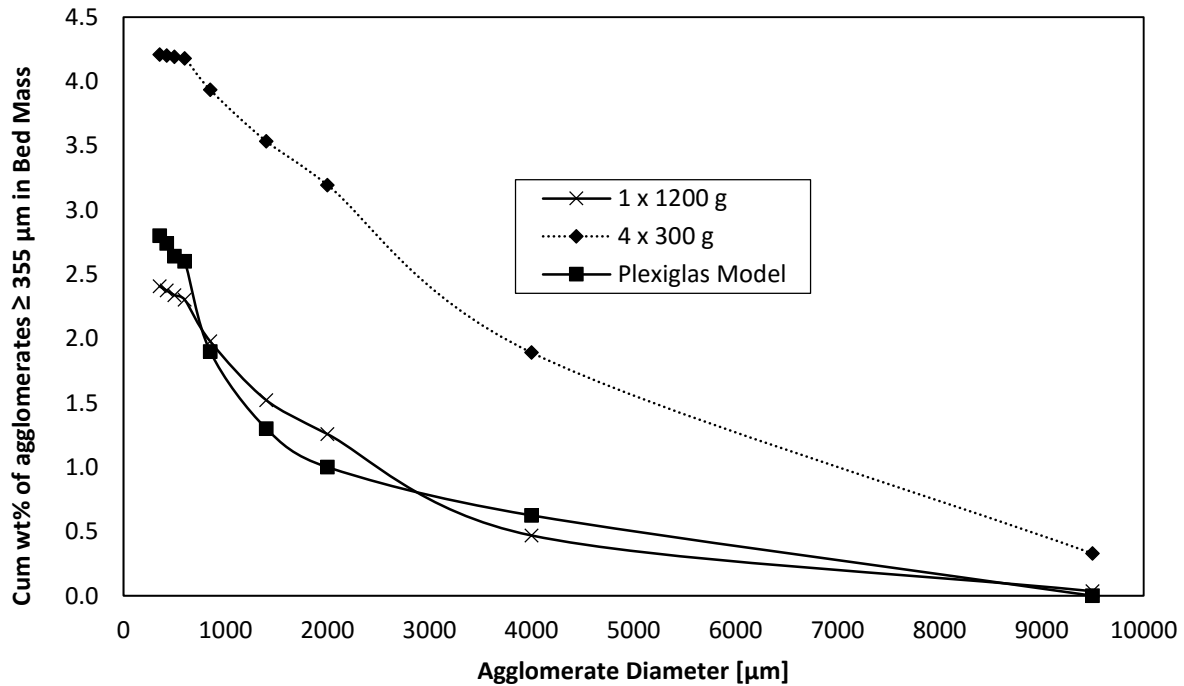


**Figure 3-4: Effect of average bed temperature (number of pulses) on agglomerate formation;  $T_0 = 130 \text{ }^\circ\text{C}$ , Solution: 5 wt% GA - 2 wt% Blue No. 1 – pH 3**

Furthermore, as the average bed temperature was increased, the viscosity of the GA solution increased and the agglomerates formed with the more viscous solution will have stronger liquid bridges (i.e. stronger agglomerates) and survive for a longer period of time (Weber, 2009).

**Figure 3-5** shows the difference in the quantity of liquid trapped with the two different injection strategies and, consequently, when the average bed temperature was changed. The agglomerates formed when doing a four pulse injection were wetter in comparison with the ones formed when doing a single pulse injection. This can be explained by the evaporation rate: for a single pulse, the liquid does not evaporate as quickly (since the drying is slower) and, therefore, the binder remains active longer to “pick up” more dry individual particles.

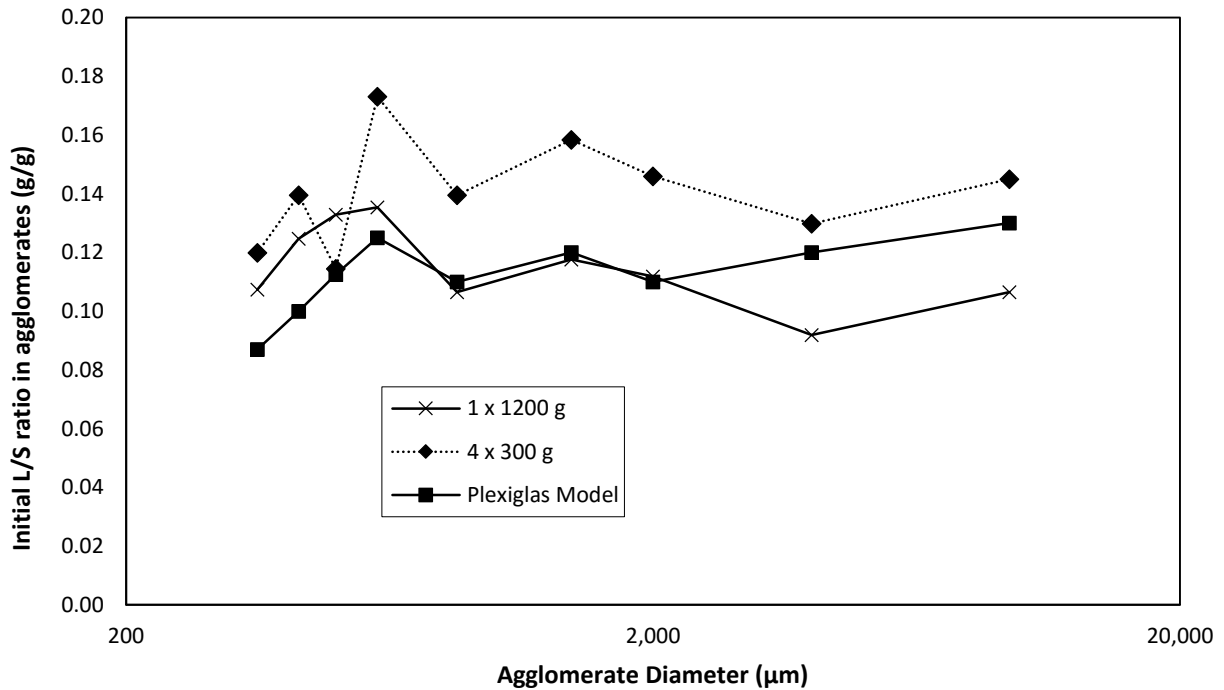


**Figure 3-5: Effect of average bed temperature (number of pulses) on the initial liquid concentration in agglomerates;  $T_0 = 130\text{ }^\circ\text{C}$ , Solution: 5 wt% GA - 2 wt% Blue No. 1 – pH 3**

A representation of the proposed drying mechanism for the agglomerates in both types of injection is displayed in **Figure 3-6**. Assuming that the initial agglomerates formed in both cases were about the same size, agglomerates formed in the four pulse injection dried in 10 seconds (injection time) and the breakage was reduced by approximately 4 times when compared with the single injection (where 40 s is the injection time). The binder crystallized faster, so that there was no opportunity for it to collect more particles.



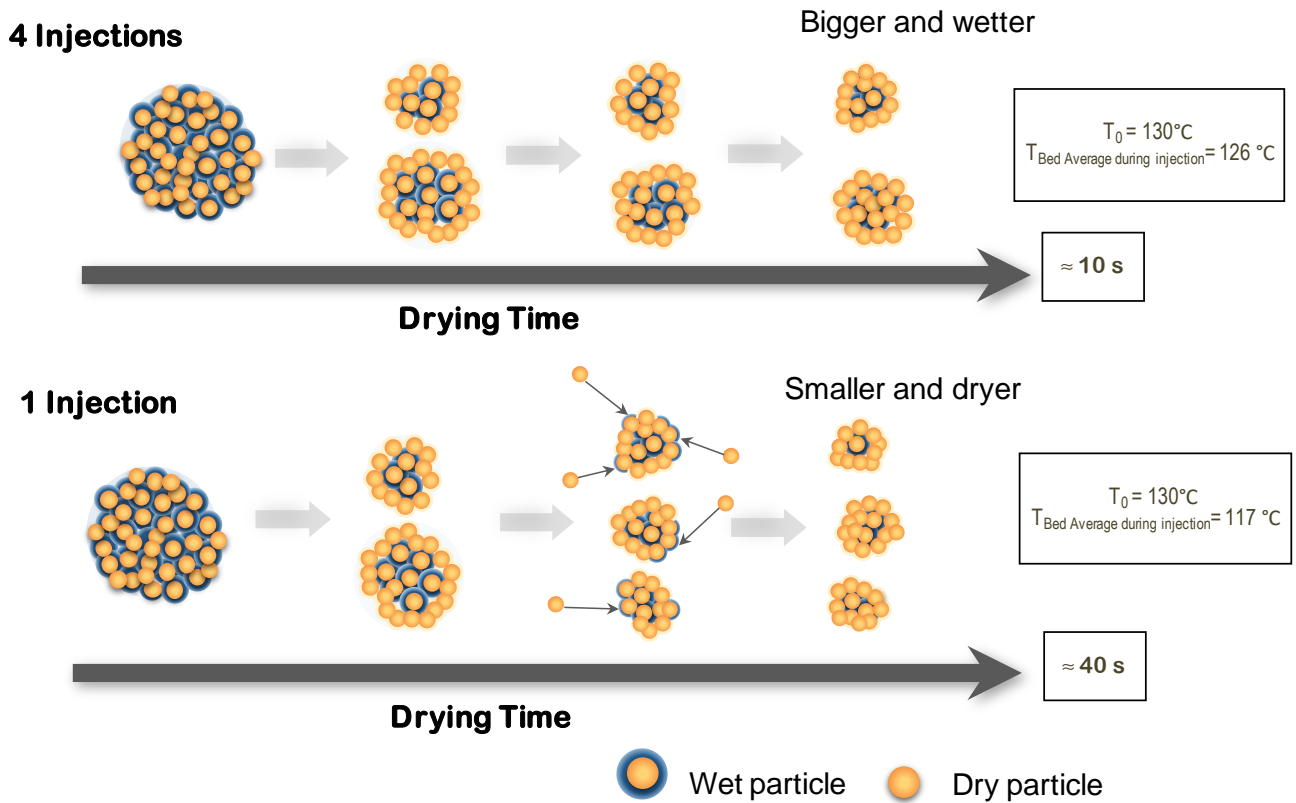


**Figure 3-6: Schematic representation of the agglomerate drying for one and four pulse injections**

Since the results obtained with the four pulse injection did not match closely the Plexiglas results (agglomeration of silica sand was increased), additional experiments with different initial bed temperatures were performed to further evaluate the effect of the average bed temperature on the agglomerate formation.

Given that results led to assume that the total mass of agglomerates obtained decreases as the average temperature decreases, it was expected that, by lowering the initial bed temperature, the total mass of agglomerates obtained would be reduced.

The temperature profiles for the experiments with initial bed temperatures of 110, 120 and 130°C are shown in **Figure 3-7**. As expected the temperature drop for all the experiments with four pulse is around 6 °C, regardless of the initial bed temperature, since it is mainly proportional to the mass that is being injected.

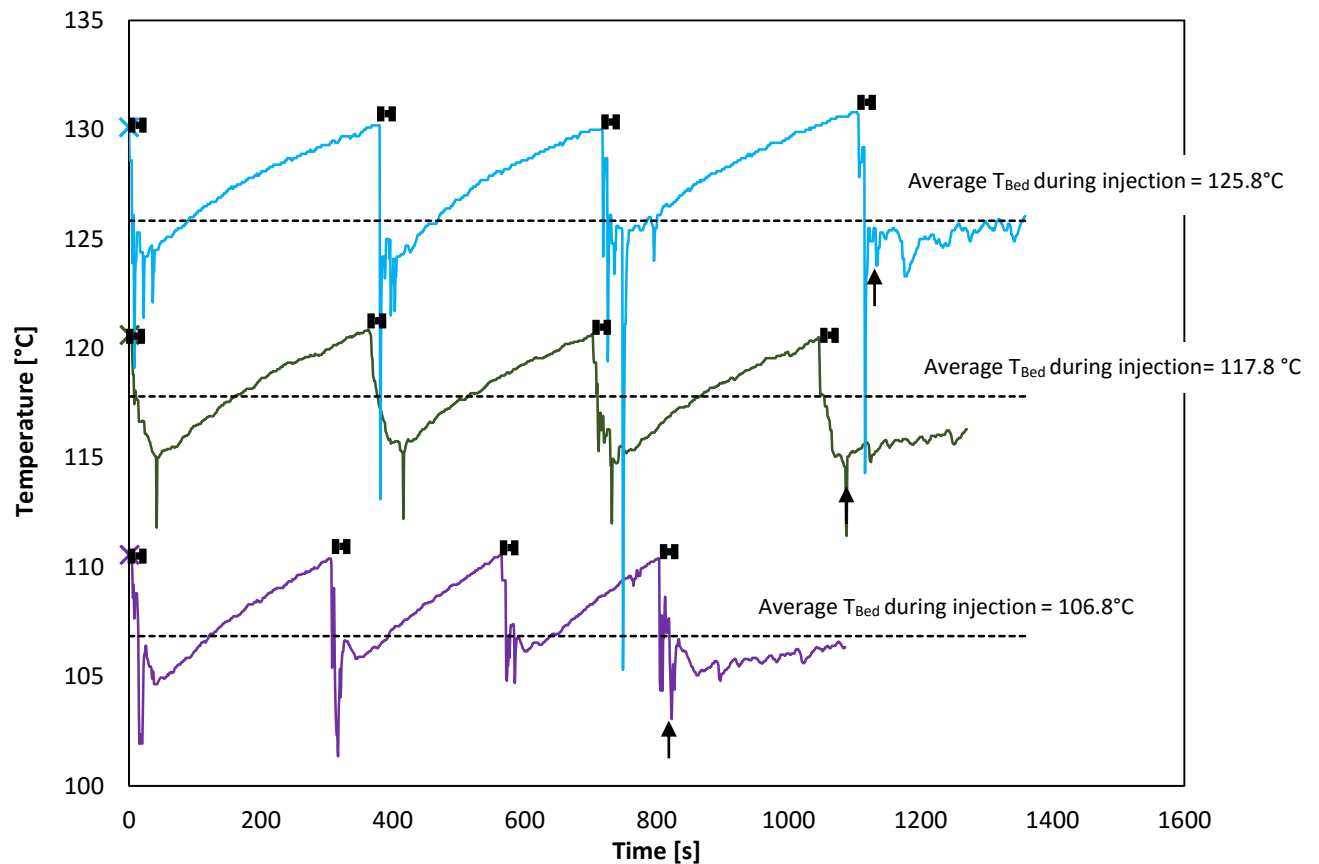


**Figure 3-7: Bed temperature for four pulse injection with different initial bed temperatures; Solution: 5 wt% GA - 2 wt% Blue No. 1 – pH 3**  
 ↑ : reduction of  $V_g$  and heating turned off  
 ─ : injection time

The results presented in **Figure 3-8** are consistent with the results obtained before: by reducing the initial bed temperature, and so the average bed temperature during injection, a smaller mass of agglomerates was formed. Lowering the temperature by 20°C reduces the mass of agglomerates by about 20%. This can be explained by the reduction in heat transfer rate in the agglomerates, which slowed down the vaporization.

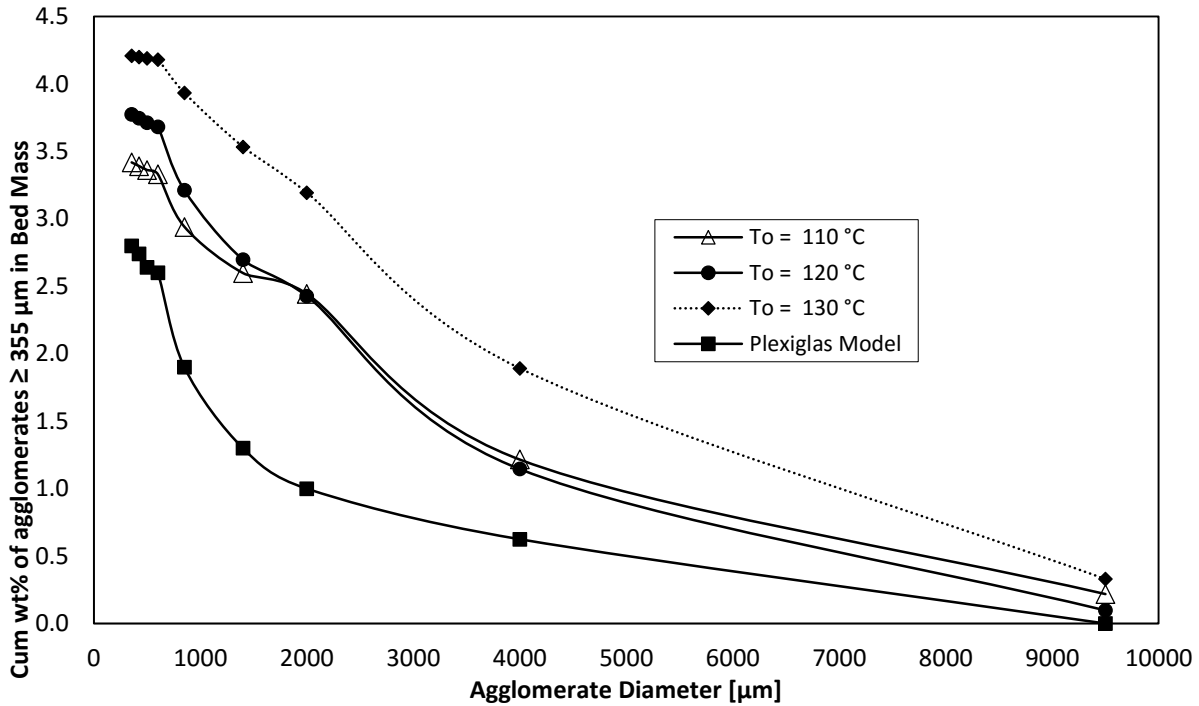


**Figure 3-8: Effect of average bed temperature (initial bed temperature) on agglomerate formation; Type of Injection: 4 x 300 g, Solution: 5 wt% GA - 2 wt% Blue No. 1 – pH 3**

Lowering the initial bed temperature gave results that approached the Plexiglas results. However, with the operating pressure, it was not possible to further reduce the temperature while maintaining continuous vaporization. Other studies could be conducted at reduced pressures (i.e. partial vacuum) to achieve lower saturations temperature, in order to analyze further if this tendency is maintained.

As with previous experiments, **Figure 3-9** shows that, at higher average bed temperatures, the agglomerates were wetter, and although the mass of agglomerates was not much larger (**Figure 3-8**), a greater proportion of the injected liquid was trapped in agglomerates. When an initial bed temperature of 130 °C was selected, 74 wt% of the injected liquid was trapped in agglomerates. On the other hand, when the initial bed temperatures of 120 and 110 °C were used, the proportion of trapped liquid was only 39 and 44 wt%, respectively. For an initial bed temperature of 110 °C, the proportion of trapped liquid approaches the results obtained with the Plexiglas model (40 wt%).

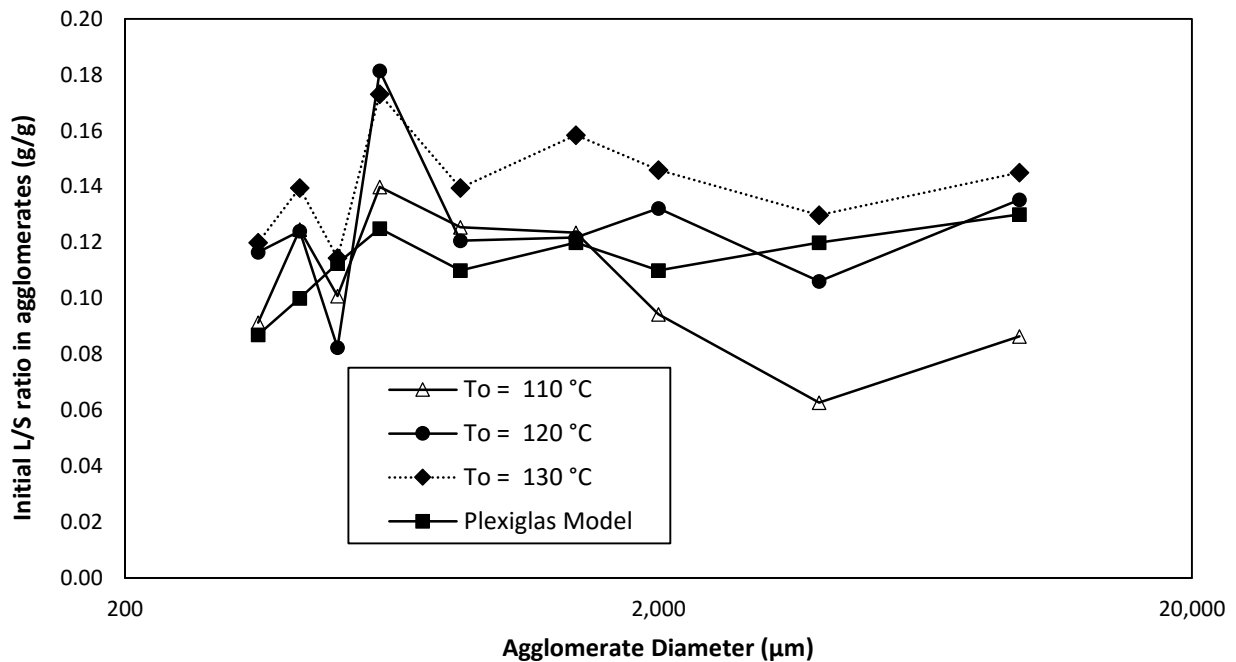


**Figure 3-9: Effect of average bed temperature (initial bed temperature) on the initial liquid concentration in agglomerates; Type of Injection: 4 x 300 g, Solution: 5 wt% GA - 2 wt% Blue No. 1 – pH 3**

For the subsequent experiments, an injection with four pulse and  $T_0 = 110\text{ }^\circ\text{C}$  was used, since the results obtained with this temperature were the closest to the Plexiglas model results.

### 3.3.4 Effect of binder concentration and pH (viscosity)

Different operating variables are changed in industrial processes to improve liquid spreading and wetting uniformity when performing wet agglomeration in fluidized beds. For instance, the binder liquid viscosity may be modified. In this study, the viscosity was reduced to decrease agglomeration and, as a consequence, to better match the GA solution and the Plexiglas results.

Considering that the viscosity of an aqueous Gum Arabic solution can be lowered by reducing the solution pH (Riddell & Davies, 1931) (Ranken & Baker, 1997), it was decided to explore the effect of modifying the pH of the GA solutions to be used.

Hydrochloric Acid was added to the GA solution to reduce its pH. A strong acid was chosen for the final tests since preliminary measurements showed that it has a greater impact in reducing the viscosity of the solution when compared to other acids (weak acids) such as Lactic Acid. **Figure 3-10** shows the viscosity of the solutions for different pH values measured in the laboratory at room temperature using a Cannon viscometer. Below a pH 1.5, there were no considerable reductions the GA solution viscosity, regardless of the GA concentration; hence, the solution with the lowest viscosity (solution 5 wt% GA – pH 1.5) was selected for the subsequent experiments.

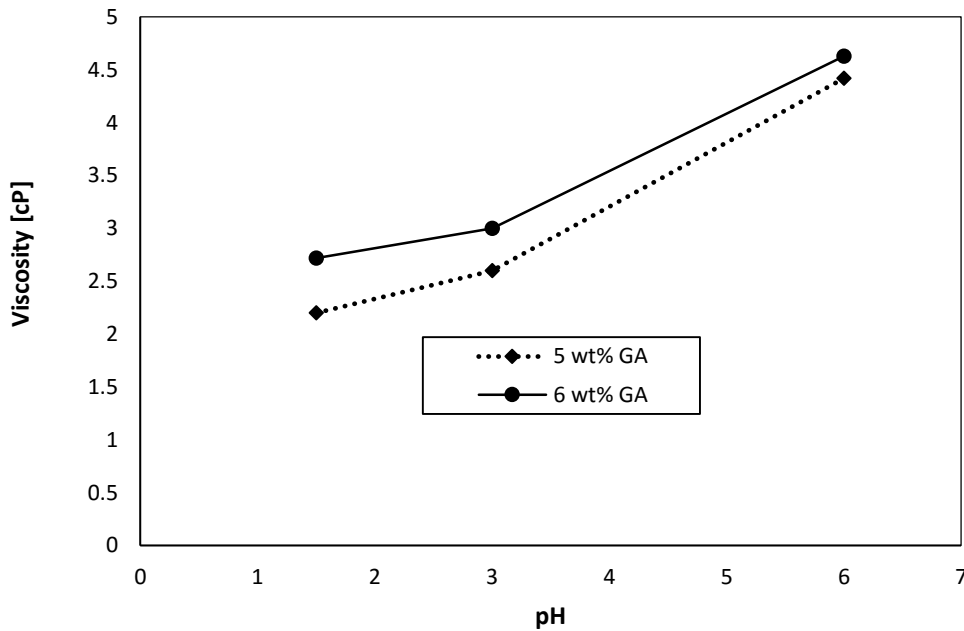


**Figure 3-10: Effect of pH and binder concentration on the viscosity of the model solutions**

**Figure 3-11** confirms that liquid spreading is improved by reducing the solution pH. Liquid bridges promote adhesion between particles and the resulting attraction forces depend on the liquid viscosity: these forces are weaker when the viscosity is lowered, promoting agglomerate breakage (Simons & Fairbrother, 2000). According to the mechanism for wet agglomeration presented by Morales (2013), the initial liquid spreading is enhanced since the droplets formed with a less viscous solution are smaller and will contact more particles that are located within the jet cavity.

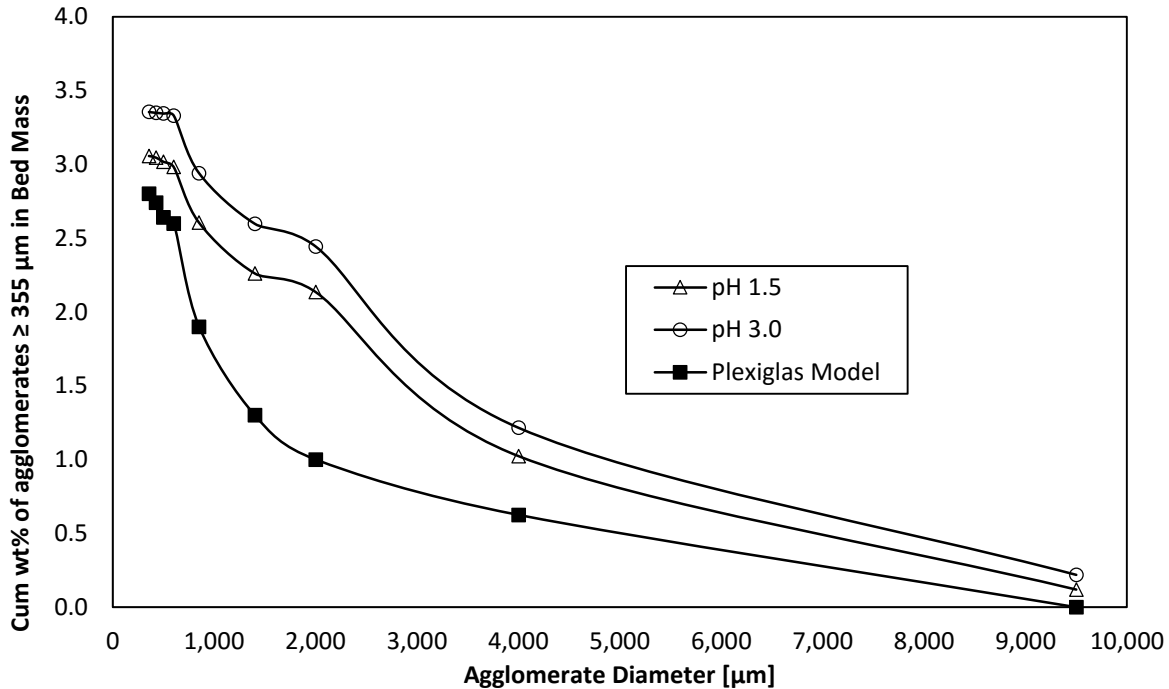


**Figure 3-11: Effect of solution pH on agglomerate formation;**  
 **$T_0 = 110 \text{ }^\circ\text{C}$ ,  $4 \times 300 \text{ g}$ , Solution:  $5 \text{ wt}\%$  GA -  $2 \text{ wt}\%$  Blue No. 1**

According to **Figure 3-11**, the total relative reduction in mass of agglomerates is around 0.5 %, which is in agreement with the results found by Weber (2009), indicating that beyond a certain liquid viscosity, reducing the liquid viscosity does not greatly affect the agglomerate stability. At such point, the effect of viscosity is minor when compared with the impact of the capillary forces (i.e. wettability and surface tension) (Pont, et al., 2001). This conclusion is also proven in this study, when the amount of agglomerates formed with the GA solution (contact angle with sand around zero) was considerably higher than that produced with the Plexiglas solution (contact angle with sand =  $45^\circ$ ).

**Figure 3-12** illustrates the differences in liquid concentration in the agglomerates for the two pH values used, and, correspondingly, for two viscosities (2.2 and 2.6 cP). Mass balances on the injected liquid showed that there was a reduction in the proportion of injected liquid trapped in agglomerates when reducing the solution viscosity. The proportion of injected liquid that was trapped in agglomerates is 39 wt% and 35 wt% for 2.6 and 2.2 cP, respectively. As in the results obtained for the total mass of agglomerates, the impact of the associated change in binder viscosity

of the proportion of liquid trapped in agglomerates was relatively small. The result was in good agreement with the 40 wt% of injected liquid trapped in agglomerates obtained for the Plexiglas model.

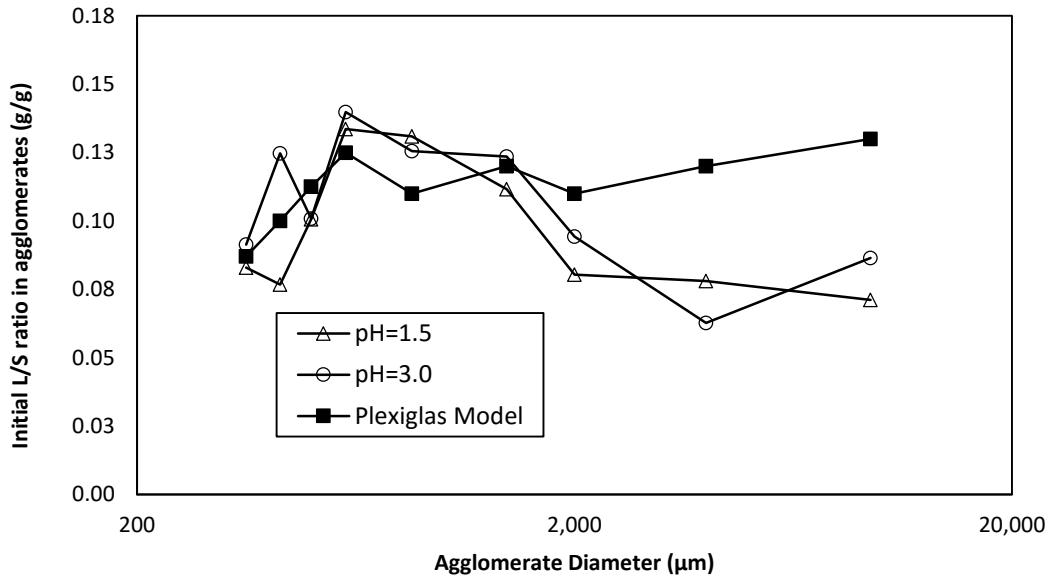


**Figure 3-12: Effect of solution pH on the initial liquid concentration in agglomerates;  $T_0 = 110\text{ }^\circ\text{C}$ , 4 x 300 g, Solution: 5 wt% GA - 2 wt% Blue No. 1**

Since further reduction in Gum concentration would have generated agglomerates so weak that they would not have survived the sieving process, the solution: **5 wt% GA - 2 wt% Blue No. 1 - pH = 1.5, with initial bed temperature  $T_0 = 110\text{ }^\circ\text{C}$  and Type of injection = 4 x 300 g**, was the one that better matches the results Plexiglas agglomerate size distribution, in terms of temperature drop, agglomerate mass, agglomerates size distribution, liquid concentration in agglomerates, and proportion of injected liquid that was trapped in agglomerates.

Currently, the GA solution and the procedure for the estimation of the liquid concentration in agglomerates are being applied in the research of Elkolaly (2015). In processes such as Fluid Coking<sup>TM</sup>, it is important to estimate the drying time of an agglomerate with a given liquid content. The author estimates the initial liquid concentration in agglomerates with the procedure developed in this thesis and then uses the information that it provides to calculate the time for full conversion of the liquid trapped in the recovered agglomerates, using the model developed by Sanchez (2013).

## Chapter 4

### 4. Impact of pulse duration on agglomerate formation, recoating and breakup

#### 4.1 Introduction

Industrial processes improve the liquid spreading quality by changing different operating variables. As illustrated in the previous chapter, for example, liquid properties and the interfacial parameters (i.e. contact angle) have a great impact. On the other hand, solids mixing (adjusted with the fluidization velocity), residence time of the solids and temperature of the inlet gas are also often modified to optimize the liquid distribution (Parikh, 2005).

Changing the liquid loading in the bed might be another possibility to enhance the liquid distribution in wet agglomeration in fluidized beds. The objective of this chapter is to describe the study on the impact of liquid pulse injection (liquid feed loading) on liquid spreading and thus, agglomerate formation and possible recoating. It is important to notice that the effect of evaporation kinetics was minimized in this section, since the average bed temperature was kept constant.

#### 4.2 Materials and methods

The experimental set up was described in Section 2.1 and the operating conditions that were used in this section are listed in **Table 4-1**. Most of the operating conditions used in this study were the same used in the previous chapter. However, the initial bed temperatures differ and they were selected to not only guarantee that the average temperature in the bed was always above the boiling point of the water, but also was the same in all experiments. As stated before, the average bed temperature was kept constant to minimize the effect of the evaporation kinetics.



**Table 4-1: Operating conditions for Injection Experiments**

Parameter	Gum Model
Spray Nozzle	TEB 2.7 mm
Solids	190 $\mu\text{m}$ Sand
Fluidization Gas	Air
Atomization Gas	Nitrogen
Mass of Solids [kg]	150
Total Liquid Injected [kg]	1.2
Liquid Flow Rate [g/s]	30
$t_{inj}$	2 x 20 s / 3 x 14 s / 6 x 7 s
Fluidization Velocity [m/s]	0.3
GLR [%]	2
$T_0$ [ $^{\circ}\text{C}$ ]	111 / 112.5 / 116

The total amount of liquid injected in the bed was always the same (i.e. 1200 g), but it was injected in different number of pulses: 2 pulses of 600 g, 3 pulses of 400 g or 6 pulses of 200 g. For all the experiments, the fluidization velocity was kept at 0.3 m/s before, during and after each pulse, so that the bed temperature returned to its initial value before the start of a subsequent pulse. At the end of the last pulse, the bed was kept at just above the minimum fluidization velocity for 10 min to fully dry the bed solids and preserve the agglomerates formed.

The physical properties of the solution selected for the experiments described in this chapter are listed in **Table 4-2**. This specific solution was selected based on the results obtained in Chapter 3, which better matched the Plexiglas model, and thus Fluid Coking<sup>TM</sup>, when injecting in pulses with and initial temperature  $T_0 = 110$   $^{\circ}\text{C}$ . These operating conditions are similar to the ones used for this part of the study: the liquid was injected in pulses (2 to 6 pulses) and the initial bed temperature fell within the range of 111 – 116  $^{\circ}\text{C}$ , and thus justifying the use of this specific solution.

Unlike the solution used in previous experiments, which only used blue dye as a tracer for the liquid, the solution injected in each pulse had a different dye added (blue, yellow or red). This modification was implemented in order to investigate the agglomerate recoating by analyzing the colour composition in individual agglomerates.

**Table 4-2: Physical properties of Gum Solutions Used**

Parameter	<i>Gum Arabic 5 wt% + wt% Dye *</i>
pH	1.5
Viscosity [cP]	2.2
Wettability: Contact angle with sand [°]	≈ 0

(\* ) 2 wt% blue, 1.2 wt% yellow or 0.5 wt% red

**Table 4-3** describes the sequence of the colours used in each experiment. As explained earlier, a different colour was used in each pulse. In the case of the six pulse injection, and since only three colours were selected, a new sequence cycle was started at pulse four, so that the layers of colour could be easily identified.

**Table 4-3: Sequence of colour injected for each type of experiment**

Mass of each liquid injected per pulse [g]	Pulse number					
	1	2	3	4	5	6
600	Blue					
600	Blue	Yellow				
400	Blue	Yellow	Red			
200	Blue	Yellow	Red	Blue	Yellow	Red

The agglomerates formed were recovered and characterized following the procedures described in Chapter 2. To characterize the distribution in individual agglomerates, the procedure explained in Section 2.3 was followed.

## 4.3 Results and Discussion

### 4.3.1 Effect of Pulse Duration on Agglomerates Formation

Few studies have been conducted to study the impact of injection duration on agglomerate formation in wet agglomeration in fluidized beds. Sabouni (2012) and Leach (2013) investigated the effect of pulsations on the liquid distribution quality; however, their studies do not apply to the present study, since the frequency of the pulsations was much higher (up to 2 Hz) and the liquid flow rate was not completely stopped between pulses. In contrast, the present work used times between injections that were of the order of minutes, and the liquid flow rate was completely stopped between pulses.

At this point it is important to remark that, with the exception of the pulse duration, time between pulses and initial bed temperature<sup>4</sup>, the operating conditions did not vary from one experiment to another (i.e. fluidization velocity, GLR, liquid flow rate and so on). The total mass of liquid injected was always kept constant as well, so that, any difference in the mass of agglomerates formed was due to pulse duration only.

As shown in **Figure 4-1**, the initial bed temperature was set at a different value for each experiment. The objective of this modification was to compensate for the differences in temperature drop due to the differences in the mass of liquid injected during each pulse. It is observed in **Figure 4-1** that the average bed temperature was the same regardless of the number of pulses (or the mass of liquid injected in each pulse) and thus, the impact of evaporation kinetics on agglomerate formation and stability was minimized.

---

<sup>4</sup> As described in Chapter 3, the bed temperature drop after any injection depends on the mass of liquid injected.

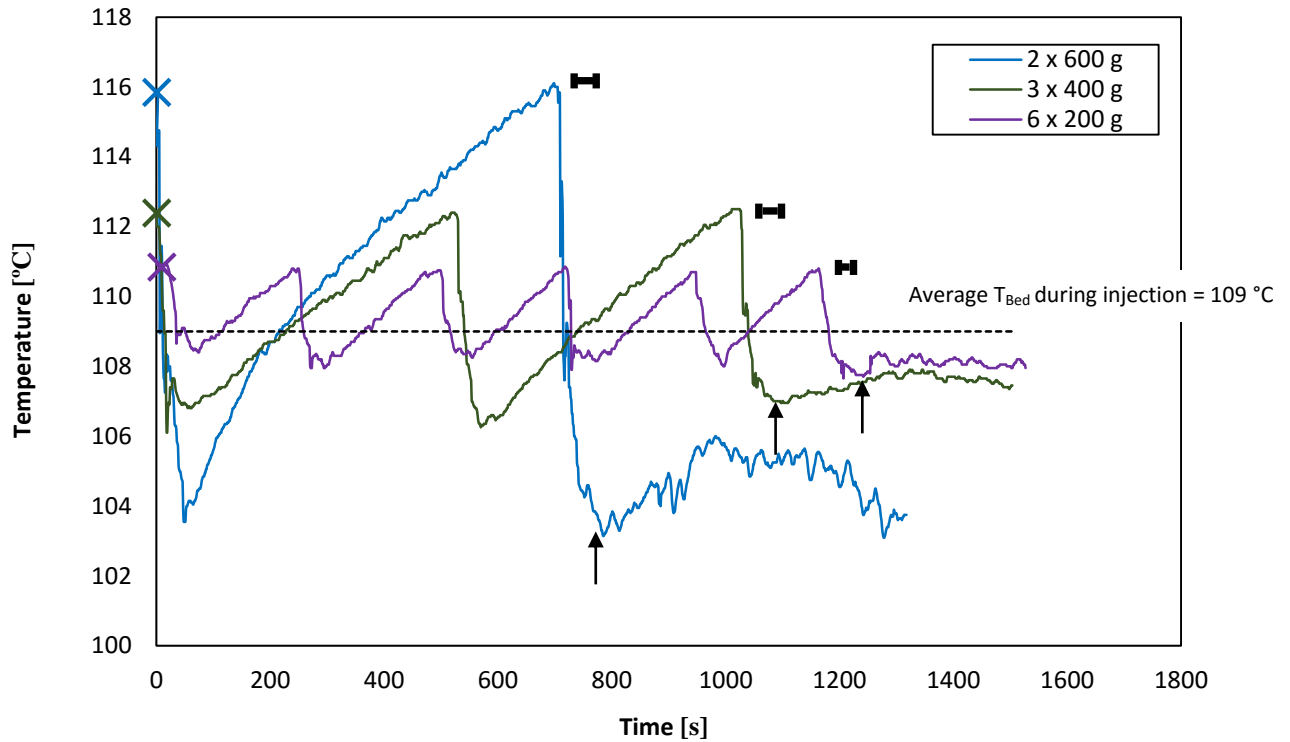


**Figure 4-1: Bed temperatures for two, three and six pulses injections;**

$$T_{0, 2 \times 600 \text{ g}} = 116 \text{ }^{\circ}\text{C}, T_{0, 3 \times 400 \text{ g}} = 112.5 \text{ }^{\circ}\text{C}, T_{0, 6 \times 200 \text{ g}} = 111 \text{ }^{\circ}\text{C}$$

↑ : reduction of  $V_g$  and heating turned off

▬: injection time

**Figure 4-2** shows that the total mass of agglomerates formed decreased when the pulses duration was reduced. Since less liquid was sprayed in each separate pulse, as the number of pulses increases (maintaining a constant flow rate), the liquid was distributed on a greater amount of solid particles and, consequently, there was less opportunity for rewetting of already wet particles. As a consequence, drier and weaker agglomerates were obtained, which could break easier than wetter agglomerates (Weber, 2009).

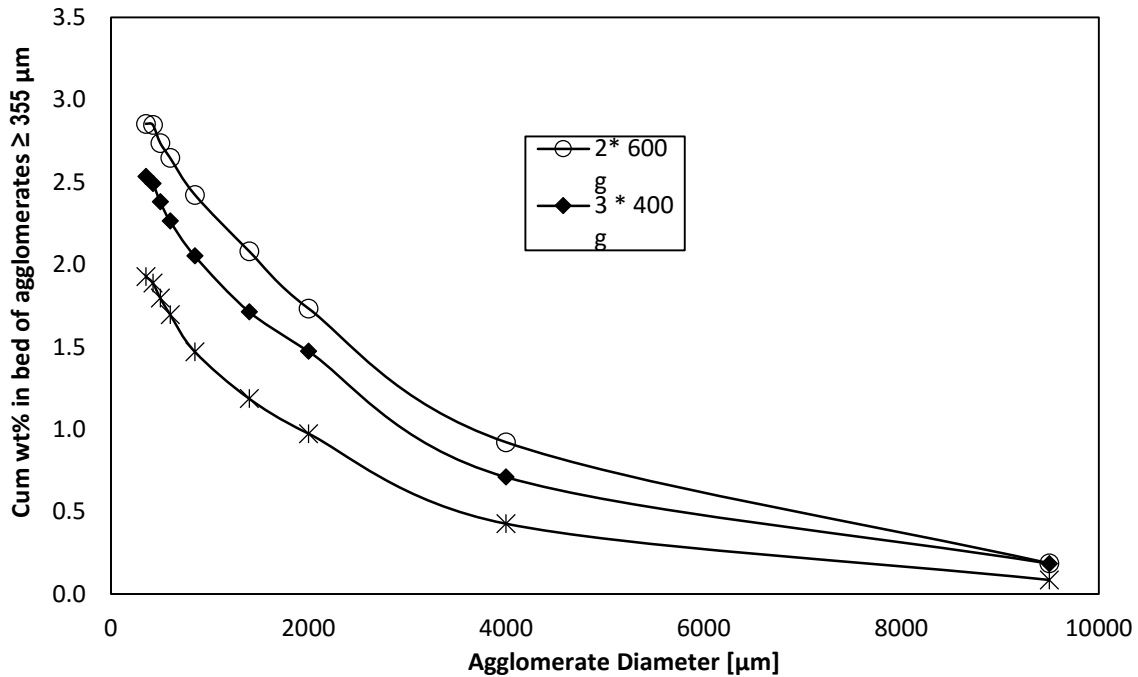


**Figure 4-2: Effect of pulse duration on agglomerate formation**

To further understand why fewer agglomerates were formed, the model described in Section 2.5 was used to calculate the average liquid concentration in the mass of wetted particles for each jet expansion (**Figure 4-3**). The model indicated that there was indeed a difference in the liquid concentration depending on the pulse duration, and when the pulse duration was decreased, the liquid concentration within the agglomerates initially formed by the spray also decreased. Moreover, as in the experimental results presented in **Figure 4-1**, the difference was more significant between the 7 second (six pulses of 200 g) and the 14 second injection (three pulses of 400 g) than between the 14 second injection and the 20 second injection (two pulses of 600 g).

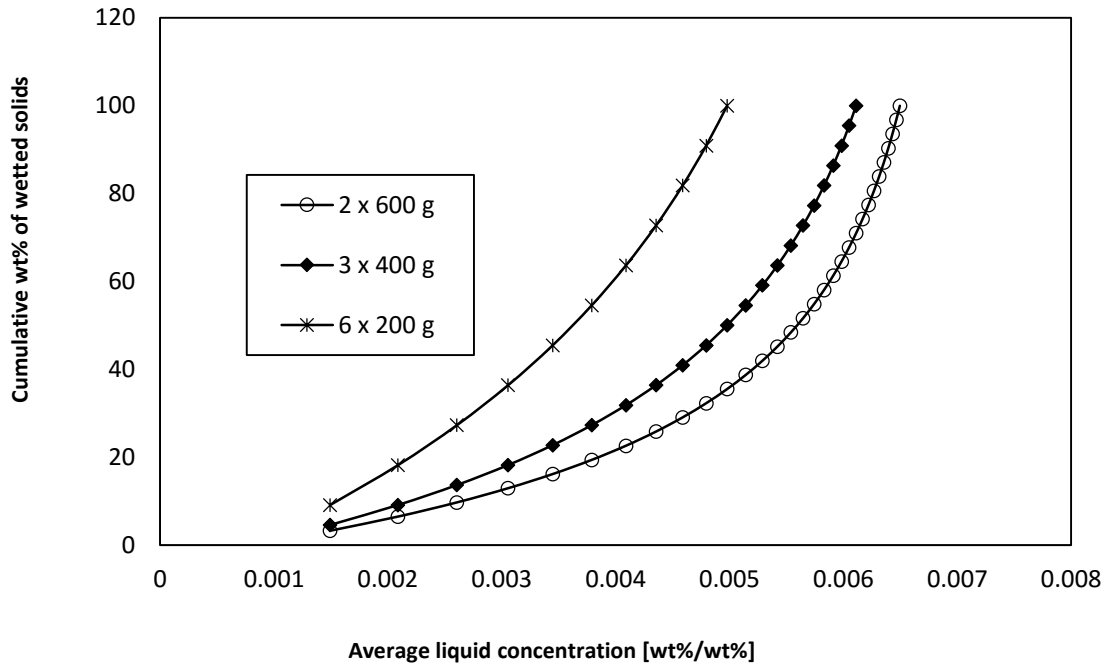


**Figure 4-3: Average liquid concentration of wetted solids obtained with the model corresponding to different injection strategies**

These results were also in agreement with those obtained with the model proposed by Mohagheghi Dar Ranji (2014), which predicts that agglomerates formed with longer injection durations are wetter. The strength of the agglomerates is proportional to the liquid content, and the higher the liquid concentration, the stronger the agglomerates (Weber, 2009). Since the agglomerates formed are stronger with longer injections, they will have greater chances of survival, resulting in a higher mass of recovered agglomerates.

Additional experiments were carried out in order to evaluate the possible impact of the recoating, independently of the effect of pulse duration, by using the same pulse duration, but a different number of injections. A single pulse injection of 600 g was performed, so that it could be compared with the two pulse injection, considering that, on the average, the pulse duration was 20 seconds.

**Figure 4-4** shows that approximately half of the mass of agglomerates was formed when half of the liquid was injected (i.e. 600 g instead of 1200 g). This might indicate that there was recoating when the liquid was injected in two pulses; however, further analysis and experiments were needed

to verify this hypothesis. The first step for such validation was to determine whether there were any differences in the agglomerate size distribution for the two experiments. Also, if there were differences, what are the sizes in which those differences could be located.

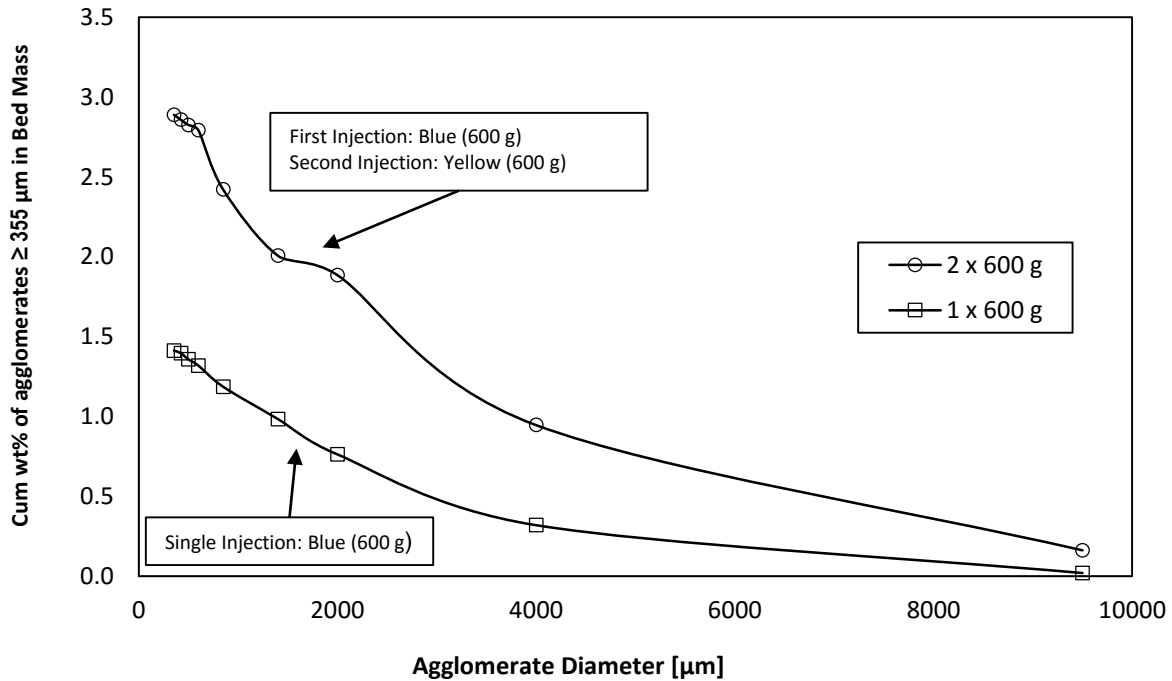


**Figure 4-4: Total mass of agglomerates formed for an experiment with a single pulse and for an experiment with two pulse of 600 g each**

**Figure 4-5** and **Figure 4-6** show agglomerate size distributions for one and two pulses. Both figures present almost the same results for the two experiments, with some differences in the tails of the graphs corresponding to largest recovered agglomerates (i.e.  $d_{\text{aggl}} \geq 9500 \mu\text{m}$ ,  $9500 \mu\text{m} > d_{\text{aggl}} \geq 4000 \mu\text{m}$ ,  $4000 \mu\text{m} > d_{\text{aggl}} \geq 2000 \mu\text{m}$ ).

These results indicated that there was some recoating of the agglomerates when the liquid was injected in two pulsations. Since some recoating was identified when having the smallest number of pulses (i.e. two pulses), it was presumed that these results could be extended to the other experiments. The number of pulses was higher and so, there would be more possibilities for the agglomerates to get recoated.

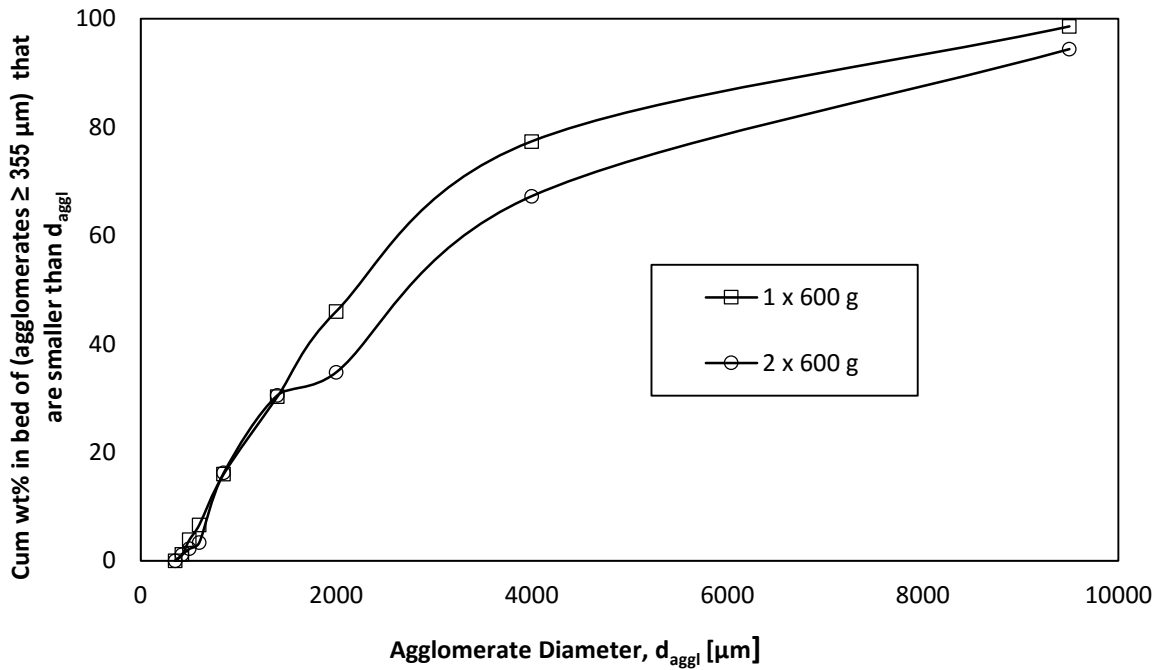


Figure 4-5: Comparison of agglomerates smaller than  $d_{agg1}$  formed for an experiment with a single pulse and an experiment with two pulse of 600 g each

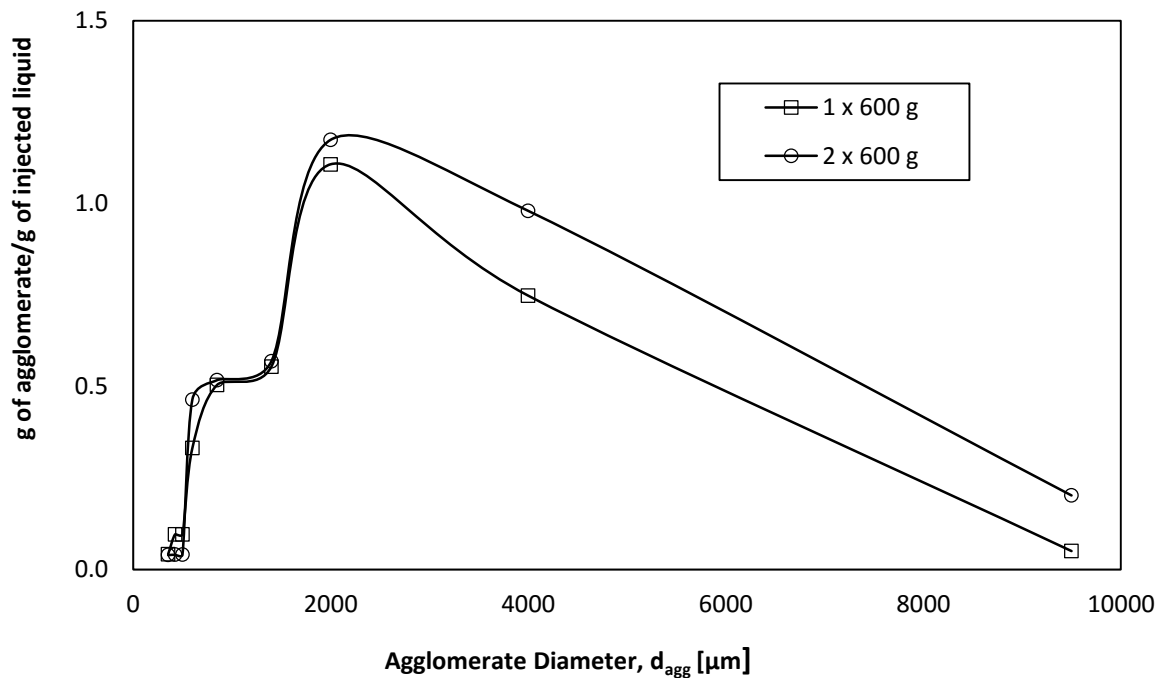


Figure 4-6: Mass of agglomerates formed per gram of liquid injected for an experiment with a single pulse and an experiment with two pulse of 600 g each



Finally, analysis of liquid-to-solid concentration for each dye was needed to determine which type of recoating was occurring. This analysis is presented in the following section.

#### 4.3.2 Effect of Pulse Duration on the Liquid Concentration

One of the main advantages of the GA model is the use of the dye. Since three different dyes could be added to the solution, it was possible not only to accurately estimate the liquid trapped in agglomerates, but also to identify from which pulse the liquid came from. In this part of the study, two different analyses were conducted to analyze how the liquid was distributed onto the bed of solid particles. The analyses were:

1. Total mass of liquid trapped in agglomerates corresponding to each pulse.
2. Colour distribution in individual agglomerates.

**Figure 4-7** shows that there was a difference in the total liquid trapped in agglomerates per pulse. The total mass of yellow liquid (second pulse) trapped in agglomerates was around 10 wt% higher compared to the blue liquid (first pulse).

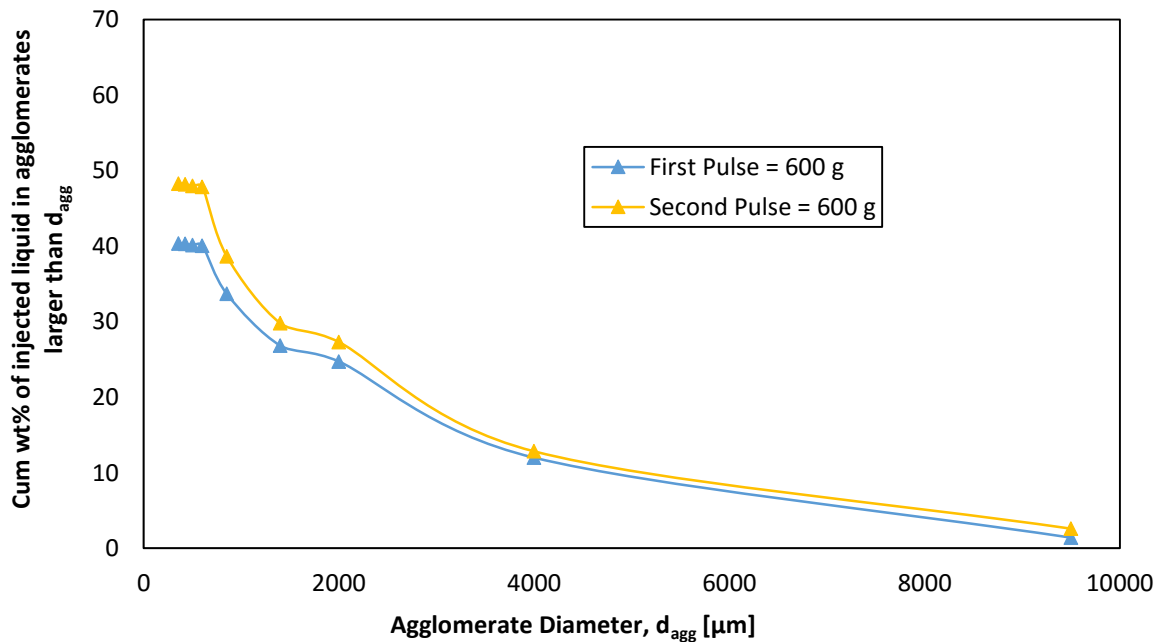


**Figure 4-7: Concentration of the liquid from the first pulse (blue) and the second pulse (yellow) in agglomerates;  $T_{0, 2 \times 600 \text{ g}} = 116 \text{ }^\circ\text{C}$**

Measurements of the particle size distribution in agglomerates were performed in order to determine whether the particles within the agglomerates had the same distribution as the bed solids or if there was some segregation in the bed mass, and some sizes of particles were being preferentially trapped in agglomerates. This could explain the differences in liquid trapped per pulse.

**Figure 4-8** shows that there was no difference in the particle size distribution, and therefore, one could state that there was no segregation during the formation of the agglomerates. Since there was no preferential agglomeration, other processes should explain why more liquid from the second pulse was trapped within the agglomerates.

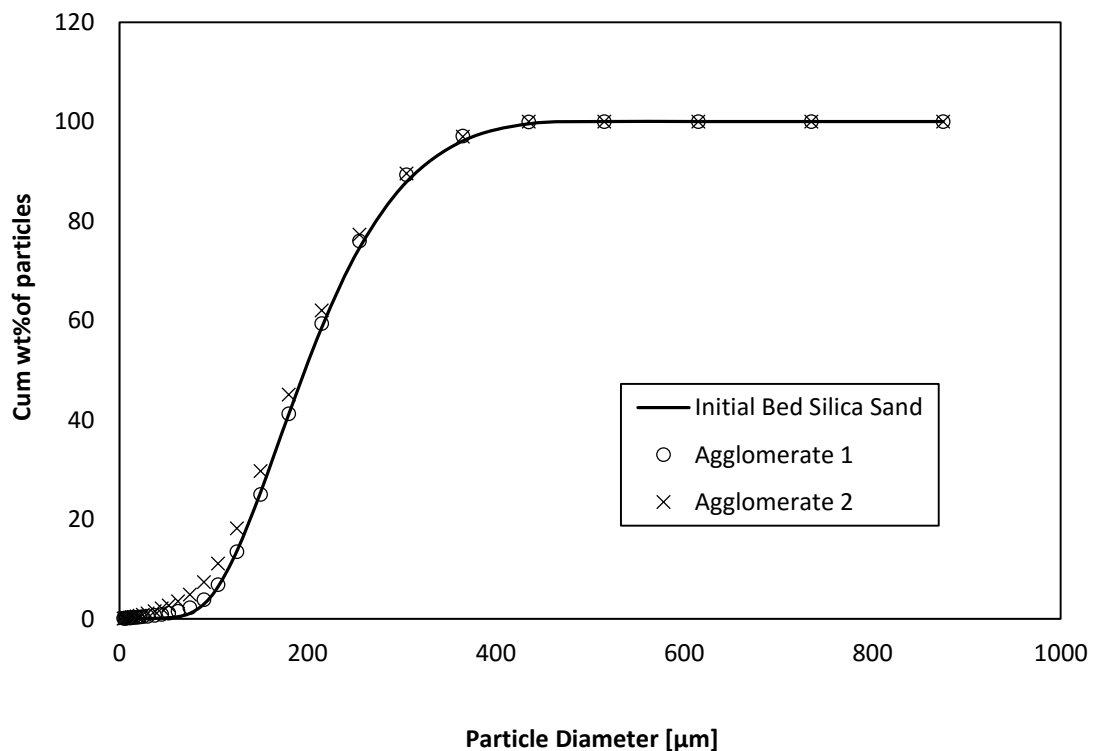


**Figure 4-8: Particle size distribution of the initial silica sand in the fluidized bed at the beginning of the experiment, and of the sand trapped in the macro-agglomerates recovered after the end of the experiment**

There were three possible explanations for this result:

1. Agglomerates formed after the first pulse (blue) were more likely to be captured by the second jet (yellow pulse).
2. Agglomerates including prior agglomerates were more stable than agglomerates including only bed particles.
3. Wet agglomerates that were breaking in the bed are more likely to capture other agglomerates than bed particles.

In order to know which one of the explanations was valid to explain the difference in liquid trapped after each individual pulse, two approaches were taken. First, a qualitative analysis of the biggest agglomerates was performed, since any layer or distinctive characteristic would be easier to identify in bigger particles. Second, the amount of agglomerates (from earlier injections) entering the jet cavity with bubbles was estimated (see Section 2.6).

In approximately 60% of the recovered agglomerates with the largest size (i.e.  $d_{\text{aggl}} \geq 9500$ ), a yellow layer recoating a blue agglomerate was identified (**Figure 4-9**). This qualitative evaluation suggested that the recoating was due to the fact that the agglomerates formed after the first pulse (blue) were more likely to be captured by the yellow jet (second pulse). If this was happening, large agglomerates formed after the blue injection must be segregating near the bottom of the bed where they could be picked up by gas bubbles and carried upward in their wake. It is also important to highlight that agglomeration by layering occurs in larger agglomerates whereas smaller ones agglomerate by coalescence (see section 1.1), therefore, the yellow layer was not identify in the small agglomerates but there was still some colour mixing.

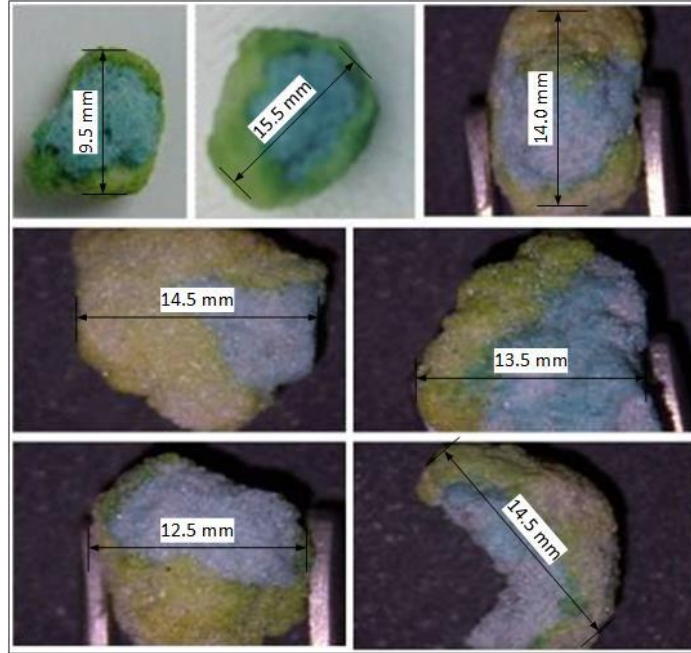


**Figure 4-9: Example of agglomerates recovered after the second pulse in an experiment of two pulse of 600 g each**

According to the calculation of the solids entering the jet cavity with bubbles wakes, approximately 77 wt% of the wetted solids originated with solids carried into the jet cavity by gas bubbles. Because large agglomerates tend to segregate in the lower bed regions, near the gas distributor, they were more likely to be carried in the wakes of the bubbles formed at the gas distributor. If the extreme case was considered (i.e. only agglomerates were being carried by the bubbles wakes), 40 wt% of dye in agglomerates should be blue and 60 wt% should be yellow. Since not all the solids carried by the bubbles wakes were agglomerates, a smaller proportion of blue than this maximum was expected.

Given these results, the colour distribution within the agglomerates was measured to determine whether it agreed with the predictions, using the procedure described in Section 2.3. Samples were taken only from the largest sizes of agglomerates because the concentration of dye in smaller agglomerates was rather small and accurate measurements using the spectrophotometer would be very difficult to obtain. For this type of injection, only the sizes:  $d_{\text{aggl}} \geq 9500 \mu\text{m}$  and  $9500 \mu\text{m} > d_{\text{aggl}} \geq 4000 \mu\text{m}$  are analyzed (**Figure 4-10** and **Figure 4-11**, respectively).

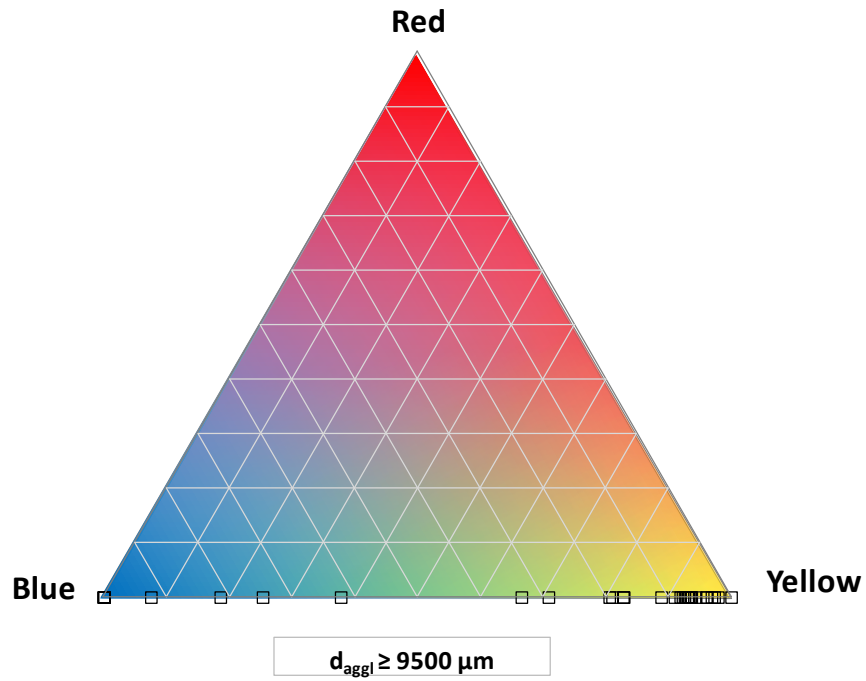


**Figure 4-10: Colour distribution in agglomerates  $d_{\text{aggl}} \geq 9500 \mu\text{m}$  for two pulse injection**

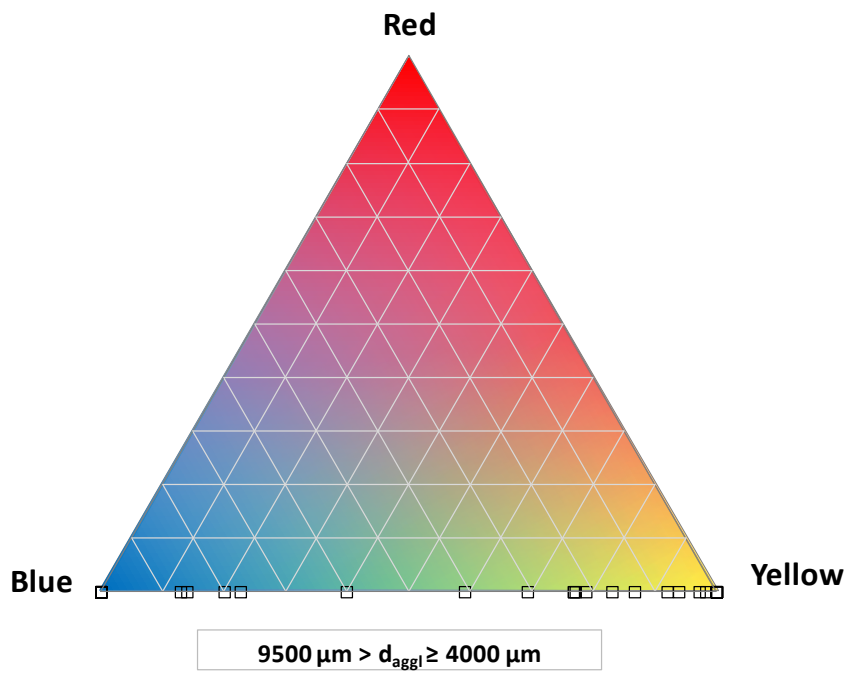


**Figure 4-11: Colour distribution in agglomerates  $9500 \mu\text{m} > d_{\text{aggl}} \geq 4000 \mu\text{m}$  for two pulse injection**

In agreement with the results presented in **Figure 4-7** and the calculation of dye in agglomerates, the concentration of yellow dye for the biggest agglomerates was higher than the blue dye concentration, with a 1:4 ratio (20% wt of blue dye and 80 wt% yellow dye) based on the total dye for recoated agglomerates. This indicated that, during the second pulse, circa 22 wt% of the solids that were being carried by the bubbles into the jet cavity were agglomerates formed after the first pulse.

In the case of the agglomerates with a diameter between 9500  $\mu\text{m}$  and 4000  $\mu\text{m}$ , **Figure 4-11** shows that the concentration of yellow in agglomerates decreased as the size of agglomerates decreased. More blue agglomerates were also found in this size range of agglomerates. The proportion of blue dye in the total dye for recoated agglomerates was around 35 wt%.

Since agglomerates formed in the first pulse (blue) were more likely to be captured by the yellow jet (second pulse), a similar behavior was expected when the number of pulses was increased from two to three and/or six. Two different experiments with three pulses injection were performed with a different colour sequence. The order of colours was inverted to verify that the specific colour added in the solution had no impact on agglomerate formation and stability.

The results presented in **Figure 4-12** are in agreement with the results obtained for the two previous injection experiments: the colour injected during the last pulse is the one that got more trapped in agglomerates (around 62 wt%), and the liquid injected in the second and the first pulse get trapped less,  $\approx 38$  wt% and  $\approx 20$  wt%, respectively.

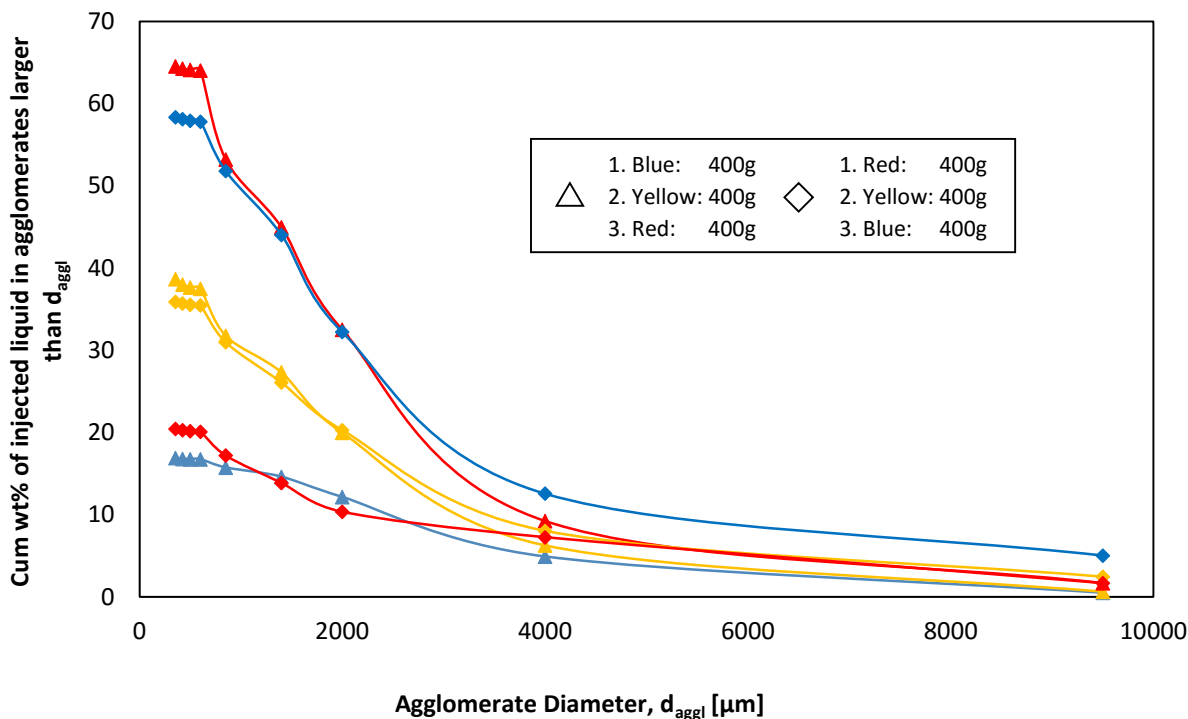


**Figure 4-12: Effect of colour sequence on the total liquid concentration in agglomerates for a three pulse injection;  $T_{0,3 \times 400 \text{ g}} = 112.5 \text{ } ^\circ\text{C}$**

In addition, it was possible to observe that, regardless of the dye that was being used, the results obtained were the same: the percentage of liquid trapped increased with the number of prior pulses. As a consequence, there was no detectable impact of the type of dye on the agglomerate formation, stability and recoating processes. The distribution of the liquid was not exactly the same in the two experiments, since there is a bit of a random process in the recoating, due to the random component in the behavior of the gas bubbles.

Some samples of the qualitative assessment for the agglomerates recovered in the experiment with the colour sequence of: blue, yellow and red are shown in **Figure 4-13**. Red colour (colour injected last) was identified in the outer layer of the agglomerates. It can be seen that in some cases a red layer recoats only blue agglomerates or only yellow agglomerates. Cases with layers of all 3 colours show an order that agrees with the colour sequence used in the experiment (bottom right).

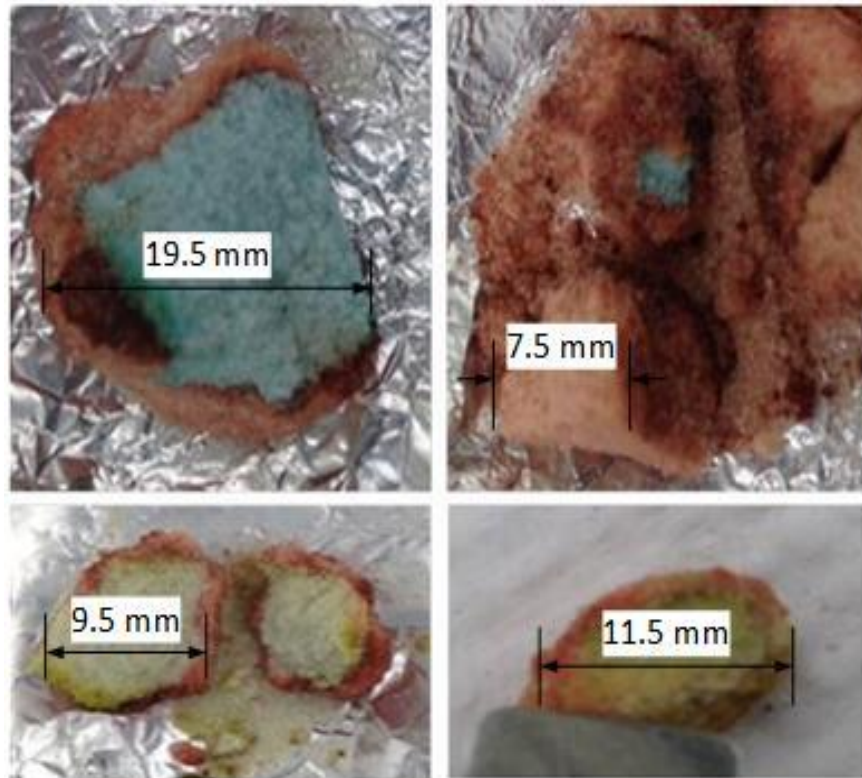


**Figure 4-13: Samples of agglomerates recovered for three pulse injection: 3 x 400 g (colour sequence of: blue, yellow and red)**



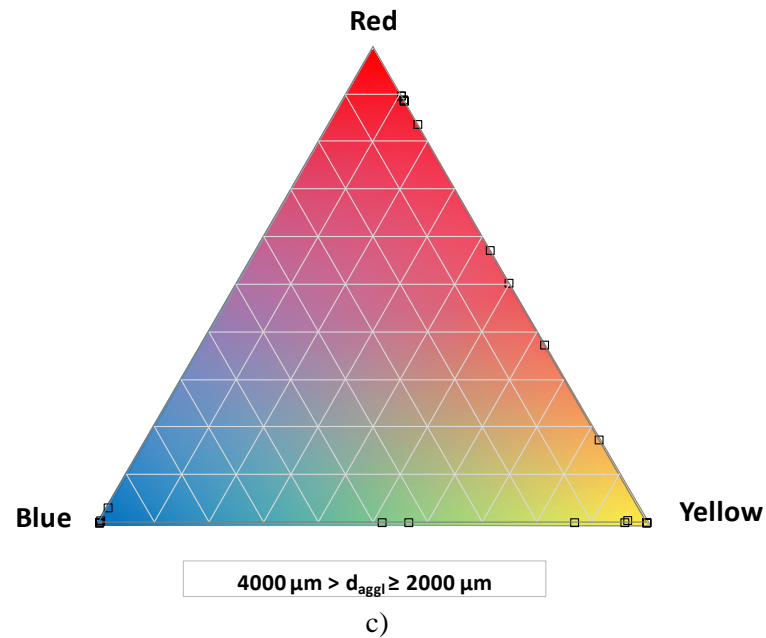
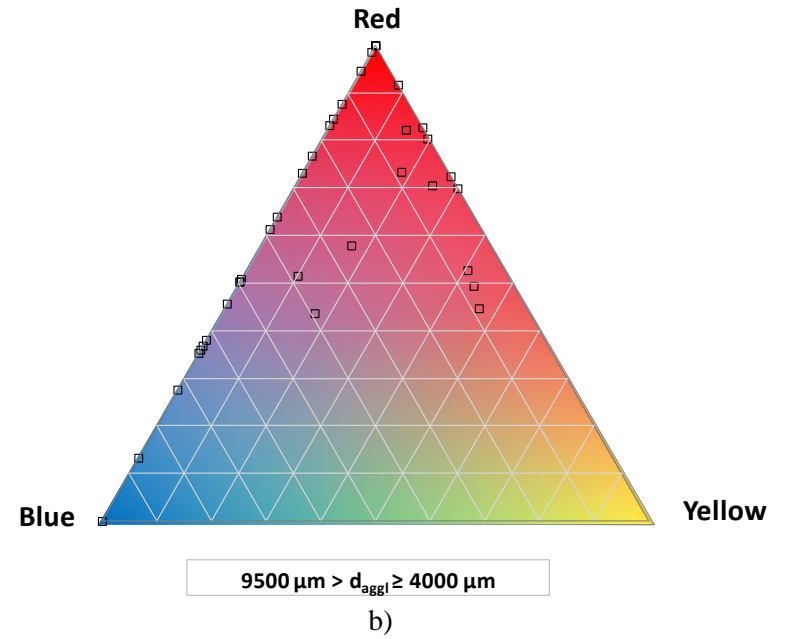
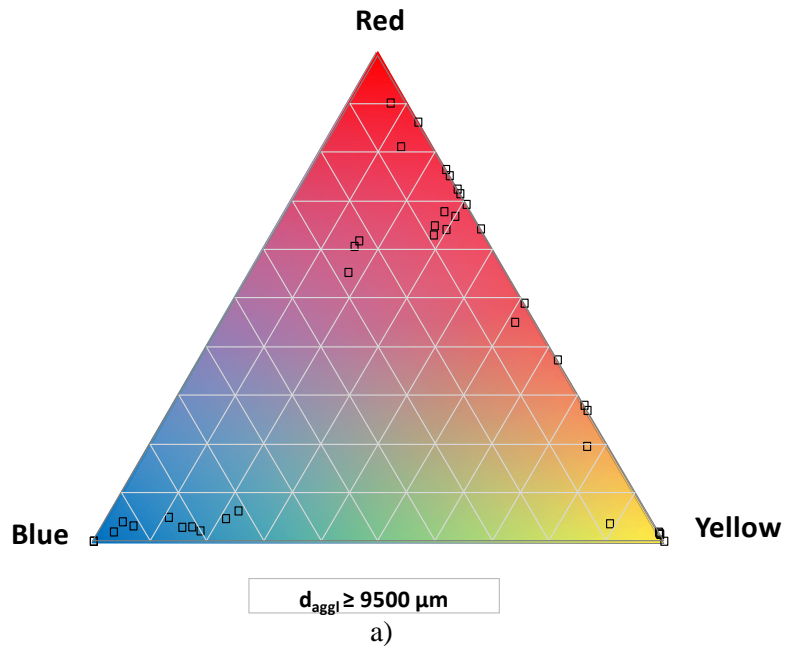


**Figure 4-14: Colour distribution in agglomerates recovered for three pulse injection (colour sequence of: blue, yellow and red)**  
 a)  $d_{\text{aggl}} \geq 9500 \mu\text{m}$  for three pulses injection b)  $9500 \mu\text{m} > d_{\text{aggl}} \geq 4000 \mu\text{m}$  c)  $4000 \mu\text{m} > d_{\text{aggl}} \geq 2000 \mu\text{m}$

The colour distribution in the agglomerates recovered from the three pulsations experiments was similar to the one found in the agglomerates of two pulsations. Similarly to the ternary plots for that experiment, **Figure 4-14** shows that the red concentration was higher in the biggest agglomerates and started decreasing with decreasing agglomerate size. For the biggest agglomerates, the concentration of red dye was around 50%, 35% for yellow and 15% for blue.

Although the second size analyzed (i.e.  $9500 \mu\text{m} > d_{\text{aggl}} \geq 4000 \mu\text{m}$ , **Figure 4-14 b**) showed a relatively little concentration of yellow in agglomerates, the general trend remained: red was the more concentrated colour and most of agglomerates were a mix of the different colours. This can be explained by considering that the process of recoating includes some randomness, and at a given time some agglomerates can be near the bottom of the bed and some might be captured by the bubbles. Based on the current configuration, it would be difficult to determine how the agglomerates formed in previous pulses were moving in the bed, and this is considered beyond the scope of the present study.

As expected, in the ternary plot that corresponds to the smallest size of agglomerates analyzed (**Figure 4-14 c**), it can be seen that the recoating was almost negligible (or at least, low enough to account for it) and the majority of the agglomerates were of a pure colour or only include two colours.

**Figure 4-15** shows the agglomerate distribution for the six pulses injection experiment. The same trend identified in the previous experiments was observed in this experiment. There was a difference in the proportion of the liquid trapped in agglomerates that belongs to each pulse and the liquid injected last was the one that got trapped the most. The difference within the colours was expected to be reduced since there were two pulses of each colour. Therefore, agglomerates from a specific colour could get captured by the bubble and get recoated with the same colour.

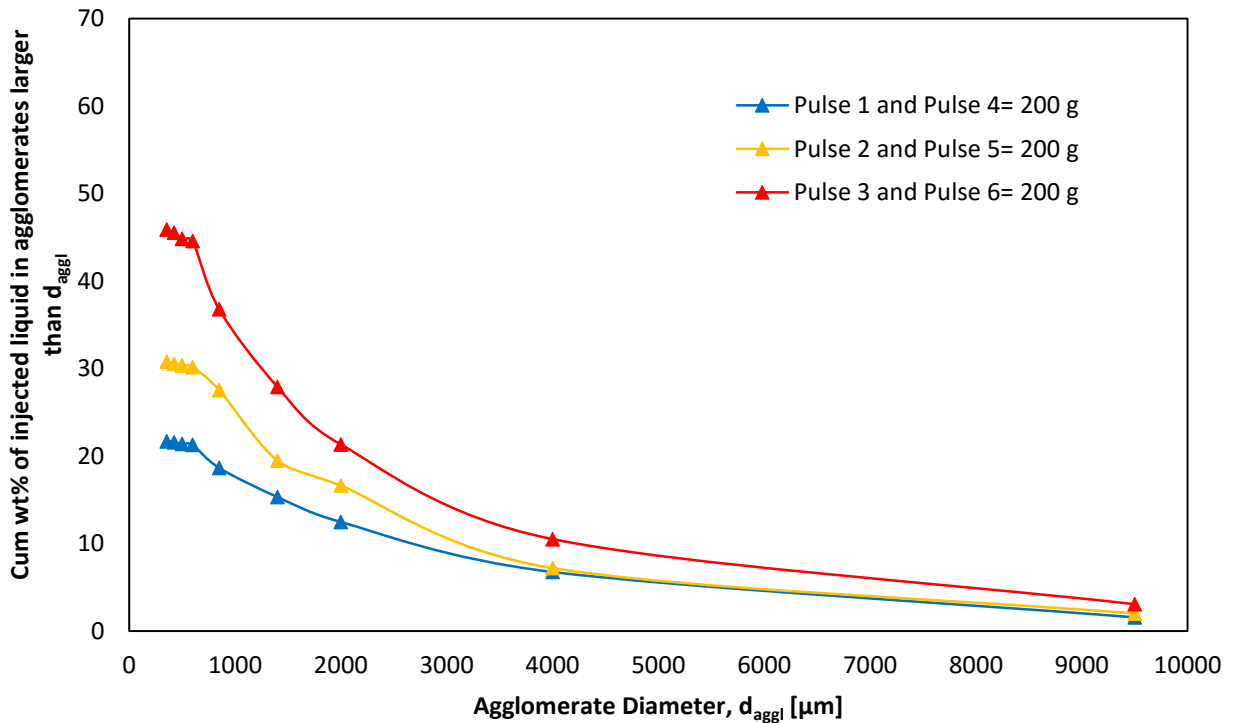


**Figure 4-15: Effect of the colour sequence on the total liquid concentration in agglomerates in a six pulse injection;  $T_{0, 6 \times 200 \text{ g}} = 111 \text{ }^\circ\text{C}$**

Finally, **Figure 4-16** displays the colour distribution for the six pulse injection. The results were consistent with previous experiments and the same colour trend was observed in the recovered agglomerates, with red being the predominant colour, and mostly in the biggest size of agglomerates. The presence of pure colour agglomerates in the smallest size of agglomerates (i.e.  $4000 \mu\text{m} > d_{aggl} \geq 2000 \mu\text{m}$ ) analyzed was lower when compared to the three pulse injections. As stated before, since there are more pulses, the recoating probability was higher, which also agrees with the results presented in **Figure 4-15**.

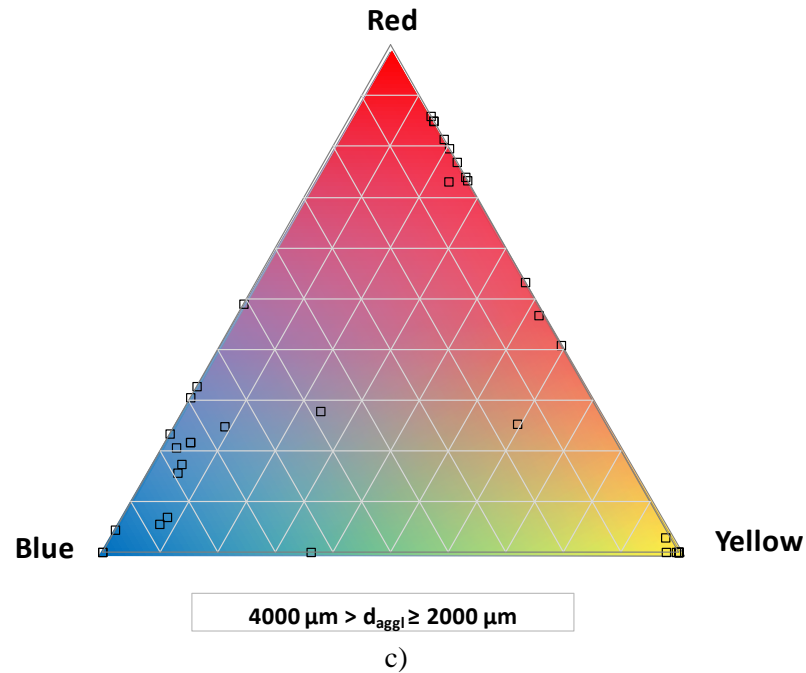
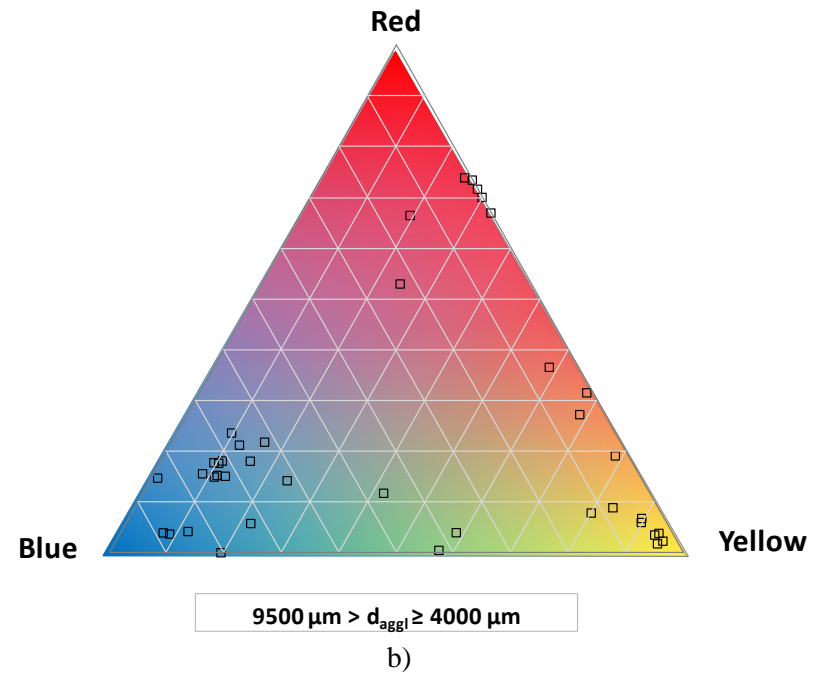
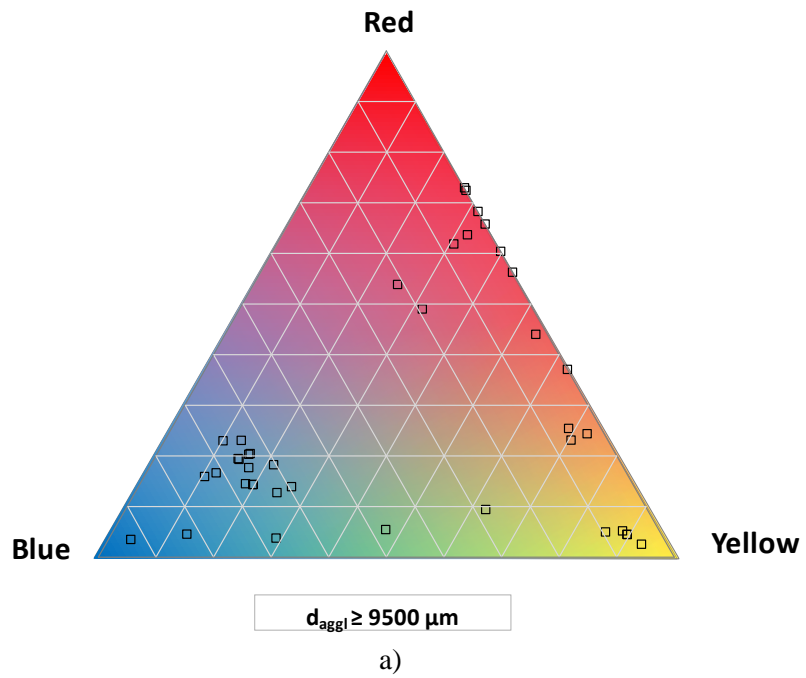
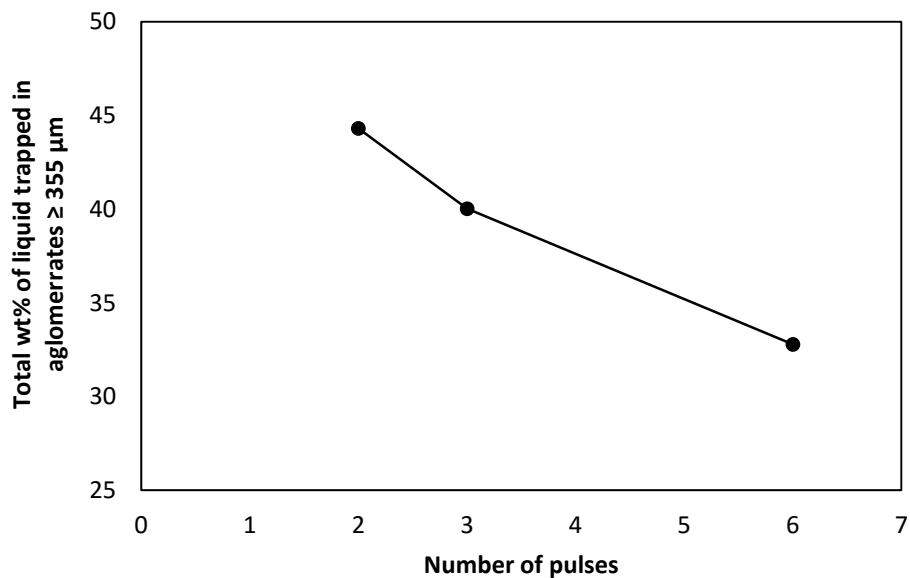


Figure 4-16: Colour distribution in agglomerates recovered for six pulse injection a)  $d_{agg} \geq 9500 \mu m$  b)  $9500 \mu m > d_{agg} \geq 4000 \mu m$  c)  $4000 \mu m > d_{agg} \geq 2000 \mu m$

It is important to highlight that the recoating of individual agglomerates is a random process (it depends on the behavior of the gas bubbles at a given time), therefore the colour distribution of the agglomerates will not be exactly the same in replicate experiments, but the trends should be the same.

The total mass of liquid trapped for each experiment is presented in **Figure 4-17**. As expected from results presented in the previous section, wetter agglomerates were obtained for a longer pulse duration (i.e. a smaller number of pulses). Additionally, the figure shows that as the number of pulses was increased, the impact of the number of pulses was initially very high and became weaker for higher numbers of pulses. According to the model (Estimation of Liquid Concentration in Solids after End of Jet Expansion), after a certain time of injection, the mass in the system reaches steady state and the percentage of wetted solids becomes constant.



**Figure 4-17: Effect of the pulse duration on the total mass of liquid trapped in agglomerates**

## Chapter 5

### 5. Evaluation of liquid spreading from wet to dry particles

#### 5.1 Introduction

The study of the liquid distribution in fluidized beds at a pilot plant scale level has mainly focused on the study of liquid trapped in agglomerates. Particles successfully wetted with a thin layer will not form agglomerates (they will form liquid bridges with other particles that are excessively weak) but they can promote liquid transfer through interparticle collisions. According to Wasylkiewicz (2014), in a Fluid Coker there are two types of liquid spreading: primary spreading, where jet-bed interactions are the determinant factors, and secondary spreading, which is due to particle-particle collisions. In the agglomerate mechanisms described by Gray (2002) and Morales (2013), the wetted particles that did not form agglomerates are not included as part of the liquid spreading.

The goal of this chapter is to achieve a better understanding of liquid spreading due to particle-particle collisions. Image analysis was used to determine the fraction of particles that came in contact with the liquid and thus, the extent to which liquid spreads from wet to dry particles.

#### 5.2 Materials and methods

The experimental procedure compared the liquid spreading in a *fluidized* bed to the liquid spreading in a *defluidized* bed. Earlier studies have shown that the liquid spreading in a defluidized bed is very slow, so the liquid distribution after drying in the defluidized state is a good approximation of the liquid distribution just before defluidization (Portghese, 2007).

### 5.2.1 Operating conditions

The experimental set up was described in Section 2.1 and the operating conditions that were used in this part of the study are listed in **Table 5-1**. In order to achieve an almost perfect liquid distribution, a special spray nozzle that produces a negligible amount of agglomerates was selected to perform the liquid injection (Mohagheghi Dar Ranji, 2014). Since virtually no agglomerates were going to be formed using this type of nozzle, the liquid was going to be distributed on the surface of individual particles and liquid spreading was going to be maximized.

In addition to the special nozzle, room temperature was selected as the initial bed temperature to perform the injection experiments, so that the drying rate was very slow. The liquid would remain on the particles surface for a time sufficiently long to maximize the possible spreading of the liquid.

**Table 5-1: Operating conditions for Injection Experiments**

Parameter	Gum Model
Spray Nozzle	Straight cylindrical tube 3.6 mm in diameter
Solids	190 $\mu\text{m}$ Sand
Fluidization Gas	Air
Atomization Gas	Nitrogen
Mass of Solids [kg]	150
Total Liquid Injected [kg]	0.3*
Liquid Flow Rate [g/s]	3.5
Fluidization Velocity [m/s]	0.1 / 0.3
Drying time [min]	10
GLR [%]	50
$T_0$ [ $^{\circ}\text{C}$ ]	16-20 $^{\circ}\text{C}$

(\*) This corresponds to a liquid to solids ratio (L/S) of 0.20 wt%. It was found by Farkhondehkavaki (2012) that at room temperature bogging will not occur below a bed-averaged liquid to solid ratio (L/S) of 0.24 wt%.

The GA solution in this part of the study was the same as the one used in the previous chapter. The concentration of dye was increased (6 wt%) to facilitate the identification of coloured particles under the microscope. The physical properties are listed in **Table 5-2**:

**Table 5-2: Physical properties of Gum Solution Used**

Parameter	Value
Colour Concentration	6% wt
pH	1.5
Viscosity	2.4 cP

### 5.2.2 Equations

To ensure that all the water in the injected liquid had been evaporated by the end of each experiment, the time required to evaporate the mass of injected liquid was calculated as shown by a previous study (Prociw, 2014):

$$F_e = \frac{m_L}{t_d} = V_{air} \times A_{bed} \times \rho_{air} \times (H^* - H_{in}) \quad 5-1$$

where  $F_e$  is the mass flow rate of evaporated liquid,  $m_L$  is the mass of injected liquid and  $t_d$  is the drying time (starting from the beginning of the spraying).  $H^*$  corresponds to the humidity of the air leaving the bed, whose temperature was monitored, assuming that the air is saturated (Portghese, 2007).  $H_{in}$  is the humidity of the gas entering the fluidized bed which was measured at the inlet air temperature, and was always below 15% (ZirGachian, et al., 2013). It is important to remark that this value was selected to maintain a safe margin during the operation.

## 5.3 Results and discussion

### 5.3.1 Characterization of initial liquid distribution

In order to estimate the maximum extent of liquid spreading under the conditions described in the previous section, a reference point (initial number of dyed particles) was necessary to determine if



there was a difference in the liquid spreading with fluidization time. As mentioned before, by defluidizing the bed just after the injection it was possible to have a good approximation of this base point. The injection experiments were performed with a solution that had a binder added in an attempt to verify that the assumption of almost perfect liquid distribution was correct.

**Figure 5-1** shows that the total mass of agglomerates obtained when the bed was defluidized just after injection was very low (under 0.15 wt%). Therefore, it was valid to assume that the liquid distribution was close to perfect. At the same time, this value represented the maximum amount of agglomerates that could be formed, since the mass of agglomerates would be reduced when the bed was kept fluidized during the drying time. The result obtained met the expectations considering that the agglomerates had more time to break due to the shear forces present inside the fluidized bed.

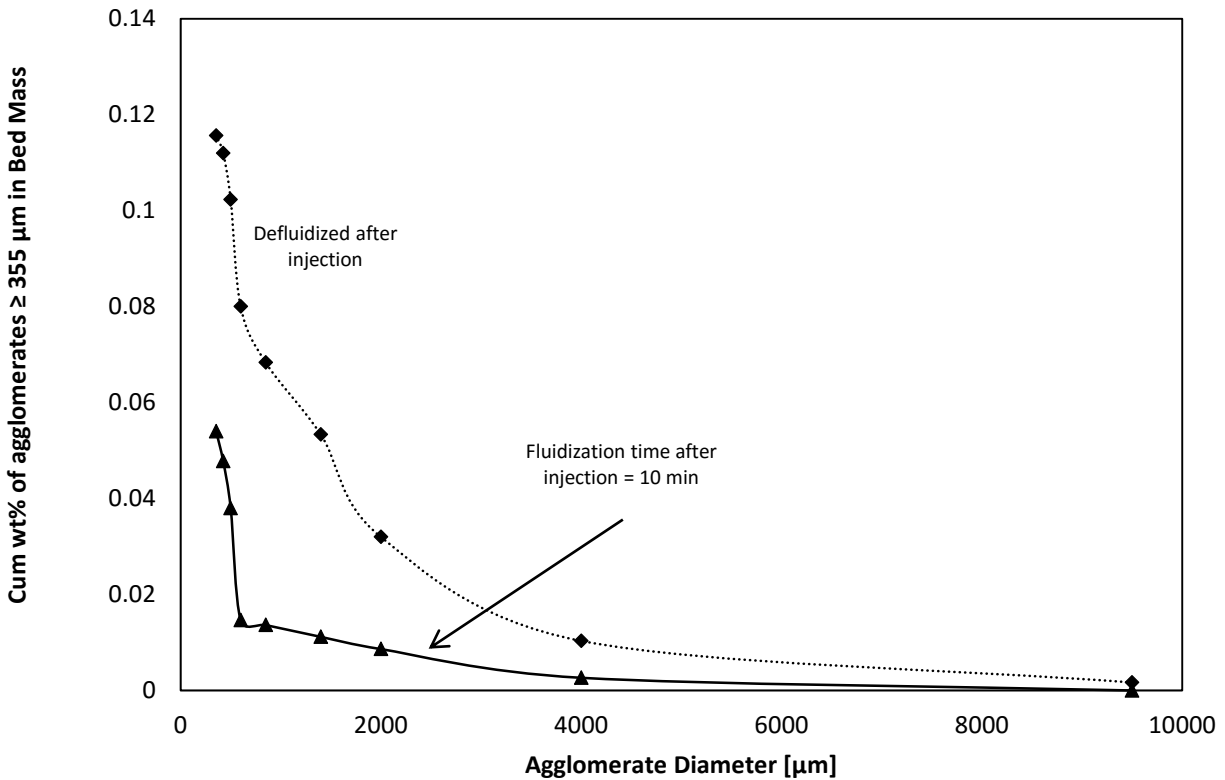


**Figure 5-1: Effect of fluidization time after injection on agglomerate formation,  $V_g = 0.3 \text{ m/s}$**

**Figure 5-2** shows that fewer agglomerates were recovered when bed fluidization was maintained during drying, but the liquid trapped in agglomerates was insignificant. Therefore, there was a negligible amount of additional liquid that was released from agglomerates during fluidization and it did not affect the results presented below. **Table 5-3** shows that almost all the liquid injected remained in the bed as a free liquid (more than 97 wt%).

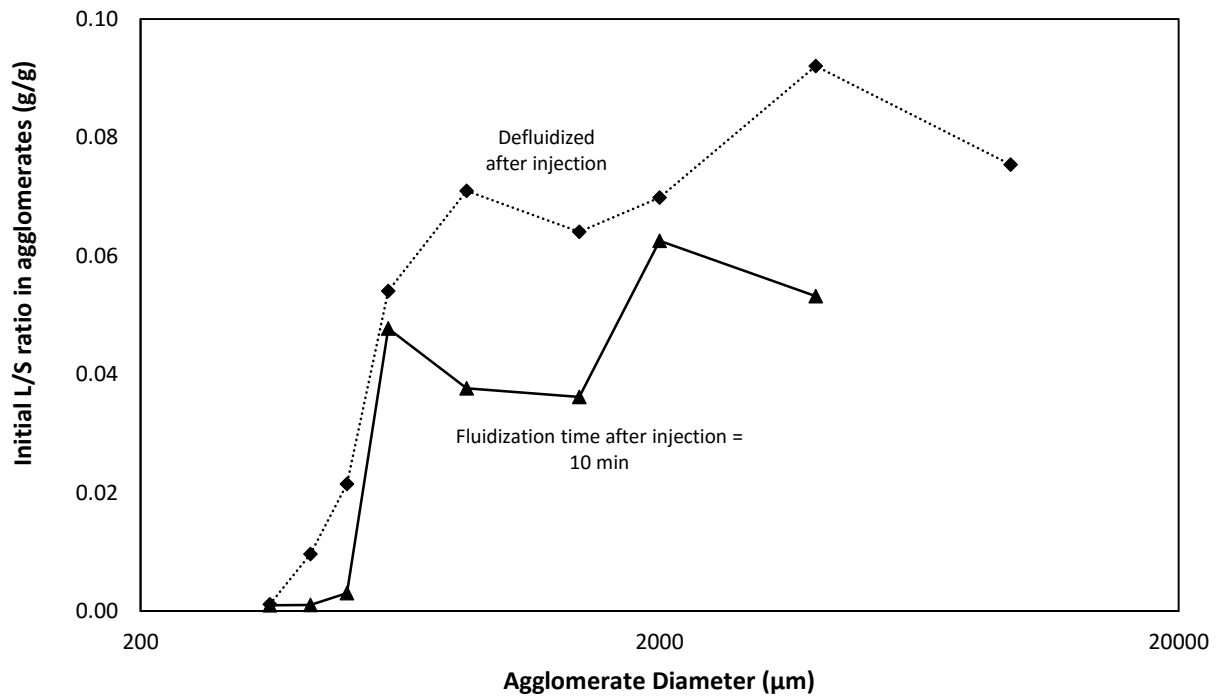


**Figure 5-2: Effect of fluidization time after injection on the initial liquid concentration in agglomerates;  $V_g = 0.3$  m/s**

**Table 5-3: Free moisture available in individual particles for experiments with different fluidization velocities**

Fluidization Time After Injection [min]	wt% of Liquid on sub-355 μm particles
0	97.4
10	99.6

The procedure to estimate the initial number of particles ( $t = 0$  min) that were in contact with the liquid was described in Section 2.7. However, it seems important to briefly recall the assumptions satisfied during the statistical analysis of the results (Chambers & Hastie, 1991):

- All observations are independent of each other.
- All observations are randomly selected.
- The distribution of each set of observations is approximately normal.
- The variances of the set of observations are close to each other.

In general, the two first assumptions were satisfied during the preparation stages and the box plots presented below could confirm that there were no highly skewed samples. Finally, the last assumption was verified for every experiment, considering the higher variance was less than twice the lower one.

**Figure 5-3** illustrates the mean fraction of dyed particles that corresponds to the three particle sizes analyzed (i.e.  $355 \mu\text{m} > d_p \geq 250 \mu\text{m}$ ,  $250 \mu\text{m} > d_p \geq 125 \mu\text{m}$  and  $125 \mu\text{m} > d_p \geq 75 \mu\text{m}$ ). Since the F value calculated was not greater than the F critical, it was not possible to reject the null hypothesis. Therefore, it could be concluded that there was no statistical difference between all means of fractions, and the differences found in the means could be due to chance.

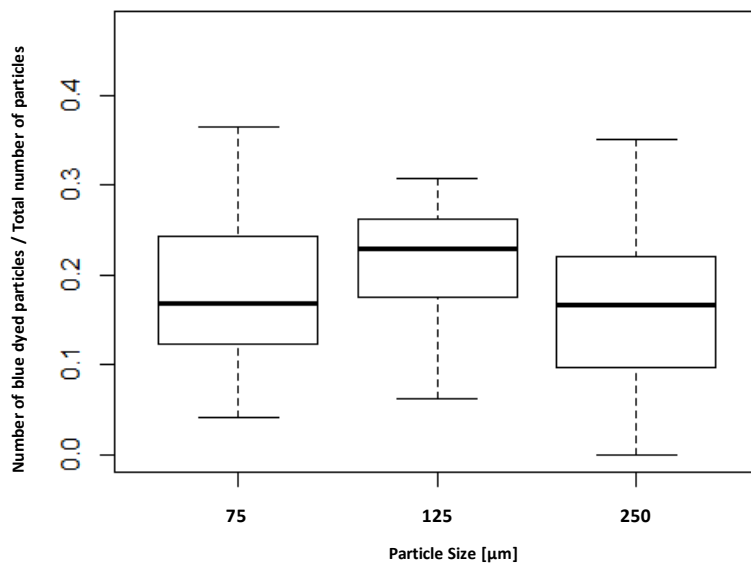


**Figure 5-3: Fraction of dyed particles for different individual size particles;  $V_g = 0.3$  m/s, defluidized just after injection**

**Table 5-4: Results for ANOVA test;  $V_g = 0.3$  m/s, Defluidized just after injection**

	Df	Sum Sq	Mean Sq	F value	Pr(>F)	F Critical
<b>Between</b>	2	0.0209	0.0104	1.1570	3.22E-01	3.1580
<b>Within</b>	57	0.5139	0.0090			

The fact that there were no differences in the values of the fraction of dyed particles means indicated that there was good mixing of solids while the liquid was being sprayed, enough to have even fraction of dyed particles in all individual particle sizes that were analyzed. The total initial fraction of dyed particles was 0.19. To verify the experimental value, the concentration of liquid in solids at steady state (after many jet expansions) was calculated, using the theoretical model described in Section 2.5. The results are illustrated in **Figure 5-4**.

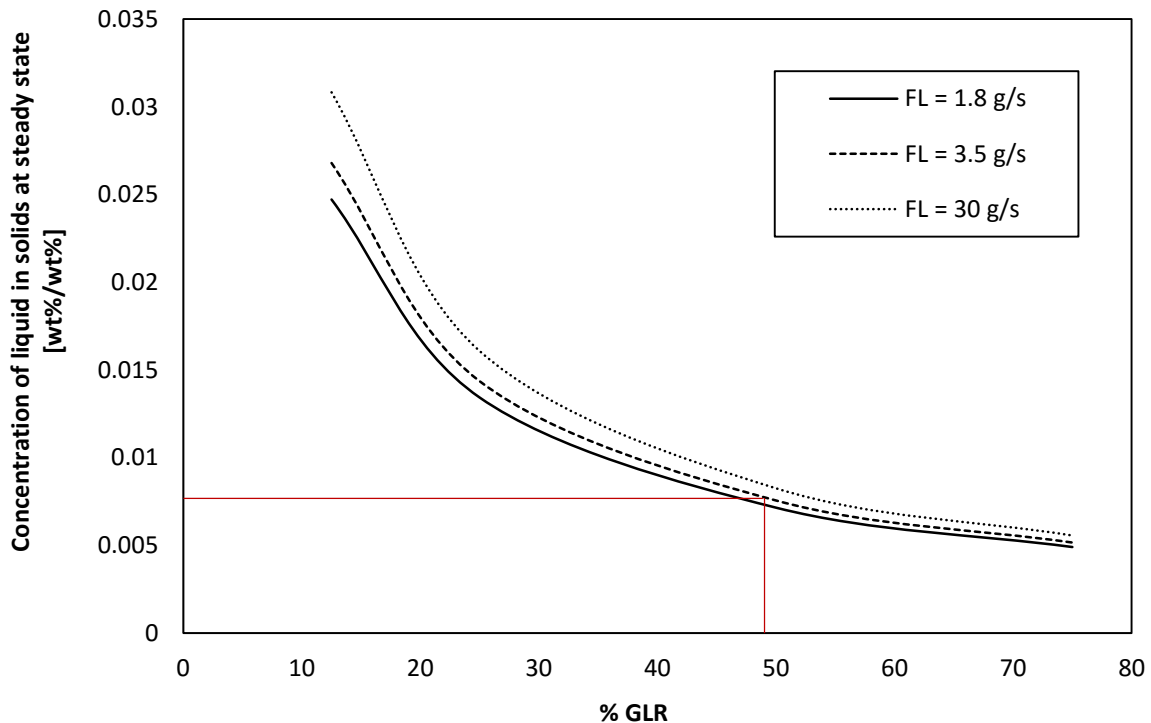


**Figure 5-4: Concentration of wetted particles according to the model for the Estimation of Liquid Concentration in Solids after End of Jet Expansion**

The ratio of the measured mass of wetted particles to the mass of wetted particles according to the model (concentration of liquid in wetted particles at steady state) was equal to 0.72. This result indicates that the model overestimates the mass of particles that are getting wet during the liquid injection.

When calculating the ratio between the solids entering the jet cavity and the ones exiting it, it was found that 11 wt% of the solids that were being carried in the wakes of the bubbles released from the jet tip were solids carried into the jet cavity by bubbles captured by the jet. The remaining 89 wt% corresponded to solids that belonged to the emulsion phase, near the jet tip. Imperfect mixing between the solids coming from the jet cavity and the solids from the emulsion phase may explain these results.

Poor mixing was much less of an issue, on the other hand, with a regular TEB feed nozzle operating at 2% GLR of the kind used in all experiments described in the previous chapters, since 70 wt% of the solids in the wake of the bubble released from the jet tip came from the jet cavity.

### 5.3.2 Spreading of liquid from wet to dry particles

Since the initial number of dyed particles was already estimated, experiments keeping the bed fluidized until complete drying were performed to determine whether the fraction of dyed particles changes.

According to **Equation 5-1**, the calculated time required to fully dry the bed solids under the operating conditions listed in **Table 5-1** was equal to ten minutes. The same fluidization velocity used during liquid injection was used during drying, so that the liquid spreading was equally promoted by the fluidization gas during both injection and drying.

As presented in **Figure 5-1** and **Figure 5-2**, the total mass of agglomerates and the liquid trapped in agglomerates were negligible and so the liquid spreading was due to the particle-particle collisions.

**Figure 5-5** and **Table 5-5** show the results of the statistical analysis. Since the calculated F value was smaller than the F critical, the null hypothesis was valid. Therefore, it could be concluded that there was no statistical difference between all means of fractions, and the differences found in the means could be due to chance. Failing of rejecting the null hypothesis was an indication that, at this velocity, the mixing of solids was even in all particle sizes.

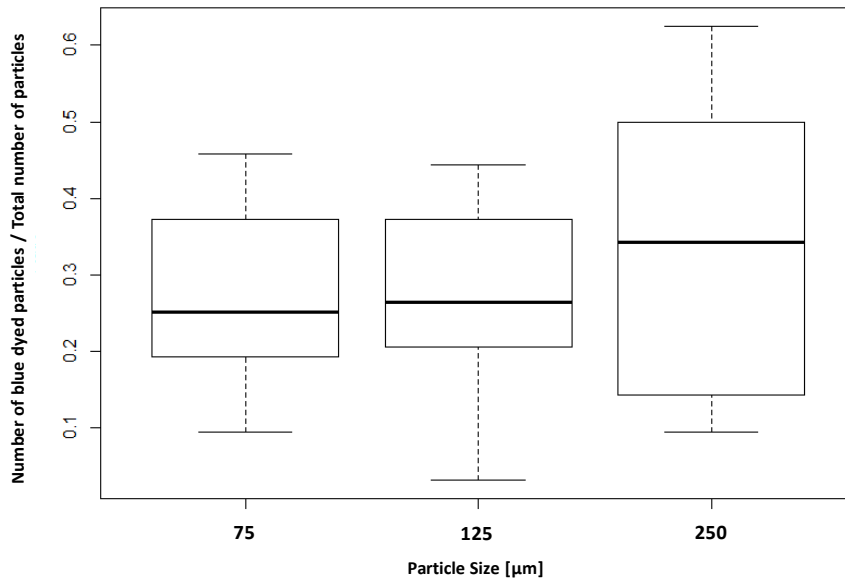


**Figure 5-5: Fraction of dyed particles for different individual size particles;  $V_g = 0.3$  m/s, Drying time = 10 min**

**Table 5-5: Results for ANOVA test;  $V_g = 0.3$  m/s, Drying time = 10 min**

	Df	Sum Sq	Mean Sq	F value	Pr(>F)	F Critical
<b>Between</b>	2	0.0472	0.0236	1.2620	2.91E-01	3.1650
<b>Within</b>	55	1.0280	0.0187			

**Figure 5-6** shows that there was an increment in the total fraction of dyed particles (from 0.19 to 0.29) when the bed was kept fluidized after the injection. The solid mixing was enhanced by keeping the fluidization gas on during injection and thus the liquid spreading was promoted by particle-particle collisions.

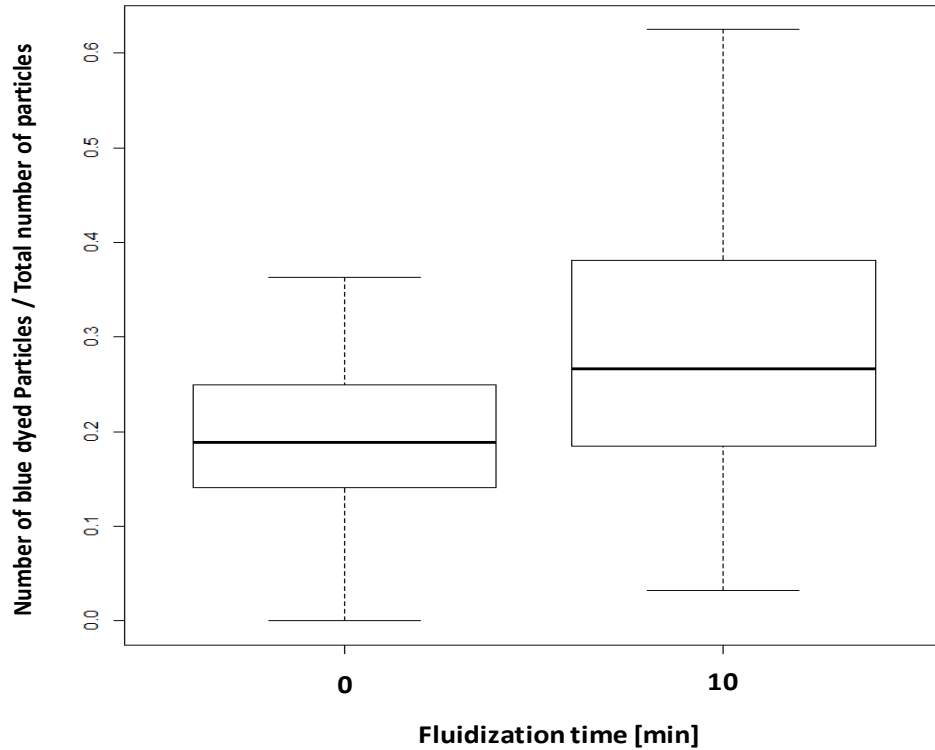
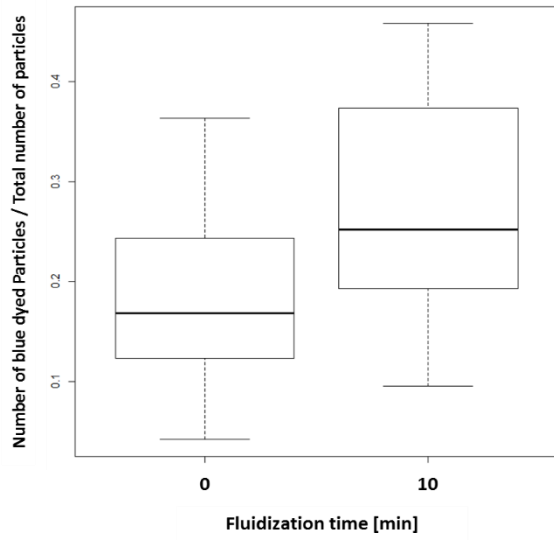
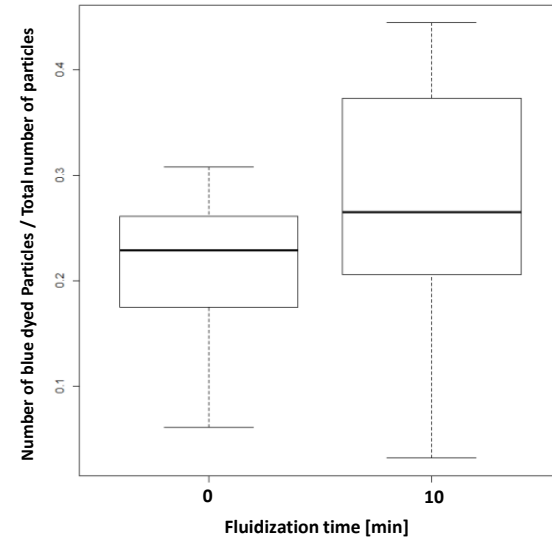


**Figure 5-6: Fraction of dyed particles for different individual size particles;  
 $V_g = 0.3 \text{ m/s}$**

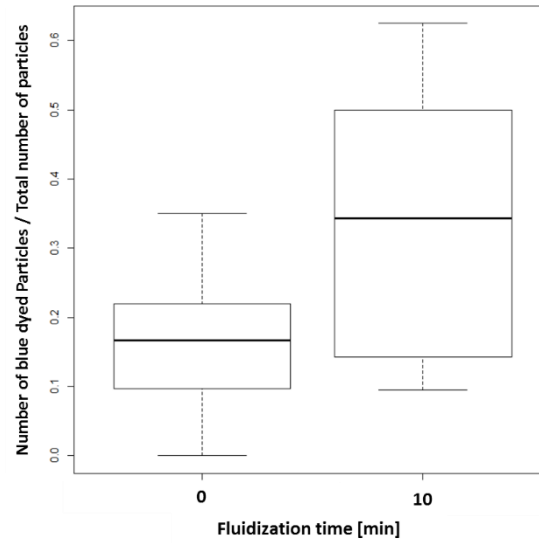
Additionally, this result indicates that each originally wet particle redistributed its moisture to about 0.5 dry particles, on the average, before drying completely. Under conditions relevant to reactors such as Fluid Cokers, drying typically occurs within a few seconds, in the absence of agglomerates (Morales M., 2013). In the current study, experiments were operated at low temperature to greatly increase the drying time (about 10 minutes) and, hence, the time for any spreading to occur. In reactors such as Fluid Cokers, liquid will therefore spread to less than 0.5 dry particles. Consequently, it can be concluded that liquid spreading is not a significant factor in such reactors.



a)



b)



c)

**Figure 5-7: Effect of fluidization time after injection in liquid spreading;  
a)  $125 \mu\text{m} > d_p \geq 75 \mu\text{m}$ ; b)  $250 \mu\text{m} > d_p \geq 125 \mu\text{m}$ ; c)  $355 \mu\text{m} > d_p \geq 250 \mu\text{m}$**



**Table 5-6: Results for Welch Two Sample t-test;  $V_g$  0.3 m/s,**

Size [ $\mu\text{m}$ ]	t	df	p-value	t critical ( $\pm$ )	95 percent confidence interval
<b>125 <math>\mu\text{m}</math> &gt; <math>d_p \geq 75 \mu\text{m}</math></b>	2.759	37.467	0.0089	2.0253	0.023 ; 0.153
<b>250 <math>\mu\text{m}</math> &gt; <math>d_p \geq 125 \mu\text{m}</math></b>	1.852	30.413	0.0737	2.0411	-0.005 ; 0.112
<b>355 <math>\mu\text{m}</math> &gt; <math>d_p \geq 250 \mu\text{m}</math></b>	3.183	28.428	0.0035	2.0470	0.58 0.265

Finally, statistical analysis was carried out for each pair of consecutive particle sizes to verify if the differences in the means were statically significant and to find out where the differences lay (**Figure 5-7**). According to the t-test results (**Table 5-6**), the means of fractions of dyed particles from each experiment significantly differed in two of three sizes analyzed.

- 125 $\mu\text{m}$  >  $d_p \geq 75 \mu\text{m}$
- 355  $\mu\text{m}$  >  $d_p \geq 250 \mu\text{m}$

Also, it shows that the difference found was not due to chance but due to the operating condition that was changed (i.e. fluidization time), i.e. there was redistribution of the moisture by particle-particle collisions.

## Chapter 6

### 6. Conclusions and recommendations

#### 6.1 Conclusions

A new cold model that simulates the agglomerate formation resulting from the injection of liquid in gas-solid fluidized beds was developed and tested at pilot plant scale. Since Fluid Coking<sup>TM</sup> was selected as an example system to model, a Plexiglas solution system that had been previously shown to model it at pilot plant scale was used as a reference. The model developed in this thesis allowed not only to analyze the agglomerate size distribution in the total mass of agglomerates formed, but also to accurately estimate the liquid concentration in all of them. The model is flexible and the agglomerate strength can be modulated by adjusting the concentration of binder or solution viscosity; the viscosity of the model solution can be reduced by reducing its pH. Moreover, the binder is stable in a wide range of temperatures (100 to approximately 200 °C)

The results of series of injection experiments showed that at higher bed average temperatures during injection more agglomerates were formed and that they are bigger and contained more liquid. These results were in agreement with previous findings that indicate that the breakage process is reduced at higher temperatures. It is believed that, at lower temperatures, the binder solution remained active for longer, so that the liquid bridges did not solidify as quickly and the agglomerates had more time to break while dry individual particles could be “picked up” making the agglomerates drier. Thus, increasing the average bed temperature worsens the quality of the liquid distribution.

On the other hand, lowering the liquid viscosity enhanced the liquid distribution and reduced the total mass of agglomerates. The initial liquid distribution was improved since solutions with lower viscosities would form smaller droplets when sprayed, and smaller droplets would distribute more uniformly over the particles surface.

Good agreement with the Plexiglas results were found. Overall, the best match of the Plexiglas agglomerate size distribution was obtained with the following injection conditions:

- 5 wt% GA - 2 wt% Blue No. 1, pH 1.5
- Initial bed temperature  $T_0 = 110\text{ }^\circ\text{C}$
- Four liquid injections of 300 g separated by enough time for full recovery of the bed temperature

Injection duration had a significant impact on the agglomerate formation and stability. Shorter pulses improved the initial liquid distribution and, as a result, fewer agglomerates were formed. The improvement stopped to be significant when the pulse duration approached the time for steady state of the liquid concentration in wetted agglomerates. It was also found that a larger proportion of the liquid that was injected in later pulses was trapped in agglomerates. This can be explained by considering that a later injection leads to the formation of new agglomerates and to the recoating of existing agglomerates formed during previous injections. Also, it was possible to determine that there was recoating of bigger agglomerates due to the fact that they were more likely to be captured by the jet of later injections. When the number of pulses was increased, more recoating was identified in individual agglomerates. Despite these phenomena, the impact of the injection duration had a greater impact on the agglomerate formation since having shorter pulses resulted in a better liquid distribution, and so less agglomerates were recovered.

There was liquid spreading (distribution of the moisture) due to particle-particle collisions from wet to dry particles after the liquid injection. However, it is not practically significant for industrial reactors such as the Fluid Cokers.

## 6.2 Recommendations

- The model showed good agreement with the agglomerate size distribution of the reference method and thus, with the Fluid Coking<sup>TM</sup> process. One drawback of the model developed in this thesis, when comparing it with the Fluid Coking<sup>TM</sup> process, is its higher latent heat

of vaporization. It is recommended to perform injection experiments heating the GA solution before injection to better match the fast evaporation in Fluid Coking™.

- The use of different dyes gave a good idea of how agglomerates are travelling in the bed. Further experiments with moving nozzles or interacting nozzles are recommended to enhance the understanding of the solids mixing in fluidized beds. Also, sampling in different sections of the bed could help to further extend the understanding of solids mixing.
- Experiments using pulses with very little time between successive pulses are recommended to prevent agglomerates from settling; this would help identify the type of agglomerates entering the jet cavity in the wake of the bubbles when enough time is given between successive pulses to allow for agglomerate segregation.
- The maximum extent of liquid spreading from wet to dry particles was estimated with a spray nozzle that uses high a gas-to-liquid ratio (GLR) and produces a negligible amount of agglomerates. Since everything is simplified under these conditions, it is recommended to use the same technique when using a real industrial nozzles, such as the TEB. This will allow to fully characterize the liquid distribution on bed solids (liquid trapped in agglomerates and distributed as a free liquid on individual particles).
- Statistically significant differences were found in the liquid spreading in a fluidized bed and the liquid spreading in a defluidized bed. However, the error in the measurements is relatively high. It is recommended to further increase the concentration of dye or increase the total mass of liquid injected, by injecting more pulses of GA solution, and thus verify the results presented in this work.

## References

- Aminu, M. O., Elliott, J. A., McCaffrey, W. C. & Gray, M. R., 2004. *Fluid Properties at Coking Process Conditions*. 43, 2929-2935 ed. s.l.:American Chemical Society.
- Andersson, M. et al., 2008. Dual Fortification of Salt with Iodine and Iron: a Randomized, Double-blind, Controlled Trial of Micronized Ferric Pyrophosphate and Encapsulated Ferrous Fumarate in Southern India. *The American Journal of Clinical Nutrition*, 88(5), pp. 1378-1387.
- Ariyapadi, S. et al., 2003. State-of-the art X-ray Imaging Technique to Study the Dispersion of Gas-Liquid Jets Injected into Fluidized Beds. *International Journal of Chemical Reactor Engineering*, 1(A56).
- Aulton, M. E., 2002. *Pharmaceutics: The Science of Dosage Form Design*. 2nd ed. s.l.:Elsievier Limited.
- Base, T. E., Chan, E. W., Kennet, R. D. & Emberley, D. A., 1999. *Nozzle for Atomizing Liquid in Two Phase Flow*. US6003789 A.
- Benali, M., Gerbaud, V. & Hemati, M., 2009. Effect of Operating Conditions and Physico-chemical Properties on the Wet Granulation Kinetics in High Shear Mixer. *Powder Technology*, 190(1–2), p. 160–169.
- Canadian Association of Petroleum Producers, 2014. *Basic Statistics*. [Online] Available at: <http://www.capp.ca/>
- Chambers, J. & Hastie, T., 1991. *Statistical Models in S*. s.l.:Chapman and Hall.
- Cozic, C. et al., 2009. Analysis of arabic gum: Study of degradation and water desorption processes. *Food Hydrocolloids*, pp. 1930-1934.
- Davies, W. L. & Gloor, W. T. J., 1972. *Batch Production of Pharmaceutical Granulations in a Fluidized Bed 11: Effects of Various Binders and Their Concentrations on Granulations and Compressed Tablets*. Vol 61 Issue 4 ed. s.l.:Journal of Pharmaceutical Sciences.
- Dhanalakshmi, K., Ghosal, S. & Bhattacharya, S., 2011. Agglomeration of Food Powder and Applications. *Critical Reviews in Food Science and Nutrition*, Volume 51, p. 432–441.

Elkolaly, H. H., 2015. *Effect of Spray Jet Interactions on the Liquid Distribution in a Fluidized Bed*. M.E.Sc. Thesis ed. s.l.:The University of Western Ontario.

ExxonMobil, 2014. *FLUID COKING™ Conversion Technology*. [Online]

Available at:

[http://www.exxonmobil.com/Apps/RefiningTechnologies/Files/sellsheet\\_05\\_fluidcoking.pdf](http://www.exxonmobil.com/Apps/RefiningTechnologies/Files/sellsheet_05_fluidcoking.pdf)

FAO, 1999. *Compendium of food additive specifications - Addendum 7*. Rome: FAO.

Farkhondehkavaki, M., 2012. *Developing Novel Methods to Characterize Liquid Dispersion in a Fluidized bed*. PhD Thesis ed. s.l.:The University of Western Ontario.

Faure, A., York, P. & Rowe, R., 2001. Process Control and Scale-up of Pharmaceutical Wet Granulation Processes: a Review. *European Journal of Pharmaceutics and Biopharmaceutics*, 52(3), pp. 269-277.

Flury, M. & Flühler, H., 1994. Brilliant Blue FCF as a Dye Tracer for Solute Transport Studies - A Toxicol. *Journal of Environmental Quality*, 23(5), pp. 1108 - 1112.

Gaonkar, A. G., Vasisht, N., Khare, A. R. & Sobel, R., 2014. *Microencapsulation in the Food Industry: A Practical Implementation Guide*. s.l.:Elsevier.

Gary, J. H. H. G. E. K. M. J., 2007. *Petroleum Refining - Technology and Economics (5th Edition)*. s.l.:Taylor & Francis.

Gray, M. R., 2002. *Fundamentals of Bitumen Coking Processes Analogous to Granulation*. Volume 80 ed. s.l.:The Canadian Journal of Chemical Engineering,.

Hoover, A. et al., 1996. An Experimental Comparison of Range Image Segmentation Algorithms. *IEEE Transactions on Pattern Analysis and Machine Intelligence*, 18(7), pp. 673-689.

House, P. K., 2007. *Interaction of Gas-Liquid Jets with Gas-Solid Fluidized Beds: Effect on Liquid-Solid Contact and Impact on Fluid Coker Operation*. PhD. Thesis ed. s.l.:The University of Western Ontario.

Imeson, A., 1997. *Thickening and Gelling Agents for Food*. 2nd ed. s.l.:Springer-Science + Business Media.

- Iveson, S. M., Litster, J. D., Hapgood, K. & Ennis, B. J., 2001. Nucleation, growth and breakage phenomena in agitated wet granulation processes: a review. *Powder Technology*, 117(3–39).
- Iveson, S. & Page, N., 2001. Tensile bond strength development between liquid-bound pellets during compression. *Powder Technology*, Volume 117, pp. 113-122..
- Jia, H., Kim, C.-S. & Kuo, C.-C. J., 2014. *Interactive Segmentation Technique: Algorithms and Performance Evaluation*. s.l.:Springer Singapore.
- Knapper, B. A., Gray, M. R., Chan, E. W. & Mikula, R., 2003. Measurement of Efficiency of Distribution of Liquid Feed in a Gas-Solid Fluidized Bed Reactor. *International Journal of Chemical Reaction Engineering*, Volume 1, p. Article A35.
- McDougall, S. et al., 2005. Effect of Liquid Properties on the Agglomerating Tendency of a Wet Gas–Solid Fluidized Bed. *Powder Technology*, Volume 149, p. 61– 67.
- McDougal, S. L., 2004. *On-line Detection of Gas-Solid Fluidized Bed Behaviour in the Precense of Liquid*. M.E.Sc Thesis ed. s.l.:The University of Western Ontario.
- Mohagheghi Dar Ranji, M., 2014. *Impact of Local Bed Hydrodynamics on Jet-Bed Interaction*. s.l.:The University of Western Ontario.
- Morales M., C. B., 2013. *Development and Application of an Experimental Model for the Fluid Coking<sup>TM</sup> Process*. M.E.Sc. ed. s.l.:The University of Western Ontatrio.
- Morales M, C. B., 2013. *Development and Application of an Experimental Model for the Fluid Coking<sup>tm</sup> Process*. s.l.:The University of Western Ontario.
- National Energy Board, 2014. *Canada’s Energy Future: Energy Supply and Demand Projections to 2035 - Crude Oil and Bitumen Highlights*. [Online]  
Available at: <http://www.neb-one.gc.ca/clf-nsi/rnrgynfmtn/nrgyrprt/nrgyfr/2011/fctsht1134crdl-eng.html>
- Nie, S.-P.et al., 2013. The core carbohydrate structure of Acacia seyal var. seyal (Gum arabic). *Food Hydrocolloids*, pp. 221-227.
- Nieuwmeyer, F., 2009. *Process Understanding on High Shear Granulated Lactose Granules During and After Drying*. PhD thesis ed. s.l.:Utrecht University.

- Ortega-Rivas, E., Juliano, P. & Yan, H., 2005. *Food Powders: Physical Properties, Processing, and Functionality*. s.l.:Food Enigeeting Series.
- Parikh, D. M., 2005. *Handbook of Pharmaceutical Granulation Technology*. 2nd ed. s.l.:Taylor and Francis.
- Parikh, D. M., 2005. *Handbook of Pharmaceutical Granulation Technology*. Boca Raton: Taylor & Francis Group.
- Parveen, F., 2011. *Stability of liquid-solid agglomerates in gas-solid fluidized beds*. M.E.Sc. Thesis ed. s.l.:The University of Western Ontario.
- Phillips, C., Haidar, N. & Poon, Y., 1985. Kinetic models for the thermal cracking of Athabasca bitumen: The effect of the sand matrix. *Fuel*, pp. 678-691.
- Pont, V., Saleh, K., Steinmetz, D. & Hémati, M., 2001. *Influence of Physicochemical Properties on the Growth of Solid Particles by Granulation in Fluidized Bed*. 97 - 104 ed. s.l.:Powder Technology.
- Portghese, F., 2007. *Interactions between Gas-Liquid Jets and Gas-Solid Fluidized Beds*. s.l.:The University of Western Ontario.
- Poutiainen, S., 2013. *Fluidized Bed Spray Granulation Process Monitoring by Acoustic Emission*. s.l.: University of Eastern .
- Prociw, N. A., 2014. *Effect of Nozzle Geometry on Jet Bed Interaction: Experiments with Commercial Scale Nozzles and Eroded Nozzles*. s.l.:The University of Western Ontario.
- Prociw, N. A., 2014. *Effect of Nozzle Geometry on Jet Bed Interaction: Experiments with Commercial Scale Nozzles and Eroded Nozzles*. M.E.Sc. Thesis ed. s.l.:The University of Western Ontario.
- Ranken, M. D. & Baker, C. G. J., 1997. *Food Industries Manual*. 24 ed. s.l.:Blackie Academic and Proffesional.
- Riddell, G. L. & Davies, C. W., 1931. *A Study of Gum Arabic, Part I. Viscosity and Adsorption Measurements*. 35 (9), pp 2722–2731 ed. s.l.:The Journal of Physical Chemistry.



ROEPER, 2015. *Raw\_Materials\_for\_Food\_Industry | Jelly Agents: Hobby Takt*. [Online]  
Available at: <http://www.hobbytakt.com/products/3856466109.pdf>

Salman, A. D., Hounslow, M. J. & Seville, J. P., 2007. *Handbook of Powder Technology*.  
Volume 11 ed. s.l.:Elsevier B.V..

Sanchez Careaga, F. J., 2014. *Hydrodynamics in Recirculating Fluidized Bed Mimicking the Stripper Section of the Fluid Coker*. PhD Thesis ed. s.l.:The University of Western Ontario.

Sato, Y., Yamamoto, Y. & Kamo, T. a. M. K., 1992. Fluid Catalytic Cracking of Alberta Tar Sand Bitumen. *Energy Fuels*, pp. 821-825.

Shamlou, P., Liu, Z. & Yates, J., 1990. Hydrodynamic Influences on Particle Breakage in Fluidized Beds. *Chemical Engineering Science*, 45(4), p. 809–817.

SIGMA-ALDRICH, 2015. *Catalog Products*. [Online]  
Available at: <http://www.sigmaaldrich.com/catalog/product/sigma/g9752>

Simons, S. & Fairbrother, R., 2000. *Direct Observations of Liquid Binder–Particle Interactions: the Role of Wetting Behavior in Agglomerate Growth*. 110 44–58. ed. s.l.:Powder Technology .

Singh, J., Kumar, S. & Garg, M., 2012. Kinetic Modelling of thermal cracking of petroleum residues: A critique. *Fuel Processing Technology*, pp. 131-144.

Speight, J., 2011. *Handbook of Industrial Hydrocarbon Processes*. s.l.:Elsevier.

Szulc, K. & Lenart, A., 2010. Effect of agglomeration on flowability of baby food powders.. *Journal of Food Science*, 75(5), pp. E276-E284.

Weber, S. C., 2009. *Agglomerate Stability in Fluidized Beds*. PhD Thesis ed. s.l.:The University of Western Ontario.

Woolard, I. N. M. & Potter, O. E., 1968. Solid Mixing in Fluidized Beds. *AIChE Journal*, 14(3), pp. 388 - 391.

Xuereb, C., Laguérie, C. & Baron, T., 1991. Etude Du Comportement De Jets Continus Horizontaux Ou Inclinés Introduits Dans Un Lit Fluidisé Par Un Gaz I: Morphologie Des Jets. 67(1).

Yadong, Y., Mohammad, A., Cheol-Ho, P. & Donghwa, C., 2012. Characterisation of Interactions between Fish Gelatin and Gum Arabic in Aqueous Solutions. *Food Chemistry*, 135(2), pp. 555-561.

ZirGachian, M. A., Soleimani, M., Briens, C. & Berruti, F., 2013. Electric Conductance Method for the Assessment of Liquid–Gas Injection into a Large Gas–Solid Fluidized. *Measurement*, 46(2), pp. 893-903.

## Appendix A

### A.1 Gum Arabic

Gum Arabic<sup>5</sup> can be defined as the “dried exudates obtained from the stems and branches of *Acacia Senegal* or *Acacia Seyal*” (FAO, 1999), which is used primarily as an adhesive agent, emulsifier, stabilizer or thickener. It is considered as a high molecular weight mixture of branched polymer of monosaccharides (i.e., galactose, rhamnose or arabinose), carboxylic acids (i.e., glucuronic acid) and their salts (SIGMA-ALDRICH, 2015) (Nie, et al., 2013).

The following figure shows a proposed structure of the molecule (ROEPER, 2015):

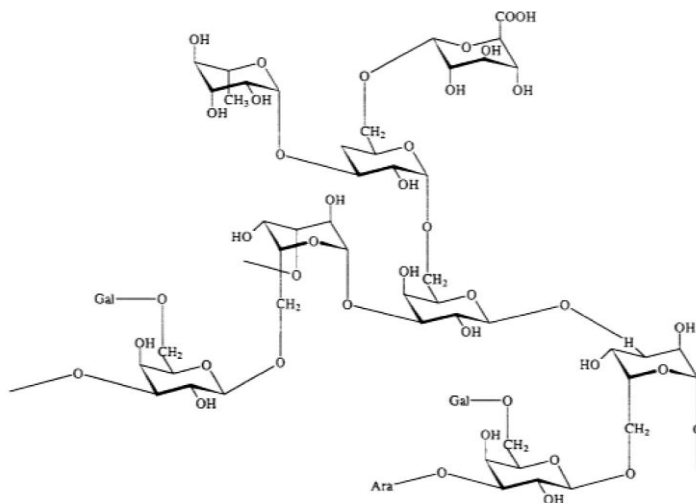


**Figure A-1: Proposed Structure of Gum Arabic. Taken from (ROEPER, 2015)**

The Arabic Gum is commonly used in food and pharmaceutical industries due to the physical properties of this mixture. **Table A-1** resumes some of the most important items:

---

<sup>5</sup> Gum Arabic is a common designation to both exudates but it is important to notice that they are indeed different products, and they are normally marketed and commercialized independently (Cozic, Picton, Garda, Marlhoux, & Le Cerf, 2009).

**Table A-1: Gum Arabic Physical Properties, adapted from (ROEPER, 2015)**

<b>Property</b>	<b>Description</b>
Colour	White – Beige in powder Transparent – white solution
Odour	Odorless
Taste	Tasteless
Solubility in Water	Soluble
Viscosity	Function of Concentration
Rheology	Newtonian Fluid when concentration < 40% Pseudoplastic at higher concentrations
pH	~ 4.5 (weakly acid) <b>Note: Solution pH has a significant effect on viscosity.</b>

Considering the experiments do not include any sensorial analysis, the odorless and tasteless characteristics of the Gum Arabic are not essential. The white-beige colour of the gum solution, on the other hand, is an important quality as it is similar to the sand colour, and it doesn't interfere with the dyes used during the analysis.

Finally, the most important characteristic is the viscosity flexibility that solutions display, based on the Gum Arabic concentration and solution pH (Riddell & Davies, 1931). It is simple to maintain the solution in the Newtonian fluid region by taking account of the mass of Gum and water, and then it is possible to adjust the viscosity of the solution by adjusting the pH of the solution. This has a very important influence in the injection droplets created, and for extension, in the agglomerates produced during the fluidization. It is important to notice that this characteristic also allows to compare the results obtained from other studies, as it is feasible to adjust GA solutions to match the viscosity and adherence characteristic of other substances.

The following figure exemplifies the flexibility of GA solutions regarding viscosity. It is observed that increasing around 10 times the GA concentration results in over 300% increase in viscosity.

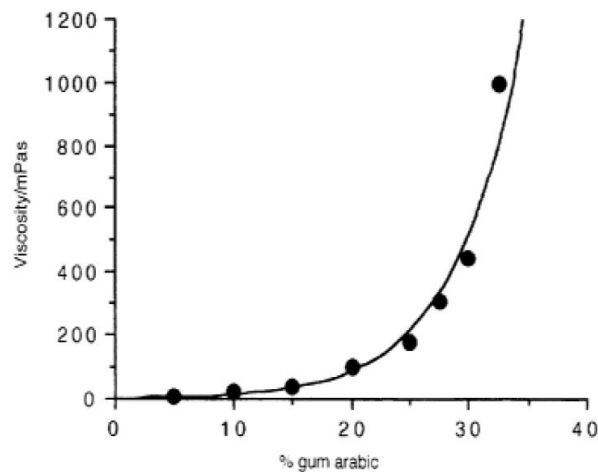


**Figure A-2: Gum Arabic solution viscosity as function of GA concentration. Taken from (ROEPER, 2015)**

## A.2 References

- Cozic, C., Picton, L., Garda, M.-R., Marlhoux, F., & Le Cerf, D. (2009). Analysis of arabic gum: Study of degradation and water desorption processes. *Food Hydrocolloids*, 1930-1934.
- FAO. (1999). *Compendium of food additive specifications - Addendum 7*. Rome: FAO.
- Nie, S.-P., Wang, C., Cui, S. W., Wang, Q., & Xie, M.-Y. (2013). The core carbohydrate structure of *Acacia seyal* var. *seyal* (Gum arabic). *Food Hydrocolloids*, 221-227.
- Riddell, G. L., & Davies, C. W. (1931). *A Study of Gum Arabic, Part I. Viscosity and Adsorption Measurements* (35 (9), pp 2722–2731 ed.). *The Journal of Physical Chemistry*.
- ROEPER. (2015, May 18). *Raw\_Materials\_for\_Food\_Industry | Jelly Agents: Hobby Takt*. Retrieved from Hobby Takt website: <http://www.hobbytakt.com/products/3856466109.pdf>
- SIGMA-ALDRICH. (2015, May 18). *Catalog Products*. Retrieved from Sigma-Aldrich Website: <http://www.sigmaaldrich.com/catalog/product/sigma/g9752>

## CURRICULUM VITAE

**Name:** Liliana Andrea Pardo Reyes

**Post-secondary Education and Degrees:** The University of Western Ontario  
London, Ontario, Canada  
2013 – 2015 M.E.Sc.

Universidad Nacional de Colombia  
Bogota, Colombia  
2003 - 2008

**Honours and Awards:** University of Western Ontario Scholarship

**Related Work Experience:** R&D Engineer  
Brinsa S.A  
Cajica, Cundinamarca, Colombia  
2008 - 2012

Research Assistant  
Instituto de Biotecnología Universidad Nacional de Colombia  
2007 – 2008